

# SPACE WEATHER INTRODUCTORY COURSE



Collaboration of



Solar-Terrestrial Centre of Excellence



Koninklijke luchtmacht



Koninklijk Nederlands  
Meteorologisch Instituut  
*Ministerie van Infrastructuur en Milieu*



## **Drivers of space weather – The eruptive Sun**

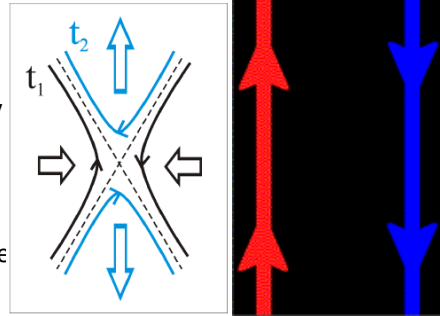
Jan Janssens

SWIC - Collaboration between STCE, Koninklijke Luchtmacht, KNMI



# Magnetic reconnection

- What
  - Antiparallel magnetic field lines
  - Break (disconnect) at X point
  - Reconnect with new partners
- Conversion
  - Magnetic energy  $\Rightarrow$  Kinetic energy
- Result
  - New topological configurations
- Solar flares
  - First observational evidence for the reconnection process
- Where
  - Solar flares
  - CME release from the Sun
  - Geomagnetic storms at Earth



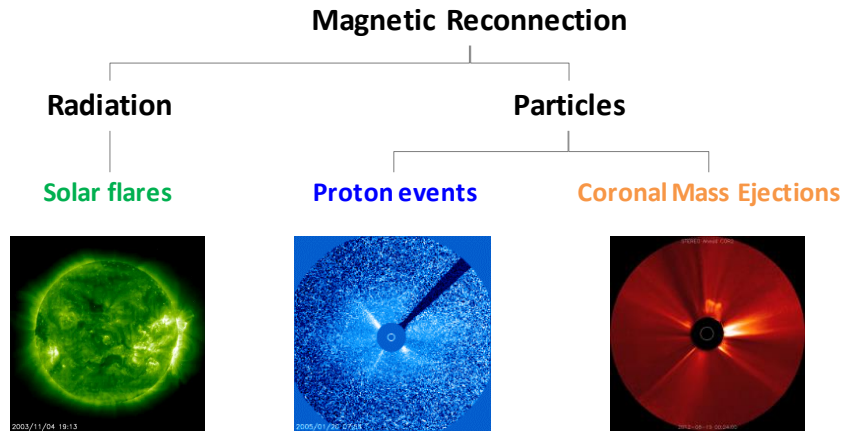
SWIC - Collaboration between STCE, Koninklijke Luchtmacht, KNMI



Text from the CISM Summer School (Boulder, August 2013) – SW101\_4\_Flares  
<https://www.bu.edu/cism/SummerSchool/summerlist.html>

Right animation from ESA: <http://sci.esa.int/cluster/36447-direct-observation-of-3d-magnetic-reconnection/>

# Solar eruptions



SWIC - Collaboration between STCE, Koninklijke Luchtmacht, KNMI



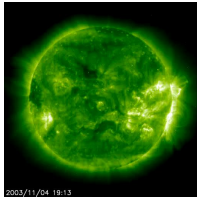
4

# Solar eruptions

**Magnetic Reconnection**

**Radiation**

**Solar flares**

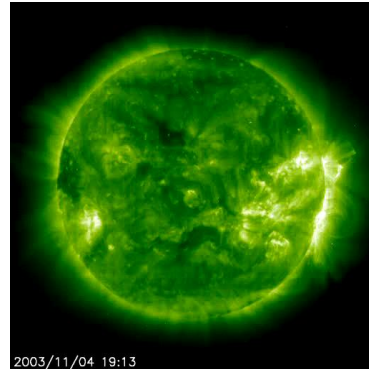


SWIC - Collaboration between STCE, Koninklijke Luchtmacht, KNMI



# Solar flares - Contents

- **Characteristics**
  - Definition
  - Standard model
  - Flare triggers
  - Flare features
- **Classification**
  - H-alpha
  - X-ray
    - Intensity, duration, frequency
  - Types of solar flares
  - Radio bursts
- **Flare predictions**
  - McIntosh
  - Hale
  - Filament eruptions

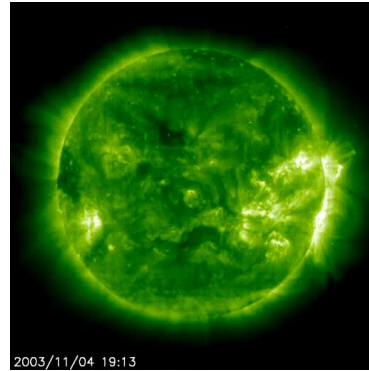


SWIC - Collaboration between STCE, Koninklijke Luchtmacht, KNMI



# Solar flare: what is it?

- Sudden burst of radiation
  - Minutes – hours
  - Gamma-rays, HXR, SXR, EUV; H-alpha, radio
- Large quantity of energy is released
  - from a small volume
  - in a short period of time
- Only viable energy source
  - intense solar magnetic fields
- *Required:*
  - *A very rapid means of converting stored magnetic energy into particle energy and radiation – magnetic reconnection*



SWIC - Collaboration between STCE, Koninklijke Luchtmacht, KNMI



From the CISM Summer School (Boulder, August 2013) – SW101\_4\_Flares  
<https://www.bu.edu/cism/SummerSchool/summerlist.html>

Solar flares are **sudden bursts of radiation** lasting minutes – hours at wavelengths that can include: Gamma-rays, HXR, SXR, EUV; H-alpha, radio

A **large quantity of energy is released** from a small volume in a **short period of time**. This requires: Either a large amount of energy stored in that small volume that can be quickly transformed and released as energetic electrons and photons. Or very efficient transport of energy into that volume where it is then converted into the observed forms.

The only viable energy source is **intense solar magnetic fields**.

*Thus we need a very rapid means of converting stored magnetic energy into particle energy and heat – magnetic reconnection.*

Magnetic energy is converted to thermal/radiative energy (flare, radio bursts) and kinetic energy (mass movement from CMEs and SEPs).

<http://solarphysics.livingreviews.org/Articles/lrsp-2011-6/>

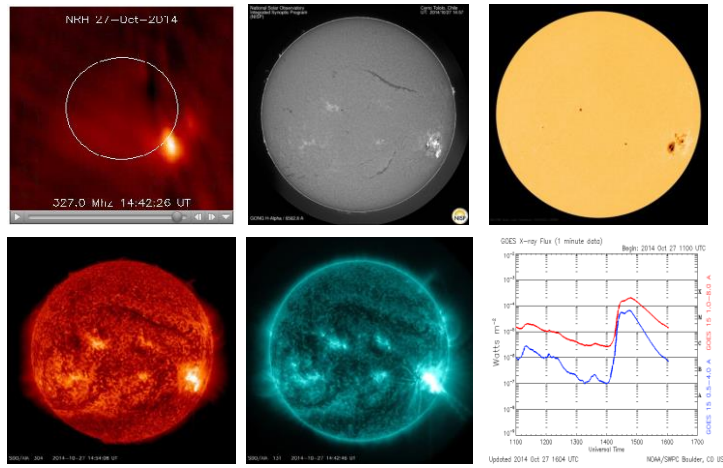
**Solar Flares: Magnetohydrodynamic Processes**

[Kazunari Shibata](#) and [Tetsuya Magara](#)

Solar flares are explosive phenomena observed in the solar atmosphere filled with magnetized plasma. Flares are observed in a wide range of electromagnetic waves such as radio, visible light, X-rays, and gamma rays.

Also, a flare usually produces high-energy particles which travel through the interplanetary space. The discovery of coronal radio and X-ray emissions from a flaring site has revealed that flares are actually coronal phenomena.

# Flares in entire E.M. spectrum



SWIC - Collaboration between STCE, Koninklijke Luchtmacht, KNMI

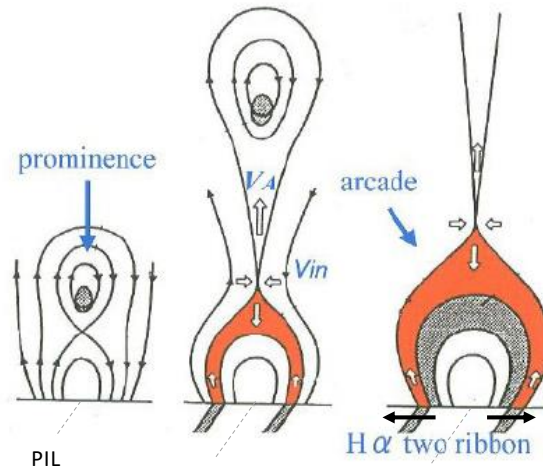


Sources:

<http://bass2000.obspm.fr/home.php> (Nançay Radio Heliograph)

<http://www.stce.be/news/279/welcome.html>

# Standard flare model: CSHKP



SWIC - Collaboration between STCE, Koninklijke Luchtmacht, KNMI



From Maria Massi (What is a solar flare?)  
<http://www3.mpi-fr-bonn.mpg.de/staff/mmassi/#coronae1>

Model proposed by Kopp and Pneuman (1976).

0) Magnetic reconnection occurs

1) It requires a „transient“ that opens up the magnetic field lines.

2) As they close down and reconnect, energy is released that goes into accelerating electrons which travel down the magnetic field lines.

3) These highly energetic particles will heat the dense chromosphere at the footpoints

4) and this plasma is heated and conducted into the loops

5) Post-eruption loop arcade appears successively high, because of the reconnection site rises with time

6) The ribbon separates with time because of the increasing distance between footpoints due to higher loop arcades

PIL: Polarity inversion line (also called neutral line): The line that separates solar magnetic fields of opposite polarity, typically determined from solar magnetograms recording the longitudinal magnetic component.

From: <https://www.swpc.noaa.gov/content/space-weather-glossary#n>

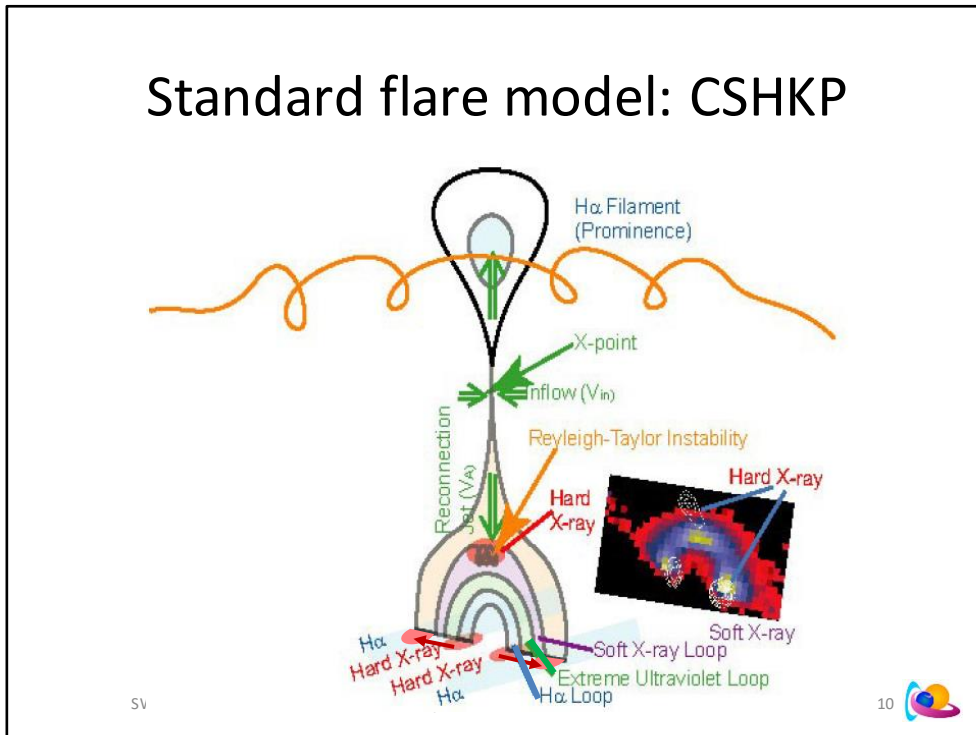
An animated model from a solar flare can be found at:

Cheung et al. (2018): A comprehensive three-dimensional radiative magnetohydrodynamic simulation of a solar flare

<http://adsabs.harvard.edu/abs/2018NatAs...3..160C>

YouTube movie at [https://www.youtube.com/watch?v=kyhsBqB2x\\_Y&feature=youtu.be](https://www.youtube.com/watch?v=kyhsBqB2x_Y&feature=youtu.be)

# Standard flare model: CSHKP



From Maria Massi (What is a solar flare?)

<http://www3.mpifr-bonn.mpg.de/staff/mmassi/#coronae1>

Model proposed by Kopp and Pneuman (1976).

0) Magnetic reconnection occurs

- 1) It requires a „transient“ that opens up the magnetic field lines.
- 2) As they close down and reconnect, energy is released that goes into accelerating electrons which travel down the magnetic field lines.
- 3) These highly energetic particles will heat the dense chromosphere at the footpoints
- 4) and this plasma is heated and conducted into the loops
- 5) Post-eruption loop arcade appears successively high, because of the reconnection site rises with time
- 6) The ribbon separates with time because of the increasing distance between footpoints due to higher loop arcades

So:

1. Magnetic reconnection occurs at the top of magnetic loop
2. Energetic particles are accelerated at the reconnection site
3. Particles precipitate along the magnetic loop (radio emission) and hit the chromosphere footpoints (Hard X-ray emission, H $\alpha$  emission and ribbon)
4. Heated chromospheric plasma evaporates into the corona (soft X-ray emission, loop arcade)

Also: **Professor Valery Nakariakov**

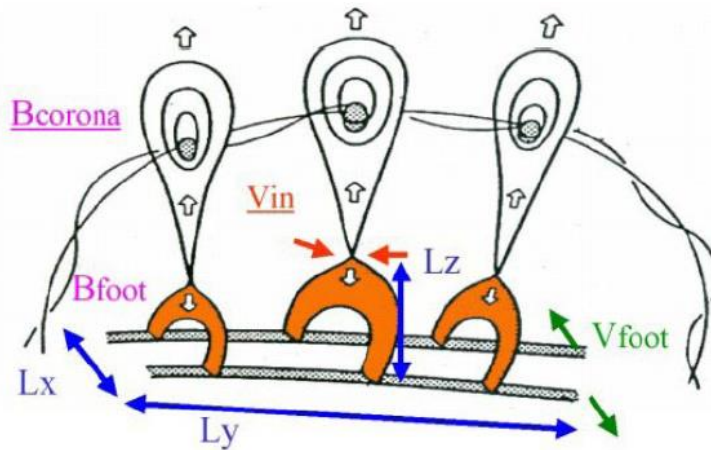
[https://www2.warwick.ac.uk/fac/sci/physics/research/cfsa/people/valery/teaching/px420/handouts/mag\\_rec\\_flare\\_res.pdf](https://www2.warwick.ac.uk/fac/sci/physics/research/cfsa/people/valery/teaching/px420/handouts/mag_rec_flare_res.pdf)

<https://warwick.ac.uk/fac/sci/physics/research/cfsa/people/valery/teaching/hse/19.pdf>

Also: Shibata

<http://cedarweb.vsp.ucar.edu/workshop/tutorials/2001/Shibata.pdf>

# Standard flare model: CSHKP



SWIC - Collaboration between STCE, Koninklijke Luchtmacht, KNMI



Hou et al. (2016): A Solar Flare Disturbing a Light Wall above a Sunspot Light Bridge  
<http://adsabs.harvard.edu/abs/2016ApJ...829L..29H>

Solar flares are energetic phenomena in the solar atmosphere, releasing dramatic electromagnetic energy spanning the range from X-ray to radio wavelengths. In the standard two-dimensional (2D) flare model (CSHKP models; Carmichael 1964; Sturrock 1966; Hirayama 1974; Kopp & Pneuman 1976), a filament rises above the neutral line and then initially drives the flare process. The rising filament pushes the overlying magnetic field lines upward, and the resulting losses of pressure below form an inward magnetic force toward the neutral sheet. This force drives antiparallel magnetic field lines to converge, leading to the formation of a current sheet, and magnetic reconnection begins to take place. Thus, the released energy heats the coronal plasma and also accelerates particles. The accelerated particles flow downward from the reconnection site along the newly formed magnetic field lines, and in the lower solar atmosphere, the flare ribbons are generated (Priest & Forbes 2002). The flare ribbons observed in  $H\alpha$  and ultraviolet (UV) wavelengths are the obvious characteristics of solar flares and are usually located on either side of the polarity inversion line. The flare ribbons move apart during the reconnection process, and the separation generally stops at the edge of the sunspots. However, Li & Zhang (2009) reported that flare ribbons sometimes sweep across the whole sunspots.

Mancuso et al. (2016): Coronal O VI emission observed with UVCS/SOHO during solar flares: Comparison with soft X-ray observations

<http://adsabs.harvard.edu/abs/2016A%26A...591A...4M>

The impulsive phase is attributed to the rapid downward acceleration of particles at the reconnection region, where magnetic energy is mainly transformed into kinetic energy of non-thermal particles, which then deposit their energy in the chromosphere and produce hard X-ray emission at the loop footpoints. The downward flux of accelerated particles generates a localized pressure pulse that drives an evaporation upflow of heated plasma into the corona, which then gradually cools as it radiates in soft X-ray and extreme ultraviolet (EUV) wavelengths. The gradual phase is thus associated with the longer lasting soft X-ray emission from chromospheric plasma evaporated into the corona.

# Standard flare model: CSHKP

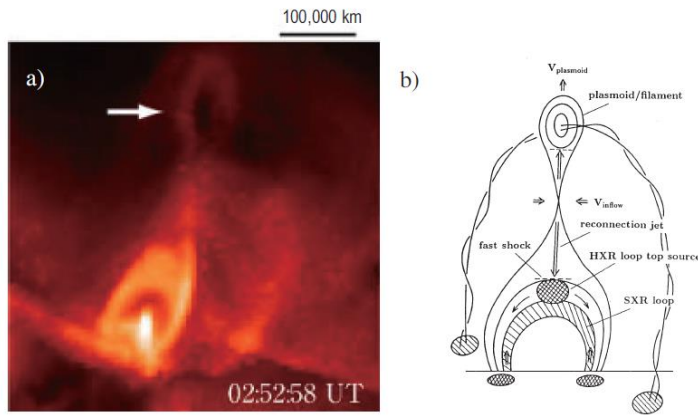


**Figure 3:** (a) Soft X-ray image of a *long-duration-event (LDE)* flare (see Section 2) observed by *Yohkoh*. (b) Schematic picture of a modified version of the CSHKP model, incorporating the new features discovered by *Yohkoh* (from *Shibata et al., 1995*).

SWIC - Collaboration between STCE, Koninklijke Luchtmacht, KNMI

12

Shibata et al. (2011): Solar Flares: Magnetohydrodynamic Processes  
<http://solarphysics.livingreviews.org/Articles/lrsp-2011-6/>

Several classic models based on magnetic reconnection have been proposed to explain the phenomenological aspect of flares: Carmichael (1964), Sturrock (1966), Hirayama (1974), and Kopp and Pneuman (1976) (see Figure 2). These models assume more or less a similar configuration of magnetic field and its dynamic process, so these models are called with a single name, CSHKP model (~ Svestka and Cliver, 1992; Sturrock, 1992; Shibata, 1999). The CSHKP model has been a standard model of flares, and the basic features of this model are explained in Figure 3.

Shibata (1999): Evidence of Magnetic Reconnection in Solar Flares and a Unified Model of Flares  
<http://adsabs.harvard.edu/abs/1999Ap%26SS.264..129S>

Shibata (1994) showed that, because there was an HXR on top of the SXR loop tops. As the HXR are produced by high energy electrons, this means that the main energy release took place outside/above the SXR loops.

# Standard flare model: CSHKP

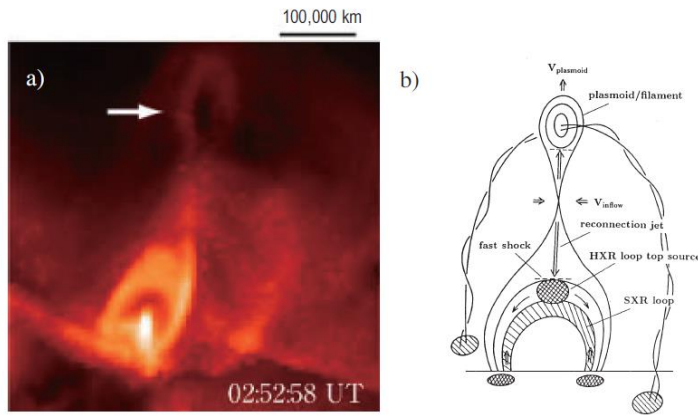


Figure 3: (a) Soft X-ray image of a long-duration-event (LDE) flare (see Section 2) observed by Yohkoh. (b) Schematic picture of a modified version of the CSHKP model, incorporating the new features discovered by Yohkoh (from Shibata *et al.*, 1995).

SWIC - Collaboration between STCE, Koninklijke Luchtmacht, KNMI

13

Shibata *et al.* (1995): Hot-Plasma Ejections Associated with Compact-Loop Solar Flares  
<http://adsabs.harvard.edu/abs/1995ApJ...451L..83S>

One of the biggest discoveries by the soft X-ray telescope (SXT) (Tsuneta *et al.* 1991) aboard Yohkoh (Ogawara *et al.* 1991) is that of cusp-shaped loop structures in long duration event (LDE) flares (Tsuneta *et al.* 1992a) and large-scale arcade loops associated with filament eruption or coronal mass ejections (Tsuneta *et al.* 1992b; Hanaoka *et al.* 1994; McAllister *et al.* 1995; Hudson, Haisch, & Strong 1995). The observed loop configurations of the LDE flares and arcade loops are quite similar to the magnetic field configuration suggested by the classical two-ribbon flare model (Carmichael 1964; Sturrock 1966; Hirayama 1974; Kopp & Pneuman 1976). This model, which is hereafter called the CSHKP model, predicts that magnetic fields are first opened up by global MHD instability associated with filament eruption to form vertical current sheet, and then magnetic field lines in the current sheet successively reconnect to form apparently growing flare loops.

Recently, using the hard X-ray telescope (HXT) (Kosugi *et al.* 1991) aboard Yohkoh, Masuda *et al.* (1994) discovered that some of impulsive compact-loop flares occurring near the solar limb, a loop top hard X-ray (HXR) source appeared well above a soft X-ray (SXR) bright loop during the impulsive phase. This indicates that the impulsive energy release did not occur within the soft X-ray loop but above the loop. This is a quite exciting discovery because bright soft X-ray loops were often considered to be evidence of "loop flares" in which energy release occurs within the loop, as discussed above. One possible physical mechanism to produce such loop top hard X-ray source is magnetic reconnection occurring above the loop; i.e., a high-speed jet is created through the reconnection and collides with the loop top, producing fast-mode MHD shock, superhot plasma, and/or high-energy electrons emitting hard X-rays. In this sense, the discovery of the loop-top HXR source may open a possibility to unify two distinct classes of flares, two-ribbon flares (or LDE flare) and compact-loop flares (or impulsive flare), by the single mechanism of magnetic reconnection (Shibata 1995).

Also: <http://solar.physics.montana.edu/magara/Research/Topics/cshkp.html>

# Standard flare model: CSHKP

P. C. H. MARTENS AND N. P. M. KUIN

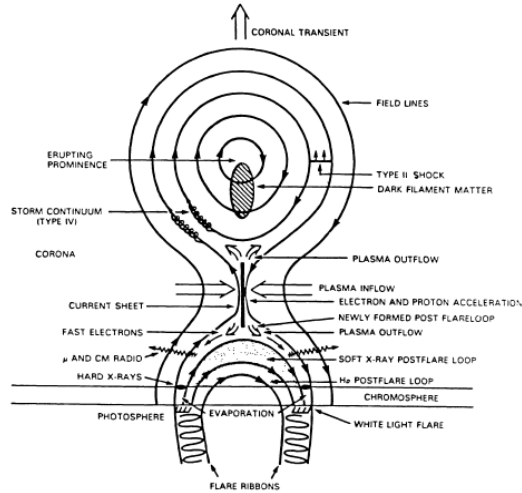


Fig. 2. The global structure of the two-ribbon flare and the location of the major observed energy conversion processes viewed in cross section along the neutral line.

14



Martens and Kuin (1989): A circuit model for filament eruptions and two-ribbon flares  
<http://adsabs.harvard.edu/abs/1989SoPh...122..263M>

Shibata et al. (2011): Solar Flares: Magnetohydrodynamic Processes  
<http://solarphysics.livingreviews.org/Articles/lrsp-2011-6/>

Several classic models based on magnetic reconnection have been proposed to explain the phenomenological aspect of flares: Carmichael (1964), Sturrock (1966), Hirayama (1974), and Kopp and Pneuman (1976) (see Figure 2). These models assume more or less a similar configuration of magnetic field and its dynamic process, so these models are called with a single name, CSHKP model (Svestka and Cliver, 1992; Sturrock, 1992; Shibata, 1999). The CSHKP model has been a standard model of flares, and the basic features of this model are explained in Figure 3.

Shibata (1999): Evidence of Magnetic Reconnection in Solar Flares and a Unified Model of Flares  
<http://adsabs.harvard.edu/abs/1999Ap%26SS.264..129S>

Shibata (1994) showed that, because there was an HXR on top of the SXR loop tops. As the HXR are produced by high energy electrons, this means that the main energy release took place outside/above the SXR loops.

Also: <http://solar.physics.montana.edu/magara/Research/Topics/cshkp.html>

Another good observational description of the solar flare phenomenon is Fletcher et al. (2011) - An Observational Overview of Solar Flares  
<http://adsabs.harvard.edu/abs/2011SSRv..159...19F>

# Various phases of solar flares

- Precursor phase
  - Slow increase EUV and SXR
  - Darkening filament (H-alpha)
- Impulsive phase
  - HXR (footpoints)
  - Particle acceleration
  - Type III radio bursts
- Flash phase
  - SXR, EUV and H-alpha max
  - More gentle energy release
  - Type II burst
- Decay phase
  - Return to pre-flare values
  - Occasionally Late EUV phase
  - Type IV radioburst
- Gradual phase
  - Flash + Decay phase

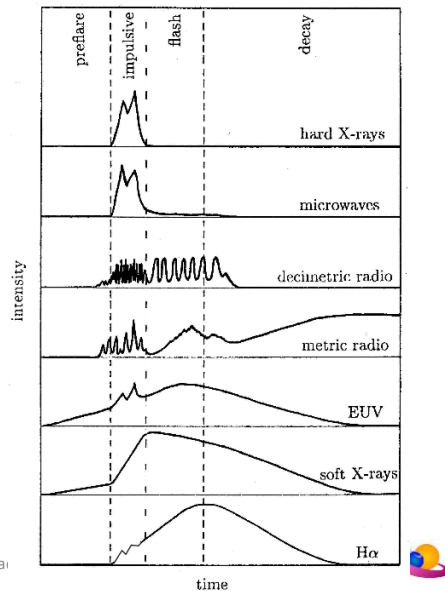


Figure source: Benz, A. O., 2008

Living Reviews: <http://solarphysics.livingreviews.org/Articles/lrsp-2008-1/>

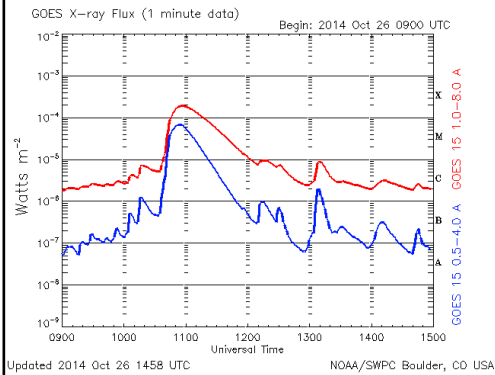
## 1.3 The phases of flares

The timing of the different emissions of the same flare is presented schematically in Figure 2. In the pre-flare phase the coronal plasma in the flare region slowly heats up and is visible in soft X-rays and EUV. A large number of energetic electrons (up to  $10^{38}$ ) and ions (with similar total energy) is accelerated in the impulsive phase, when most of the energy is released. The appearance of hard X-ray footpoint sources at chromospheric altitude is a characteristic of this phase (Hoing et al., 1981). Some high-energy particles are trapped and produce intensive emissions in the radio band.

The thermal soft X-ray and H $\alpha$  emissions finally reach their maxima after the impulsive phase, when energy is more gently released, manifest in decimetric pulsations, and further distributed. The rapid increase in H $\alpha$  intensity and line width has been termed flash phase. It coincides largely with the impulsive phase, although H $\alpha$  may peak later. In the decay phase, the coronal plasma returns nearly to its original state, except in the high corona ( $>1.2R$ , where R is the photospheric radius), where magnetic reconfiguration, plasma ejections and shock waves continue to accelerate particles, causing meter wave radio bursts and interplanetary particle events.

[Kane, 1974: The gradual phase consists of the flash phase and the decay phase. Here, the flash phase concerns the energy release as the sudden brightening. (Fundamentals of Solar astronomy, Figure 5.40).]

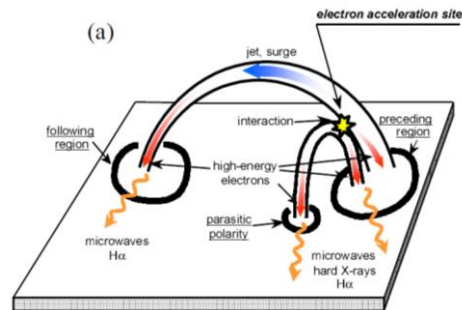
## Exercise – Various phases of solar flares



- In this GOES soft x-ray curve of an X2.0 flare, which of the typical flare phases can be distinguished?
  - Precursor phase
  - Impulsive phase
  - Flash phase
  - Decay phase
  - Gradual phase

# Triggers of solar flares

- Magnetic restructuring
- Magnetic flux emergence
- Helical energy storage
  - Sigmoid
  - Kink instability
    - Twisted magnetic flux bundle
- Instability surrounding fields
  - Long/high filaments
  - Moreton/EIT wave
- Interaction with nearby CH
- ...



SWIC - Collaboration between STCE, Koninklijke Luchtmacht, KNMI

17 

Top: From Hanaoka et al., 1999: Radio and X-ray Observations of the Flares Caused by Interacting Loops

[http://solar.nro.nao.ac.jp/meeting/nbym98/PDF/hanaoka\\_2.pdf](http://solar.nro.nao.ac.jp/meeting/nbym98/PDF/hanaoka_2.pdf)

And

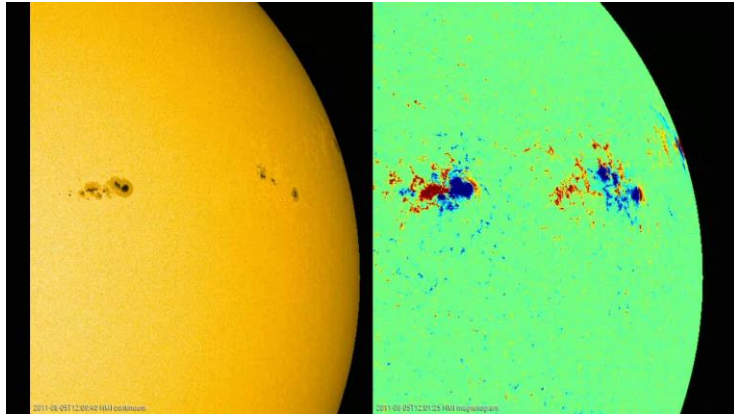
Bottom: From Maria Massi (What is a solar flare?)

<http://www3.mpi-fr-bonn.mpg.de/staff/mmassi/#coronae1>

Other example: Solar flare mechanism: <http://www.stce.be/news/265/welcome.html>

# Triggers of solar flares

## Magnetic flux emergence



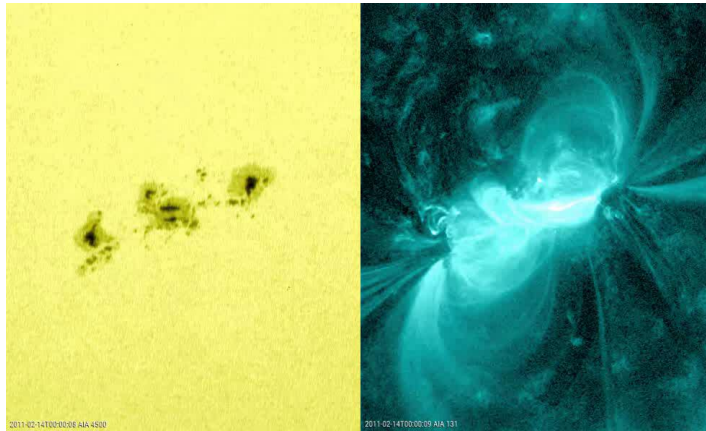
SWIC - Collaboration between STCE, Koninklijke Luchtmacht, KNMI

18 

Magnetic flux emergence: X6.9 flare on 9 August 2011: <http://www.stce.be/news/353/welcome.html>  
Blue/black is negative (inward) magnetic polarity, red/white is positive (outward) polarity

# Triggers of solar flares

## Helical energy storage



SWIC - Collaboration between STCE, Koninklijke Luchtmacht, KNMI



Helical energy storage: X2.2 flare on 15 February 2011

Velareddi et al. (2012): On the role of rotating sunspots in the activity of solar active region NOAA 11158

<http://iopscience.iop.org/article/10.1088/0004-637X/761/1/60/pdf>

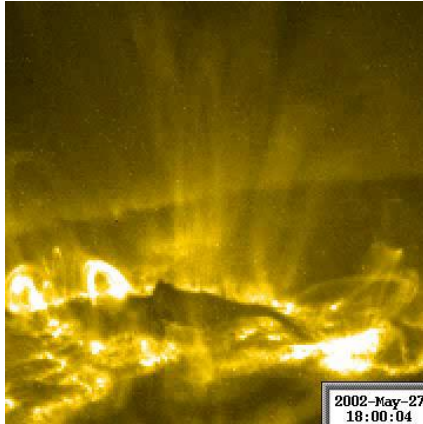
Jiang et al. (2011): Rapid sunspot rotation associated with the X2.2 flare on 2011 February 15

<http://iopscience.iop.org/article/10.1088/0004-637X/744/1/50>

Also at PhysOrg: <https://phys.org/news/2011-04-rotating-sunspots-super-solar-flare.html>

# Triggers of solar flares

## Kink instability



## Unstable magnetic fields



SWIC - Collaboration between STCE, Koninklijke Luchtmacht, KNMI



## Kink instability

Török et al. (2010): The writhe of helical structures in the solar corona

[https://www.aanda.org/articles/aa/full\\_html/2010/08/aa13578-09/aa13578-09.html](https://www.aanda.org/articles/aa/full_html/2010/08/aa13578-09/aa13578-09.html)

<http://www.lmsal.com/TRACE/POD/TRACEpodarchive14.html#movie61> (27 May 2002; M2 ; NOAA 9957)

Unstable if twist  $\sim 2.5\pi$  (Török et al., 2003:

<https://www.aanda.org/articles/aa/pdf/2003/30/aah4206.pdf>).

## Unstable magnetic fields

Collateral damage: <http://www.stce.be/news/361/welcome.html>

Shen et al. (2014): A Chain of Winking (Oscillating) Filaments Triggered by an Invisible Extreme-ultraviolet Wave

<http://adsabs.harvard.edu/abs/2014ApJ...786..151S>

# Post-eruption coronal loops



SWIC - Collaboration b

21



STCE: <http://www.stce.be/news/316/welcome.html>

STCE: <http://www.stce.be/news/331/welcome.html>

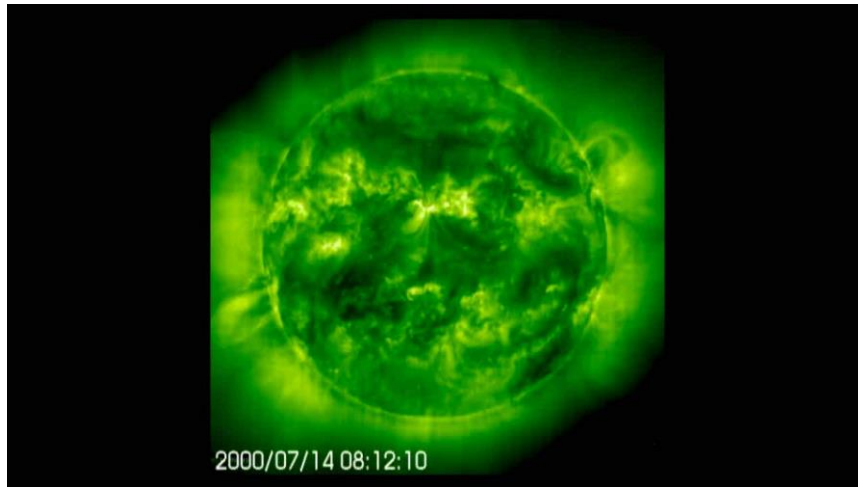
STCE: <http://www.stce.be/news/274/welcome.html>

The M2-event finished with an arcade, which is the technical term for a series of post-flare coronal loops. Interestingly, these post-flare loops continued to grow, first reaching the limit of AIA's Field-Of-View (FOV) on 15 October around 17:00UT, then continuing to grow even beyond AIA's FOV.

Fortunately, PROBA2's wider-field SWAP telescope came to the rescue and was able to monitor this arcade in its full glory till its disappearance around noon on 17 October. So, the loops of this long duration arcade were visible for about 2.5 days (60 hours!), and at their maximum height, they were towering at least 340.000 km above the solar surface. That's not far from the average Earth-Moon distance!

# Post-eruption coronal loops

## Arcade



SWIC - Collaboration between STCE, Koninklijke Luchtmacht, KNMI



An arcade is a series of post-eruption coronal loops

Bastille Day event

SOHO: <https://soho.nascom.nasa.gov/gallery/Movies/flares.html>

TRACE: <http://soi.stanford.edu/results/SolPhys200/Schrijver/TRACEpodarchive3.html>

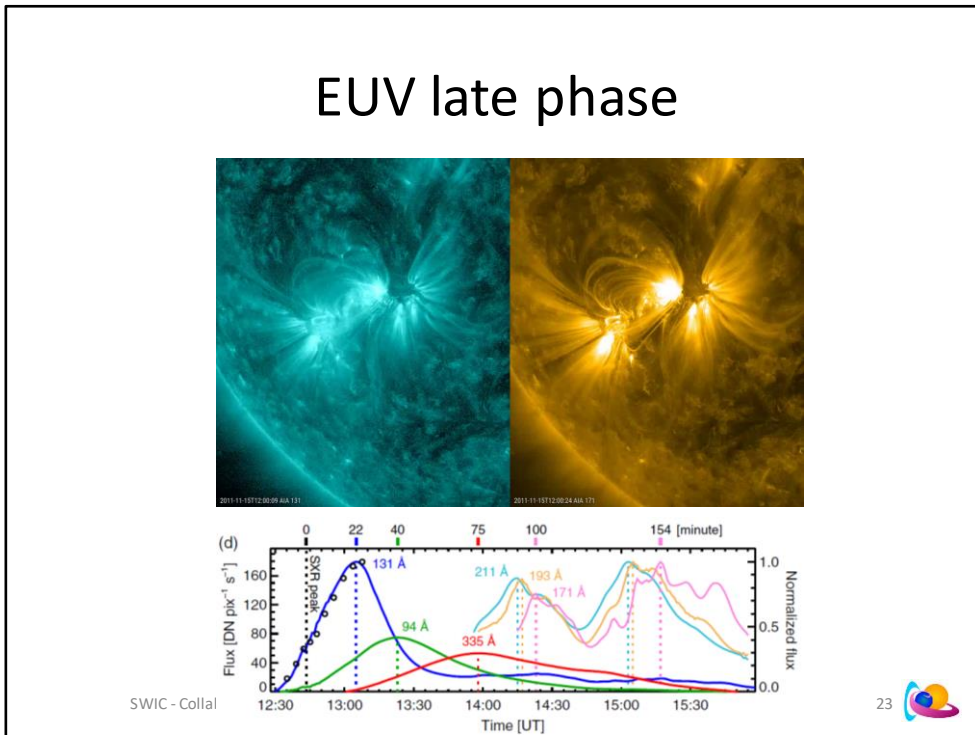
Yashiro et al. (2013): Post-Eruption Arcades and Interplanetary Coronal Mass Ejections

<http://adsabs.harvard.edu/abs/2013SoPh..284....5Y>

<https://cdaw.gsfc.nasa.gov/publications/yashiro/yashiro2013SolPhys.pdf>

Two-ribbon flares are characterized by a pair of bright ribbons observed in H-alpha and ultraviolet (UV) images. The ribbons are located on either side of a magnetic polarity inversion line and they separate from each other as the flare progresses. Two-ribbon flares are often associated with filament eruptions and coronal mass ejections (CMEs). After the launch of the filament, long-lived arcades are formed connecting the two ribbons across the polarity inversion line. The emerged assembly of arches is called a post-eruption arcade (PEA). The PEAs are observed at multiple wavelengths and are known also as long-duration (or decay) events (LDEs; Pallavicini, Serio, and Vaiana, 1977) in X-ray observations. The erupting filament becomes the core of the associated CME (Webb and Hundhausen, 1987; Gopalswamy *et al.*, 2003), thus PEAs are considered as surface signatures of CMEs (Tripathi, Bothmer, and Cremades, 2004).

# EUV late phase



STCE: <http://www.stce.be/news/268/welcome.html> (concerns the 10 September 2014 flare)

One can see that the EUV emissions peak 6-12 minutes later than those from x-ray. This is due to the cooling of the post-flare coronal loops, whose emissions become then better visible in the less energetic EUV passbands. The AIA 094 emissions also show a second peak about 30 minutes after its maximum. This second peak is not visible in x-ray. This "extra" EUV emission does not originate from the original flare site, but most probably from a volume of higher coronal loops. This may indicate there's additional post-flare loop reconnection, but at a lower temperature than during the flare's main peak. This is called the "EUV late phase".

Sun et al. (2013): Hot Spine Loops and the Nature of a Late-phase Solar Flare (graph - This concerns the 15 November 2011 flare)

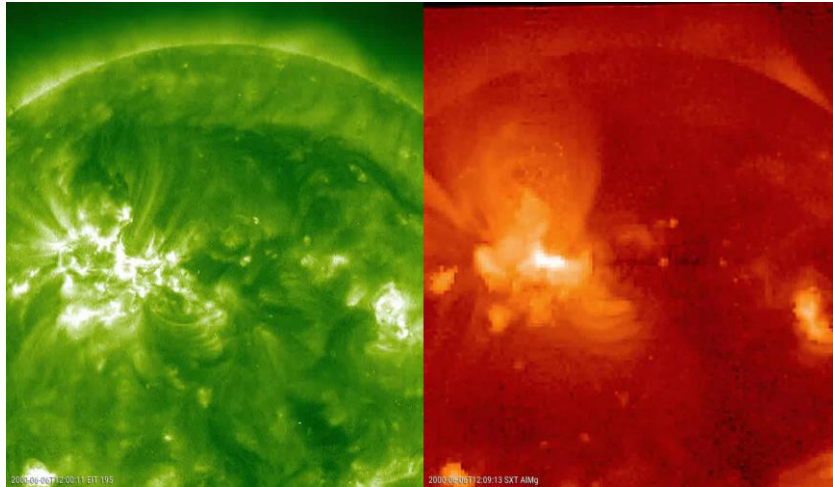
<http://adsabs.harvard.edu/abs/2013ApJ...778..139S>

This event also features an extreme-ultraviolet (EUV) late phase, i.e., a delayed secondary emission peak in warm EUV lines (about 2–7 MK). We show that this peak comes from the cooling of large post-reconnection loops beside and above the compact fan, a direct product of eruption in such topological settings. The long cooling time of the large arcades contributes to the long delay; additional heating may also be required. ... If the fan is small compared to the pre-existing AR, the post-reconnection loops can be very different in size. They will cool at different rates during the initial, conduction-dominated stage, when the cooling time scales with the loop length squared (for recent review, see Reale 2010). Because emission in the warm EUV lines increases only after the hot loops cool down, peaks from A2 and A3 loops will appear at a much later time compared to A1, as already noted in Woods et al. (2011). Additional heating from ongoing, weak reconnection may also contribute (Hock et al. 2012). The two mechanisms need not be mutually exclusive.

NASA: <https://svs.gsfc.nasa.gov/10817>

The solar EUV radiation creates our Earth's ionosphere (plasma in our atmosphere), so solar flares disturb our ionosphere and consequently our communication and navigation technologies, such as Global Positioning System (GPS), that transmit through the ionosphere. ... With these new SDO EVE results, they now recognize that additional ionospheric disturbances from these later EUV enhancements are also a concern.

# Cusp



SWIC - Collaboration between STCE, Koninklijke Luchtmacht, KNMI



JHV: Flare from 06 June 2000 (SOHO, Yohkoh: X1.1 in NOAA 9026)

More on this and other cusps: [http://solar.physics.montana.edu/takeda/evt\\_archive/cusp\\_flare.html](http://solar.physics.montana.edu/takeda/evt_archive/cusp_flare.html)

Another example of a cusp: <http://www.stce.be/news/298/welcome.html> (06 March 2015)

Another example of a cusp: <http://www.stce.be/news/173/welcome.html> (19 January 2012)

Another example of a cusp: <http://www.stce.be/news/238/welcome.html> (25 February 2014; X4.9)

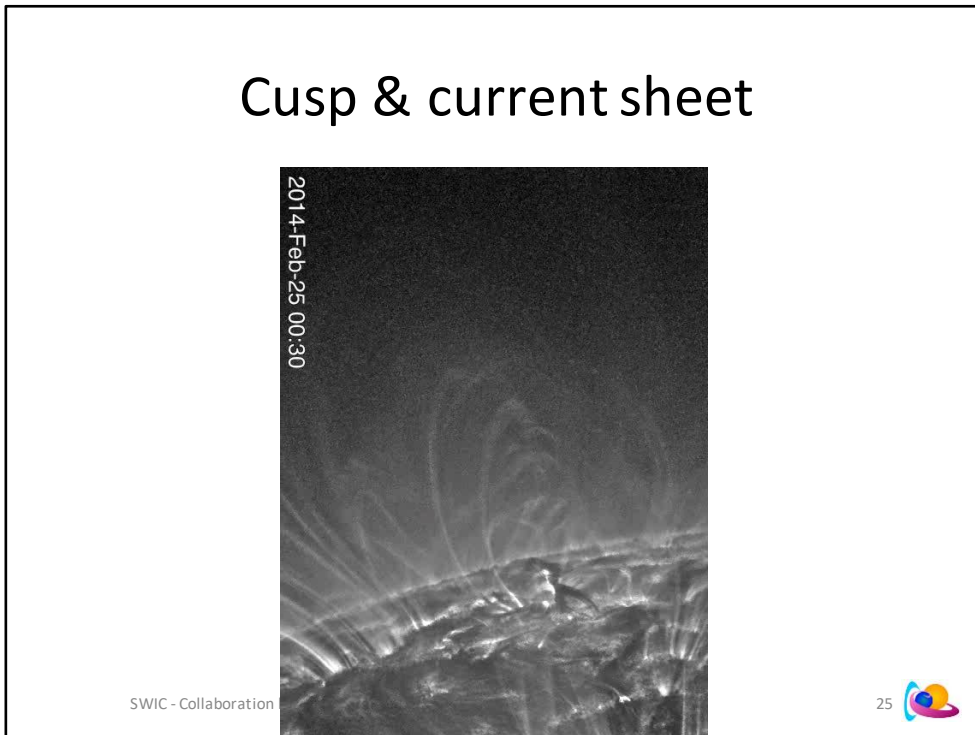
Yokoyama et al. (2001): Clear Evidence of Reconnection Inflow of a Solar Flare

<http://adsabs.harvard.edu/abs/2001ApJ...546L..69Y>

Magnetic reconnection (Petschek 1964; Sweet 1958; Parker 1963)—the reorganization caused by local diffusion of antiparallel magnetic field lines and the consequent release of magnetic energy—has been thought to be the cause of solar flares (e.g., Shibata 1996). Many indirect pieces of evidence for this process have been found by recent spacecraft observations. There was, however, almost no direct evidence, such as inflow or outflow (reconnection jet) that carries the field lines toward or from the magnetic neutral point where the local dissipation occurs (except for McKenzie & Hudson 1999). We report here the first discovery of reconnection inflow during a flare on 1999 March 18.

Solar flares are now thought to be caused by magnetic reconnection (Fig. 1; e.g., Shibata 1996; Yokoyama & Shibata 1998). In this model, the antiparallel field lines dissipate in a certain local point in the corona. The tension force of the reconnected field lines then accelerates the plasma out of the dissipation point. In response to this outflow, the ambient plasma is drawn in. The inflowing plasma carries the ambient magnetic field lines into the dissipating point. These field lines continue the reconnection cycle. In this manner, the magnetic energy stored near the neutral point is released to become the thermal and bulk-flow energy of plasma. ... The supporting evidence for this model is the observation of a cusp-shaped soft X-ray flare loop (Tsuneta et al. 1992). The tip of the cusp is thought to be the remnant of the kink of the reconnected field lines. This cusp-shaped flare loop increases its height and the distance between the footpoints, which might be the consequence of the piling up of the shrunk magnetic field lines (see also Forbes & Acton 1996; Hiei, Hundhausen, & Sime 1993). Flare observation by Masuda et al. (1994) demonstrates a hard X-ray source above the soft X-ray loop. This source suggests that some high-energy process, such as acceleration of electrons associated with reconnection, is occurring above the soft X-ray loop.

# Cusp & current sheet

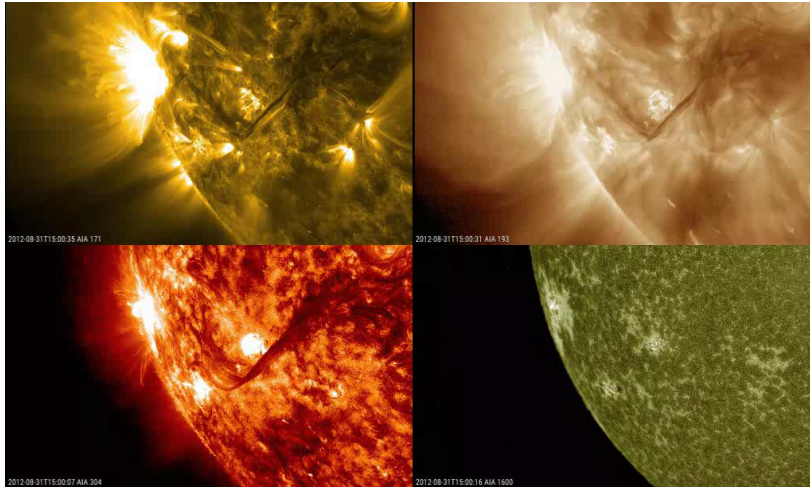


Seaton et al. (2017): Observations of the Formation, Development, and Structure of a Current Sheet in an Eruptive Solar Flare  
<http://adsabs.harvard.edu/abs/2017ApJ...835..139S>

**Figure 2.** Evolution of current sheet structure in the 131 Å AIA channel, beginning with its appearance in the wake of a strong CME. Early on (upper left) the structure is long and narrow, and only later (upper right) do background features begin to appear. These features are first seen as shrinking loops, which later broaden (middle left, black arrow) into a more fan-like structure, while the sheet itself (middle left, white arrow) begins to broaden. As the sheet broadens, shrinking loops are clearly visible in the cusp region at the current sheet's base (middle right). Even later (lower left) dark inflows, presumably SADs [Supra-Arcade Downflows], become visible in the diffuse background emission. At very late times (lower right) some material appears to flow into the sheet itself, triggering bifurcated up-down flows along the sheet structure.

The structures we report on in this paper were formed in association with a large and complex filament eruption that occurred on the east limb of the Sun in NOAA Active Region 11990 at about 00:40 UT on 2014 February 25. This eruption was also associated with an ... X4.9 class flare, which peaked about 10 minutes after the onset of the eruption, and a very energetic CME with a reported velocity of more than  $2100 \text{ km s}^{-1}$  in the CDAW CME Catalog (for a description of CDAW, see Yashiro et al. 2004).

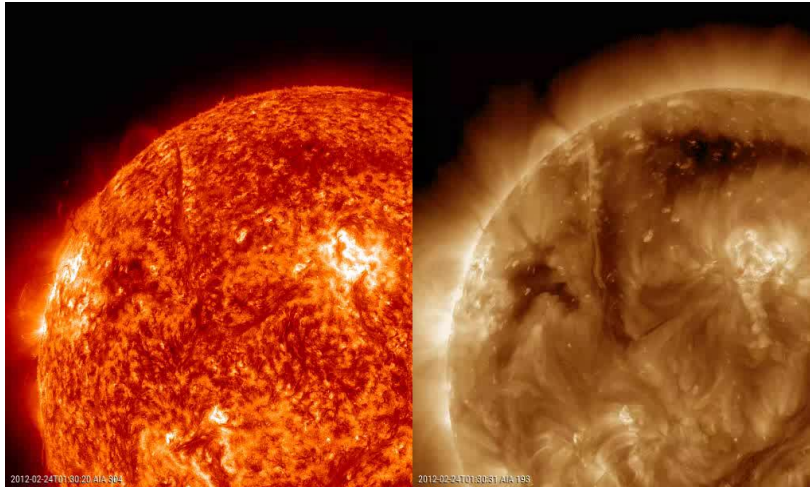
# Two ribbon flare



SWIC - Collaboration between STCE, Koninklijke Luchtmacht, KNMI

<http://www.stce.be/news/157/welcome.html>  
<http://www.stce.be/news/218/welcome.html>

# Canyon of fire



SWIC - Collaboration between STCE, Koninklijke Luchtmacht, KNMI



<http://www.stce.be/news/255/welcome.html>

The eruption was not associated to an obvious x-ray flare, but a disturbance was noted in the EUV imagery, parallel to the original position of the erupted filament on both the east and west side (see annotated image above). The disturbance propagated through the corona at a speed of 2-5 km/s. Just as the expanding flare ribbons ("parallel ribbons") and the post-flare coronal loops that often can be seen after a solar flare, also this phenomenon is an effect of the reconnection higher up in the solar atmosphere. The charged particles get accelerated towards the denser inner solar atmosphere, where they collide with other particles and heat the local chromospheric environment and make it evaporate. It is not an EIT wave, characteristics of which were described in a previous newsletter (see <http://www.stce.be/news/241/welcome.html> for more details). The footpoints of some faint coronal loops can be seen embedded in the expanding disturbance in the combo movies.

Another example of a canyon-of-fire

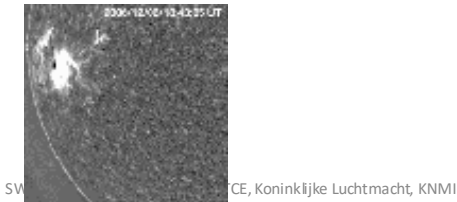
NASA: <https://www.nasa.gov/content/goddard/nasa-releases-movie-of-suns-canyon-of-fire>

NASA: <https://www.nasa.gov/content/solar-filament-eruption-canyon-of-fire>

# Moreton waves & EIT waves

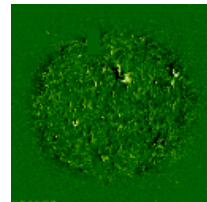
## Moreton waves

- Chromospheric ( $H\alpha$ ) waves
- Fast: 500-2000 km/s
- More arc-like (90-120°)
  - Filament blinking
- Fast mode MHD waves?
- More related to flares



## EIT waves

- Coronal (EUV) waves
- Rather slow: 200-600 km/s
- More isotropic (halo like)
  - Stopped at CH boundaries
- Fast Magnetosonic wave?
- More related to CMEs



Another name for this kind of features is « solar tsunami »

They are expanding large-scale waves in the solar atmosphere usually associated to strong solar eruptions (flares and CMEs).

### Animation sources:

- Moreton wave: 6 December 2006 event:

[https://en.wikipedia.org/wiki/Moreton\\_wave#/media/File:MoretonWaveAnimation200612.gif](https://en.wikipedia.org/wiki/Moreton_wave#/media/File:MoretonWaveAnimation200612.gif)

With associated press release at

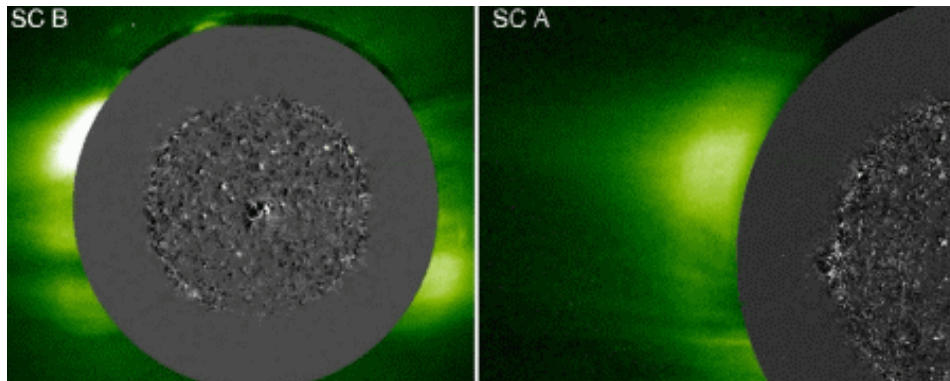
<http://www.nso.edu/sites/www.dev.nso.edu/files/files/press/archive/SolarTsunami.pdf>

- EIT wave: 12 May 1997 event: <http://umbra.nascom.nasa.gov/eit/cme/may12/>

### References:

- "EIT waves" and coronal mass ejections, Chen et al. (2011): [http://www.ncra.tifr.res.in:8081/~basi/ASICS\\_2/229-chen.pdf](http://www.ncra.tifr.res.in:8081/~basi/ASICS_2/229-chen.pdf)
- Synthesis of CME-associated and EIT-wave features from MHD simulations, Chen et al. (2005): <http://astronomy.nju.edu.cn/~chenpf/paper/ssr01.pdf>
- Large-scale coronal propagating fronts... , Nitta et al. (2013) : <http://iopscience.iop.org/article/10.1088/0004-637X/776/1/58/pdf>
- Observation of a Moreton wave and wave-filament interactions... , Liu et al. (2013) : <http://iopscience.iop.org/article/10.1088/0004-637X/773/2/166/pdf>
- On the nature of EIT waves, EUV dimmings and their link to CMEs, Zhukov et al. (2004) : <https://www.aanda.org/articles/aa/pdf/2004/44/aa0351-04.pdf>
- SOHO/EIT Observations of the 1997 April 7 Coronal Transient: Possible Evidence of Coronal Moreton Waves, Thompson et al. (1999): <http://adsabs.harvard.edu/abs/1999ApJ...517L.151T>

# EIT wave: another example



SWIC - Collaboration between STCE, Koninklijke Luchtmacht, KNMI



More examples:

**Moreton waves:** <http://www.stce.be/news/222/welcome.html>

**EIT waves:** <http://www.stce.be/news/222/welcome.html> and <http://www.stce.be/news/241/welcome.html>

EIT-waves are named after the Extreme-ultraviolet Imaging Telescope (EIT) onboard SOHO, with which this phenomenon was discovered in 1996-1997. They are large-scale bright fronts observed in extreme ultraviolet (EUV) and propagating over a significant portion of the solar surface. 17 years later, the true nature of these waves remains under debate, though there is a gradual convergence towards it being primarily a fast magnetosonic wave (directly related to the presence of a coronal mass ejection, CME, rather than a flare), but often also with a contribution from the CME expansion (see Note 1). Other typical characteristics are its relatively low average speed of 200-600km/s, and that these fronts can be stopped at the boundary of coronal holes or near active regions.

**Note 1** - A fast magnetosonic wave is a longitudinal wave of charged particles in a magnetized plasma propagating in all directions, including perpendicularly and parallel to the magnetic field. See image underneath (Source: Wikipedia).

**Example above on EIT wave** from: <https://cor1.gsfc.nasa.gov/>

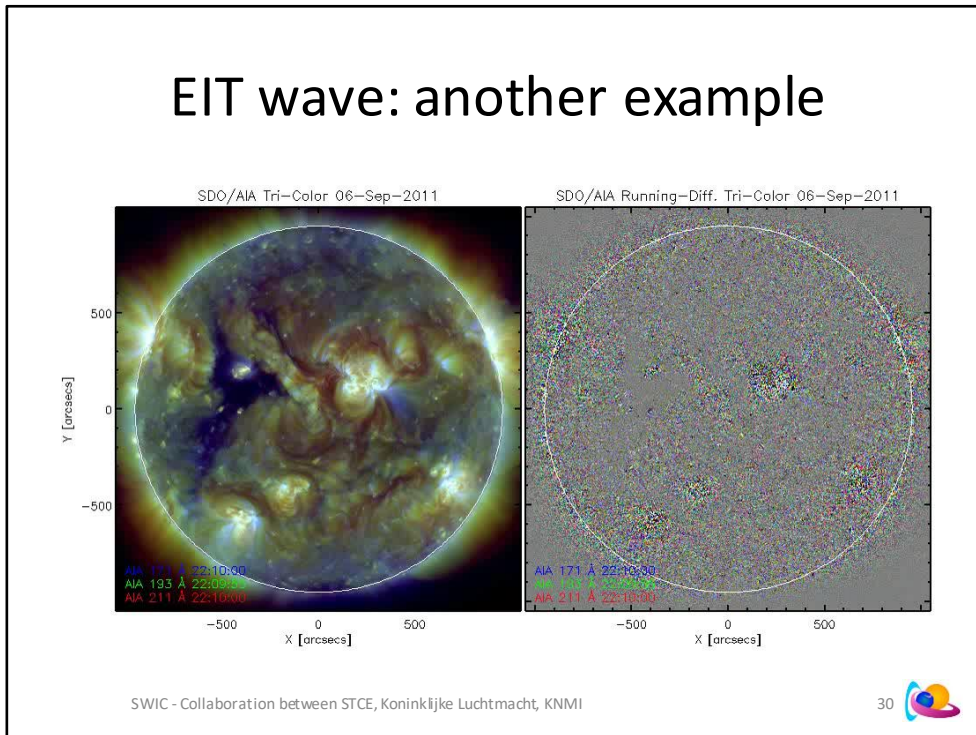
November 24, 2009: Sometimes you really can believe your eyes. That's what NASA's STEREO (Solar Terrestrial Relations Observatory) spacecraft are telling researchers about a controversial phenomenon on the sun known as the "solar tsunami."

Years ago, when solar physicists first witnessed a towering wave of hot plasma racing along the sun's surface, they doubted their senses. The scale of the thing was staggering. It rose up higher than Earth itself and rippled out from a central point in a circular pattern millions of kilometers in circumference. Skeptical observers suggested it might be a shadow of some kind—a trick of the eye—but surely not a real wave.

"Now we know," says Joe Gurman of the Solar Physics Lab at the Goddard Space Flight Center. "Solar tsunamis are real."

The twin STEREO spacecraft confirmed their reality in February 2009 when sunspot 11012 unexpectedly erupted. The blast hurled a billion-ton cloud of gas (a "CME") into space and sent a tsunami racing along the sun's surface. STEREO recorded the wave from two positions separated by 90 degrees,

# EIT wave: another example



Shen et al. (2014): A Chain of Winking (Oscillating) Filaments Triggered by an Invisible Extreme-ultraviolet Wave  
<http://adsabs.harvard.edu/abs/2014ApJ...786..151S>

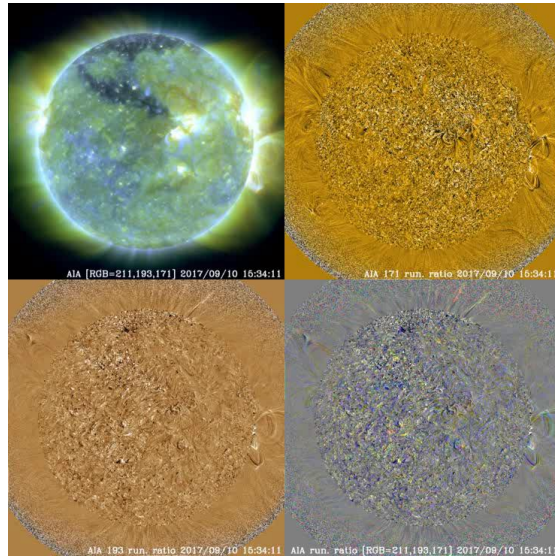
In this paper, we present the observations of a chain of winking filaments and a subsequent jet that are observed right after the X2.1 flare in AR11283. The event also produced an extreme-ultraviolet (EUV) wave that has two components: an upward dome-like wave ( $850 \text{ km s}^{-1}$ ) and a lateral surface wave ( $554 \text{ km s}^{-1}$ ) that was very weak (or invisible) in imaging observations. By analyzing the temporal and spatial relationships between the oscillating filaments and the EUV waves, we propose that all the winking filaments and the jet were triggered by the weak (or invisible) lateral surface EUV wave. The oscillation of the filaments last for two or three cycles, and their periods, Doppler velocity amplitudes, and damping times are 11-22 minutes, 6-14  $\text{km s}^{-1}$ , and 25-60 minutes, respectively. We further estimate the radial component magnetic field and the maximum kinetic energy of the filaments, and they are 5-10 G and  $\sim 10^{19}$  J, respectively. The estimated maximum kinetic energy is comparable to the minimum energy of ordinary EUV waves, suggesting that EUV waves can efficiently launch filament oscillations on their path. Based on our analysis results, we conclude that the EUV wave is a good agent for triggering and connecting successive but separated solar activities in the solar atmosphere, and it is also important for producing solar sympathetic eruptions.

In this paper, we present an interesting observational study of a chain of winking filaments that was in association with a GOES X2.1 flare in the NOAA active region AR11283 (N13W18) on 2011 September 6. The flare was produced with a remarkable EUV wave propagating mainly in the northwest direction, which not only triggered the oscillation of three filaments in the northwest of AR11283, but also launched the oscillation of a long filament and the occurrence of a small jet in the eastern hemisphere, where the wave signature is very weak or even invisible.

According to previous studies, winking filaments are often triggered by either chromospheric Moreton waves or coronal EUV waves (Eto et al. 2002; Okamoto et al. 2004). In the present case, we do not detect any significant signature of Moreton waves in H $\alpha$  observations. On the other hand, as the EUV wave mainly propagated in the northwest of AR11283, it is hard to understand the trigger mechanisms of the F1's oscillation and the occurrence of the small coronal jet.

# Global EIT wave from X8 flare

## 10 September 2017



SWIC - Collaboration between STCE, Koninklijke Luchtmacht, KNMI

[© Liu et al., 2018](#)

31



Liu et al. (2018): A Truly Global Extreme Ultraviolet Wave from the SOL2017-09-10 X8.2+ Solar Flare-Coronal Mass Ejection

<http://adsabs.harvard.edu/abs/2018ApJ...864L..24L>

**ABSTRACT** - We report Solar Dynamics Observatory/Atmospheric Imaging Assembly (SDO/AIA) observations of an extraordinary global extreme ultraviolet (EUV) wave triggered by the X8.2+ flare-CME eruption on 2017 September 10. This was one of the best EUV waves ever observed with modern instruments, yet it was likely the last one of such magnitudes of Solar Cycle 24 as the Sun heads toward the minimum. Its remarkable characteristics include the following. (1) The wave was observed, for the first time, to traverse the full-Sun corona over the entire visible solar disk and off-limb circumference, manifesting a truly global nature, owing to its exceptionally large amplitude, e.g., with EUV enhancements by up to 300% at 1.1 Rs from the eruption. (2) This leads to strong transmissions (in addition to commonly observed reflections) in and out of both polar coronal holes (CHs), which are usually devoid of EUV waves. It has elevated wave speeds  $>2000$  km/s within the CHs, consistent with the expected higher fast-mode magnetosonic wave speeds. The CHs essentially serve as new “radiation centers” for the waves being refracted out of them, which then travel toward the equator and collide head-on, causing additional EUV enhancements. (3) The wave produces significant compressional heating to local plasma upon its impact, indicated by long-lasting EUV intensity changes and differential emission measure increases at higher temperatures (e.g.,  $\log T=6.2$ ) accompanied by decreases at lower temperatures (e.g.,  $\log T=6.0$ ). These characteristics signify the potential of such EUV waves for novel magnetic and thermal diagnostics of the solar corona on global scales.

# Coronal dimming (Transient CHs)



SWIC - Collaboration between STCE, Koninklijke Luchtmacht, KNMI



<http://www.stce.be/news/362/welcome.html>

Mason et al. (2016): Relationship of EUV Irradiance Coronal Dimming Slope and Depth to Coronal Mass Ejection Speed and Mass

<http://adsabs.harvard.edu/abs/2016ApJ...830...20M>

Large regions of temporary dimming or darkening of preexisting solar coronal emission often accompany coronal mass ejections (CMEs) and may trace field lines opened during the CME. The plasma of the solar corona responds in a number of ways to an eruptive event. Mason et al. (2014) provide details about the physics behind coronal dimming and the observational effects to be considered during analysis. Therein, the case is made for two hypotheses: that the slope of deconvolved, extreme-ultraviolet (EUV) dimming irradiance light curves should be directly proportional to CME speed, and similarly, that dimming depth should scale with CME mass. Dimming regions can be extensive, representing at least part of the “base” of a CME and the mass and magnetic flux transported outward by it.

Extensive surveys of EUV images containing coronal dimming events and their relation to CMEs have been performed by Reinard & Biesecker (2008, 2009). For their sample of 100 dimming events, Reinard & Biesecker (2008) found mean lifetimes of 8 hr, with most disappearing within a day. Reinard & Biesecker (2009) studied CMEs with and without associated dimmings, finding that those with dimmings tended to be faster and more energetic. Bewsher et al. (2008) found a 55% association rate of dimming events with CMEs and conversely that 84% of CME events exhibited dimming.

The timescale for dimming development is typically several minutes to an hour. This is much faster than the radiative cooling time, which implies that the cause of the decreased emission is more dependent on density decrease than temperature change (Hudson et al. 1996). Studies have demonstrated that dimming regions can be a good indicator of the apparent base of the white light CME (Thompson et al. 2000; Harrison et al. 2003; Zhukov & Auchère 2004). Thus, dimmings are usually interpreted as mass depletions due to the loss or rapid expansion of the overlying corona (Hudson et al. 1998; Harrison & Lyons 2000; Zhukov & Auchère 2004).

# Coronal dimming (Transient CHs)



SWIC - Collaboration between STCE, Koninklijke Luchtmacht, KNMI

33 

<http://www.stce.be/news/362/welcome.html>

Cheng et al. (2016): The Nature of CME-flare-Associated Coronal Dimming

<http://adsabs.harvard.edu/abs/2016ApJ...825...37C>

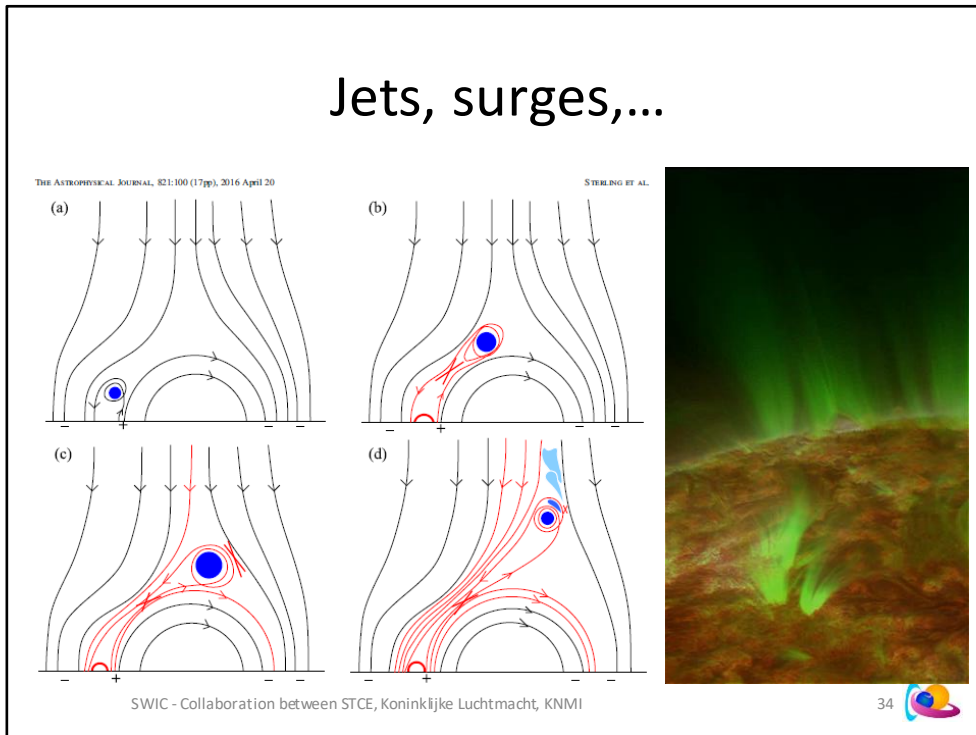
During the eruptive events, transient coronal holes, or coronal dimmings, are often observed (Thompson et al. 2000; Harrison et al. 2003; Zhukov & Auchère 2004). Coronal dimming was first observed in Skylab data and characterized as transient coronal holes (Rust & Hildner 1976; Rust 1983). Subsequently, similar observations have been analyzed to study the relationship of dimming with CMEs, flares, and other associated phenomena ... By these series of studies, dimmings are usually interpreted as mass depletion due to the loss or rapid expansion of the overlying corona (Hudson et al. 1998; Harrison & Lyons 2000; Zhukov & Auchère 2004). This interpretation is supported by imaging observations of simultaneous and co-spatial dimming in several coronal lines (e.g., Zarro et al. 1999; Sterling et al. 2000), as well as spectroscopic observations (Harra & Sterling 2001; Tian et al. 2012). Although CMEs are also observed to occur without dimming, Reinard & Biesecker (2009) found that non-dimming CMEs all have speeds of less than  $800 \text{ km s}^{-1}$ , suggesting a more intimate connection between fast CMEs and dimming properties. Krista & Reinard (2013) found further correlations between the magnitudes of dimmings and flares, and the CME mass by studying variations between recurring eruptions and dimmings.

Coronal dimming can be produced by various processes, although the main contributor is mass depletion. As summarized by Mason et al. (2014), several different mechanisms have been proposed to explain coronal dimming.

- (1) Mass-loss dimming: the mass-loss dimming is produced by the ejection of emitting plasma (Harrison & Lyons 2000; Harra & Sterling 2001), which causes darkening of the areas in and near the erupting active region.
- (2) Thermal Dimming: ... this is due to the heating of coronal plasmas to higher temperatures, so that heated areas appear dark in extreme ultraviolet...
- (3) Obscuration Dimming: ... (4) Wave Dimming: ... (5) Doppler Dimming: ...

Among these mechanisms the mass-loss dimming is considered to be the main process of coronal dimming, and this scenario is supported by many recent studies (Sterling & Hudson 1997; Reinard & Biesecker 2008, 2009; Aschwanden et al. 2009).

# Jets, surges,...



Sterling et al. (2016): Minifilament Eruptions that Drive Coronal Jets in a Solar Active Region

<http://adsabs.harvard.edu/abs/2016ApJ...821..100S>

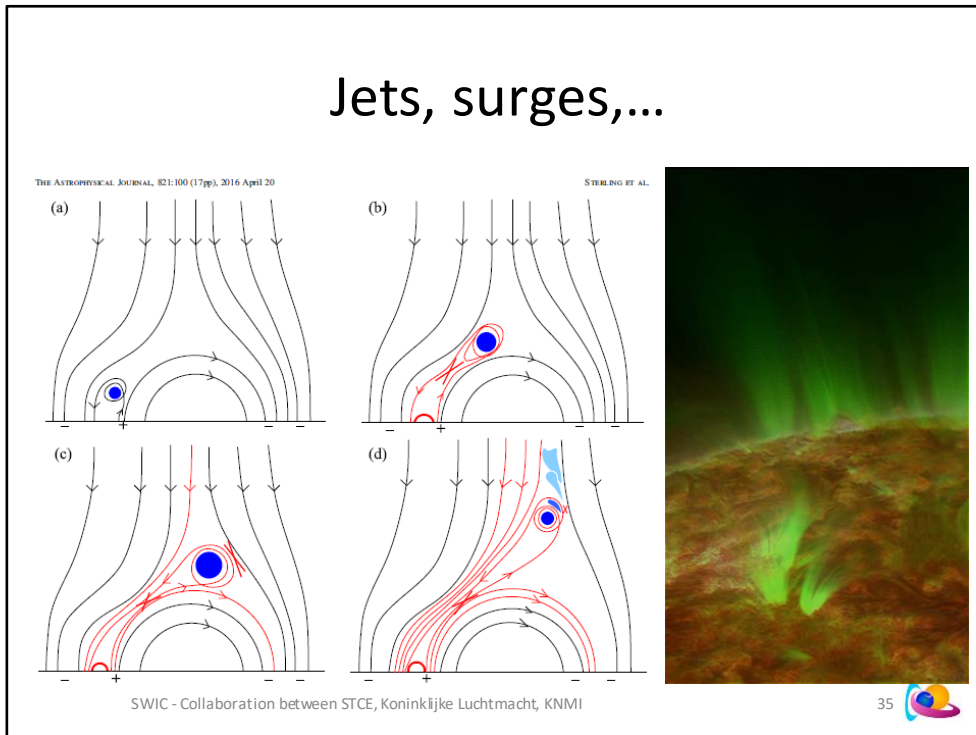
Figure 1. Schematic showing in 2D the formation process of jets, as suggested by Sterling et al. (2015). The bold horizontal black line is the photosphere, curved black lines represent magnetic field that has not undergone magnetic reconnection, curved red lines show field that has undergone reconnection, and red crosses show locations where reconnection is taking place. (a) A compact bipole carrying a mini-filament (blue) resides next to a larger-scale bipole, in a background ambient open coronal field. (b) Due to an unspecified process, the mini-filament-carrying field erupts outward. Its field orientation is such that magnetic reconnection with the surrounding field external to the erupting bipole does not occur, as long as the erupting bipole is on the near side (i.e., the side from which the eruption originated) of the apex of the larger bipole. Reconnection does, however, occur among the field internal to the erupting bipole itself ("internal reconnection"), just as in typical larger scale filament eruptions that result in typical solar flares and CMEs. In the large-scale flares the internal reconnection results in a "normal" solar flare, while in this case the internal reconnection beneath the erupting mini-filament-carrying field results in the jet bright point (JBP) (bold red semicircle). (c) When the erupting field reaches the far end of the larger bipole's apex, its orientation is favorable for reconnection with the ambient field ("external reconnection"), resulting in a new open field line, and new field loops over the large bipole. A hot coronal jet occurs on the newly reconnected open field lines. (d) If the external reconnection of the ejected mini-filament-carrying field envelope progresses far enough into that field's core, then the mini-filament material (blue and light blue), which is in the core, will escape along new open field lines, resulting in a cool component of the coronal jet.

Example from "Leaving on a jet": <http://www.stce.be/news/293/welcome.html> (30 January 2015): What seems to have happened in this case is that a small filament became unstable and, while erupting, got in contact with the "leg" of a low-lying coronal loop. There, the reconnection took place and the material was ejected along the open field lines into space. The point of reconnection and the jet itself seem to be somewhat off-set, hence the name lambda jet (the more symmetrical case is called "Eiffel tower jet"). With some imagination, the greek letter can indeed be seen in the loops and jet. Some further analysis may be required to have a final answer (line-of-sight effects,...). The imagery underneath is a composition of EUV images from AIA 304, 171 and 094 filters.

SWPC glossary: <https://www.swpc.noaa.gov/content/space-weather-glossary>

**Surge:** A jet of material from active regions that reaches coronal heights and then either fades or returns into the chromosphere along the trajectory of ascent. Surges typically last 10 to 20 minutes and tend to recur at a rate of approximately 1 per hour. Surges are linear and collimated in form, as if highly directed by magnetic fields.

# Jets, surges,...



Liu et al. (2016): On the Observation and Simulation of Solar Coronal Twin Jets  
<http://adsabs.harvard.edu/abs/2016ApJ...817..126L>

Decades have passed since the first observations on solar jets (named as surges in Newton 1934), which are thought to play an important role in solar wind acceleration and coronal heating (e.g., Tsiropoula & Tziotziou 2004; Tian et al. 2014). A generalized definition of solar jets includes the terms of H $\alpha$  surges (e.g., Canfield et al. 1996; Jibben & Canfield 2004), UV/EUV/X-ray jets (e.g., Schmieder et al. 1988; Patsourakos et al. 2008; Tian et al. 2014; Liu et al. 2015) and spicules (e.g., De Pontieu et al. 2007; Shibata et al. 2007), among which their different names come from different dominant temperatures and sizes. As shown in many previous works (Shibata et al. 1996, as a review), different jets obtain quite different physical characteristics such as length and axial speed, which range from a few to hundreds of megameters and tens to thousands of kilometers per second, respectively. Despite the different properties of different jets, it is believed that they are triggered by a similar mechanism (except type I spicules, De Pontieu et al. 2007). Reconnections between newly emerging twisted loops with pre-existing ambient open fields (e.g., Moreno-Insertis et al. 2008) lead to the heating and initiation of bulks of plasma, which are observed as materials of a jet (Savcheva et al. 2007). Twists transferred from the emerging flux then lead to the rotational motion of jets, as observed and studied widely through observation and simulation (e.g., Xu et al. 1984; Shibata & Uchida 1985; Canfield et al. 1996; Shimojo et al. 2007; Pariat et al. 2010; Liu 2009; Fang et al. 2014; Liu et al. 2014).

Example from "Leaving on a jet": <http://www.stce.be/news/293/welcome.html>

Also:

Cheung et al. (2014): Flux Emergence (Theory)  
<http://adsabs.harvard.edu/abs/2014LRSP...11....3C>  
 Chapter 4 and Fig. 53.

SWPC glossary: <https://www.swpc.noaa.gov/content/space-weather-glossary>

:Issued: 2014 Apr 17 1325 UTC  
:Product: documentation at <http://www.sidc.be/product/sft/ot>  
#-----#  
# DAILY BULLETIN ON SOLAR AND GEOMAGNETIC ACTIVITY from the SIDC #  
#-----#  
SIDCURSIGRAM 40417  
SIDCSOLAR BULLETIN 17 Apr 2014, 1304UT



SIDC FORECAST (valid from 1230UT, 17 Apr 2014 until 19 Apr 2014)  
SOLAR FLARES : Active (M-class flares expected, probability >=50%)  
GEOMAGNETISM : Quiet (A<20 and K<4)  
SOLAR PROTONS : Quiet

PREDICTIONS FOR 17 Apr 2014 10CM FLUX: 180 / AP: 013  
PREDICTIONS FOR 18 Apr 2014 10CM FLUX: 184 / AP: 007  
PREDICTIONS FOR 19 Apr 2014 10CM FLUX: 188 / AP: 005

COMMENT: Eleven sunspot groups were reported by NOAA today. NOAA ARs 2035, 2036, and 2037 (Catania numbers 24, 25, and 26 respectively) maintain the beta-gamma configuration of the photospheric magnetic field. The strongest flare of the past 24 hours was the M1.0 flare peaking at 19:59 UT yesterday in the NOAA AR 2035 (Catania number 24). The flare was associated with an EIT wave and a weak coronal dimming, but the associated CME was narrow and is not expected to arrive at the Earth.

We expect further flaring activity on the C-level, especially in the NOAA ARs 2035 and 2037 (Catania numbers 24 and 26 respectively) as well as in the NOAA AR 2042 (no Catania number yet) that yesterday appeared from behind the east solar limb, with a good chance for an M-class event.

Since yesterday evening the Earth is situated inside a solar wind structure with an elevated interplanetary magnetic field magnitude (occasionally up to 10 nT). It may be a weak ICME or the compression region on the flank of an ICME that missed the Earth. The solar origin of this structure is not clear. The north-south magnetic field component Bz was not strong, so no significant geomagnetic disturbance resulted (Kindex stayed below 4). Currently the solar wind speed is around 380 km/s and the IMF magnitude is around 8 nT.

We expect quiet to unsettled (K index up to 3) geomagnetic conditions, with active geomagnetic conditions (K=4) possible, but unlikely.

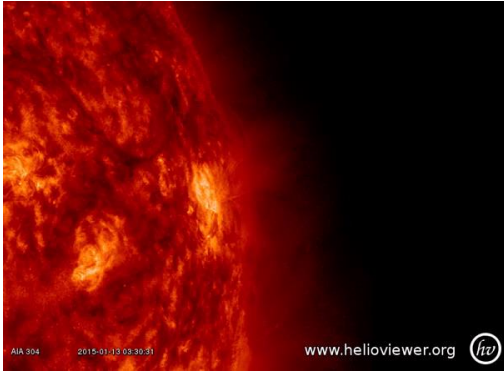
TODAY'S ESTIMATED ISN : 145, BASED ON 17 STATIONS.  
99999

SOLAR INDICES FOR 16 Apr 2014  
WOLF NUMBER CATANIA : ///  
10CM SOLAR FLUX : 184  
AK CHAMBON LA FORET : 012  
AK WINGST : 004  
ESTIMATED AP : 004  
ESTIMATED ISN : 139, BASED ON 29 STATIONS.

*Flare features*

NOTICEABLE EVENTS SUMMARY  
DAY BEGIN MAX END LOC XRAY OP 10CM Catania/NOAA RADIO\_BURST\_TYPES  
16 1954 1959 2004 S14E09 M1.0 1N 24/2035 I/2  
END

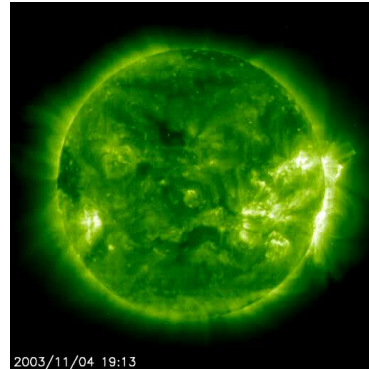
## Exercise: Solar flare feature recognition



- Which of the following solar flare features can be seen in this EUV clip of the 13 January 2015 flare?
  - Flash
  - Post-eruption coronal loops
  - Jets
  - Cusp
  - Coronal dimming
  - EIT wave

# Solar flares - Contents

- Characteristics
  - Definition
  - Standard model
  - Flare triggers
  - Flare features
- **Classification**
  - H-alpha
  - X-ray
    - Intensity, duration, frequency
  - **Types of solar flares**
  - **Radio bursts**
- Flare predictions
  - McIntosh
  - Hale
  - **Filament eruptions**

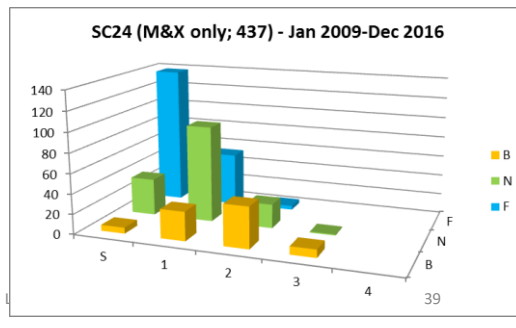


SWIC - Collaboration between STCE, Koninklijke Luchtmacht, KNMI

# Solar flare classification: H-alpha

- H-alpha
  - Visual!
  - Importance
    - Area @ max. brightness
    - S, 1, 2, 3, 4
  - Brightness
    - Faint, Normal, Brilliant
  - Optical class
    - E.g. SF, 3B,...
  - Limited correlation with geophysical effects

| Importance | $A_c$ (MH)            | $A_c$ ( $^{\circ}2$ )  |
|------------|-----------------------|------------------------|
| S          | $10 \leq A_c < 100$   | $0,2 \leq A_c < 2,1$   |
| 1          | $100 \leq A_c < 250$  | $2,1 \leq A_c < 5,2$   |
| 2          | $250 \leq A_c < 600$  | $5,2 \leq A_c < 12,4$  |
| 3          | $600 \leq A_c < 1200$ | $12,4 \leq A_c < 24,7$ |
| 4          | $1200 \leq A_c$       | $24,7 \leq A_c$        |



H-alpha flare classification: Australian SWS: <http://www.sws.bom.gov.au/Educational/2/4/2>  
 H-alpha observing: <http://users.telenet.be/j.janssens/Halpha/Halfaeng.html#Flares>

From SWPC's « The Weekly » User guide  
 ([https://www.swpc.noaa.gov/sites/default/files/images/u2/Usr\\_guide.pdf](https://www.swpc.noaa.gov/sites/default/files/images/u2/Usr_guide.pdf); page 4)

Optical Information (Op): The optical classification and location of an associated flare, observed in H $\alpha$ . It contains an importance and a Brightness parameter:

\* Importance is the corrected area of the flare in heliospheric square degrees at **maximum brightness**, observed in the H $\alpha$  line (656.3 nm).

S - Subflare (area  $\leq 2.0$  deg. $^2$ )

1 - Importance 1 ( $2.1 \leq \text{area} \leq 5.1$  deg.  $^2$ )

2 - Importance 2 ( $5.2 \leq \text{area} \leq 12.4$  deg.  $^2$ )

3 - Importance 3 ( $12.5 \leq \text{area} \leq 24.7$  deg.  $^2$ )

4 - Importance 4 (area  $\geq 24.8$  deg.  $^2$ )

\* Brightness is the relative maximum brightness of flare in H $\alpha$ .

F – faint ; N – normal ; B – brilliant

\* Location ( $^{\circ}$ Lat.  $^{\circ}$ CMD) gives the spherical, heliographic coordinates of the solar flare in H $\alpha$  as a distance in degrees from the solar equator (heliographic latitude), and distance in degrees from a line extending from the north solar rotational pole to the south solar rotational pole through the center of the solar disk as viewed from Earth (central meridian). The field is blank for x-ray events with no optical correlation (no optical flare observed or no optical patrol at the time) and for flares that occasionally occur in unassigned regions).

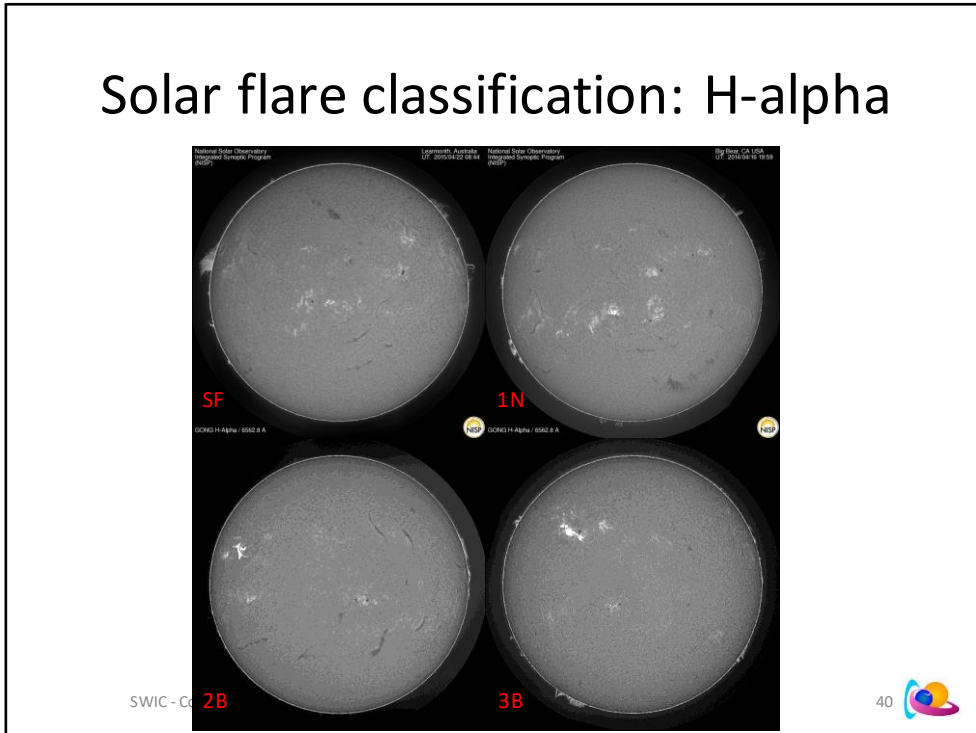
This classification is still widely used, e.g. in the daily SWPC (event) reports, The Weekly, the SIDC's Ursigrams and weekly bulletins,...

A detailed analysis of H-alpha flare properties is by Temmer et al. (2001)

**Statistical analysis of solar H flares**

<https://www.aanda.org/articles/aa/pdf/2001/33/aa1413.pdf>

# Solar flare classification: H-alpha



| DAY | BEGIN       | MAX   | END  | LOC  | XRAY   | OP   | 10CM | Catania/NOAA | RADIO_BURST_TYPES |               |
|-----|-------------|-------|------|------|--------|------|------|--------------|-------------------|---------------|
| SF: | 22 Apr 2015 | -0830 | 0844 | 0858 | S09E05 | M1.1 | SF   |              |                   |               |
| 1N: | 16 Apr 2014 | -1954 | 1959 | 2004 | S14E09 | M1.0 | 1N   | 24/2035      | II/2              |               |
| 2B: | 02 Apr 2014 | -1318 | 1405 | 1428 | N14E53 | M6.5 | 2B   | 3700         | 09/2027           | II/1IV/2      |
| 3B: | 07 Mar 2012 | -0002 | 0024 | 0040 | N17E27 | X5.4 | 3B   | 7200         |                   | IV/1,II/2,V/2 |

Data are from the SIDC / Daily Ursigrams (<http://www.sidc.be/archive> )  
 Images are from GONG/NSO H-alpha Network (<ftp://gong2.nso.edu/HA/hag/> )

Cont's (H-alpha classification)

The size (or importance) of a flare can also be measured in MH. From the wikipedia site:  
[https://en.wikipedia.org/wiki/Solar\\_flare#H-alpha\\_classification](https://en.wikipedia.org/wiki/Solar_flare#H-alpha_classification)

## H-alpha classification

An earlier flare classification is based on [H \$\alpha\$](#)  spectral observations. The scheme uses both the intensity and emitting surface. The classification in intensity is qualitative, referring to the flares as: (f)aint, (n)ormal or (b)rilliant. The emitting surface is measured in terms of *millionths* of the hemisphere and is described below. (The total hemisphere area  $A_H = 15.5 \times 10^{12}$  km<sup>2</sup>.)

Classification Corrected Area [millionths of hemisphere]

S < 100

1 100 – 250

2 250 – 600

3 600 – 1200

4 > 1200

A flare then is classified taking S or a number that represents its size and a letter that represents its peak intensity, v.g.: **Sn** is a *normal subflare*.<sup>[10]</sup>

[Tandberg-Hanssen, Finar](#); *Emslie, A. Gordon (1988). Cambridge University Press, ed. "The physics of solar flares".*

# Solar flare classification: H-alpha

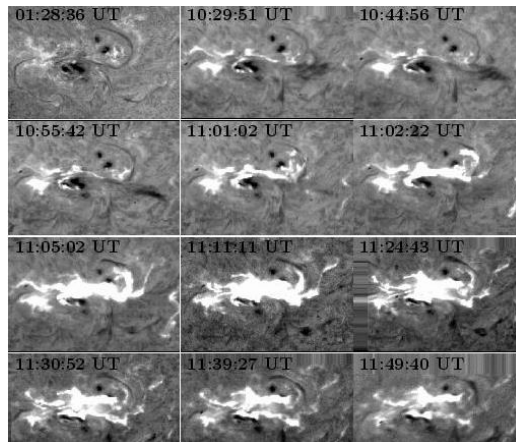


Fig 1: Evolution of historical **4B/X17.2** class solar flare in H-alpha on 28 October 2003 from super-active region NOAA 10486. Observed from ARIES, Nainital (<http://www.aries.res.in/research/solar/>)



Cont'd (H-alpha classification)

From Townsend et al. (1982): A source book of the solar-geophysical environment  
<http://www.dtic.mil/dtic/tr/fulltext/u2/a138682.pdf> (pp. 105 and 107):

One optical flare intensity or "brilliance" classification is based on the Doppler shift of the hydrogen-alpha line. This Doppler shift is a measure of emitting gas particle velocity and is used by the observer in making his subjective estimate of flare intensity. Using this system we classify flares as follows:

**Intensity**

- Faint (F)
- Normal (N)
- Brilliant (B)

**Doppler Shift of Flare Emission**

- Seen over a line width of 0.8 Angstrom or greater.
- Seen over a line width of 1.2 Angstrom or greater.
- Seen at + and/or - 1.0 Angstrom off line center.

The SOON (Solar Observing Optical Network) telescopes are capable of directly measuring the intensity of optical flare emissions. The SOON observatories report as their flare brightness the measured flare intensity. However, the observed intensity is strongly dependent on the seeing conditions, and only a slight amount of atmospheric pollution can drastically alter the measured intensity.

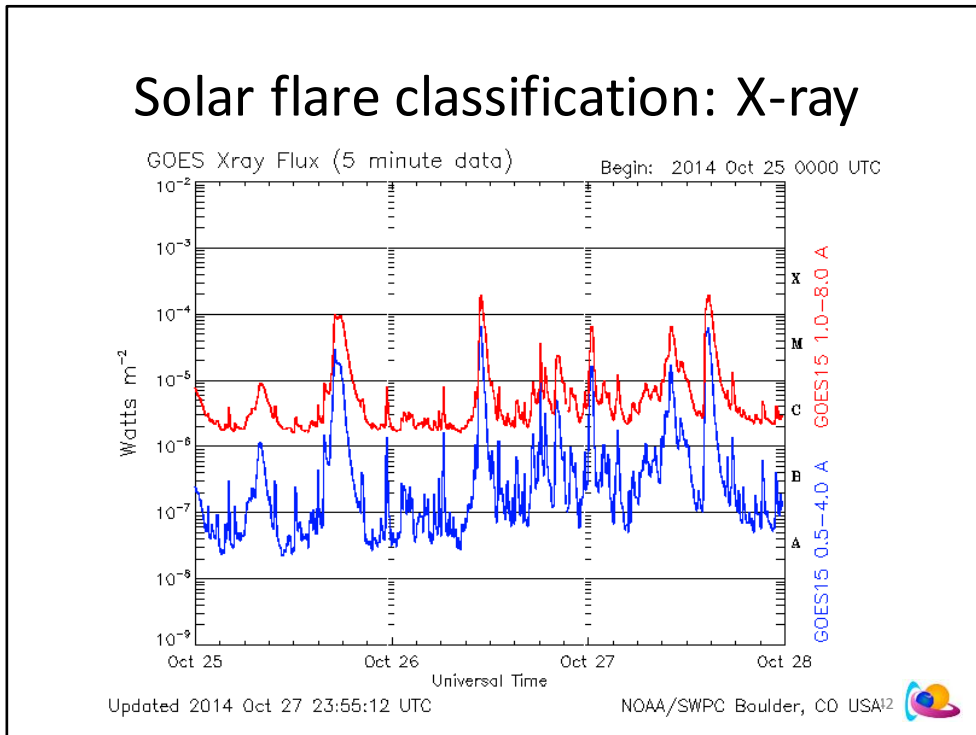
History of H-alpha observations:

<http://adsabs.harvard.edu/abs/1966SSRv...5..388S>

Optical Observations of Solar Flares, [Švestka, Zdeněk](#), 1966

The H-alpha flare classification system was approved by Commission 10 of the IAU in 1966 (Zirin, 1988: Astrophysics of the Sun, pp. 347).

# Solar flare classification: X-ray



Source: <http://iopscience.iop.org/article/10.1086/304521/fulltext/36016.text.html>

From SWPC's « The Weekly » User guide

([https://www.swpc.noaa.gov/sites/default/files/images/u2/Usr\\_guide.pdf](https://www.swpc.noaa.gov/sites/default/files/images/u2/Usr_guide.pdf); page 2)

The letter classification of solar flares used in these definitions (Table 1) was initiated on 01 January 1969. This classification ranks solar activity by its peak x-ray intensity in the 0.1-0.8 nm band as measured by the Geostationary Operational Environmental Satellites (GOES). This x-ray classification offers at least two distinct advantages compared with the standard optical classifications: it gives a better measure of the geophysical significance of a solar event, and it provides an objective means of classifying geophysically significant activity regardless of its location on the solar disk.

Table 1. The SWPC x-ray flare classification

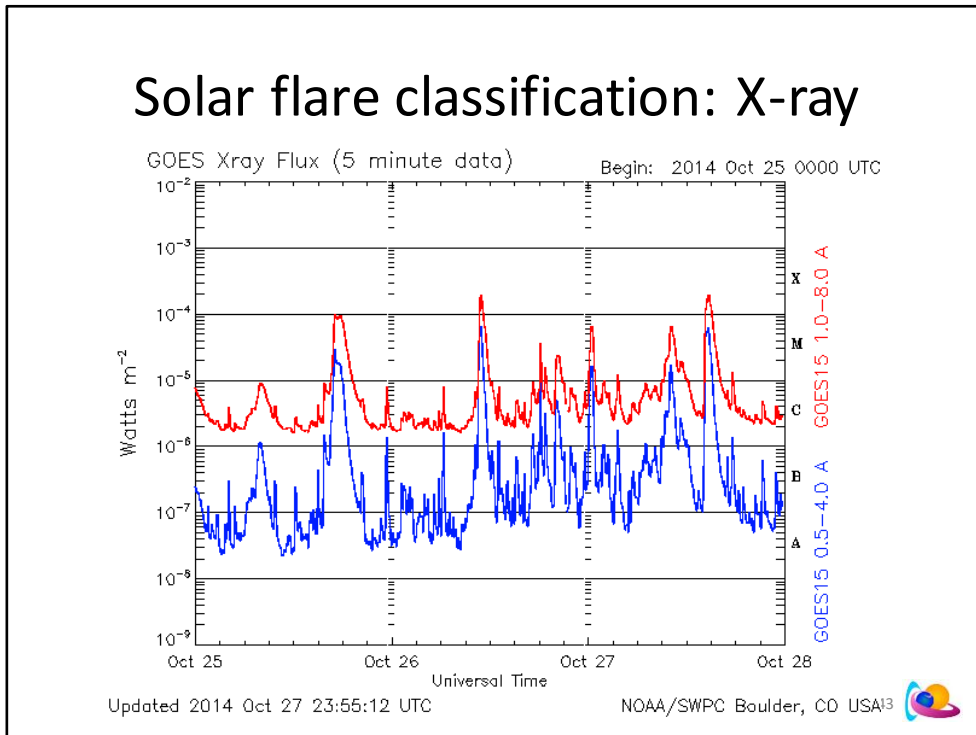
Peak Flux Range (0.1-0.8 nm)

| Classification | mks system ( $W m^{-2}$ )     |                               | cgs system ( $erg cm^{-2}s^{-1}$ ) |
|----------------|-------------------------------|-------------------------------|------------------------------------|
| A              | $\Phi < 10^{-7}$              |                               | $\Phi < 10^{-4}$                   |
| B              | $10^{-7} \leq \Phi < 10^{-6}$ | $10^{-4} \leq \Phi < 10^{-3}$ |                                    |
| C              | $10^{-6} \leq \Phi < 10^{-5}$ | $10^{-3} \leq \Phi < 10^{-2}$ |                                    |
| M              | $10^{-5} \leq \Phi < 10^{-4}$ | $10^{-2} \leq \Phi < 10^{-1}$ |                                    |
| X              | $10^{-4} \leq \Phi$           |                               | $10^{-1} \leq \Phi$                |

The letter designates the order of magnitude of the peak value and the number following the letter is the multiplicative factor. A C3.2 event for example, indicates an x-ray burst with  $3.2 \times 10^{-6} W m^{-2}$  peak flux. Solar flare forecasts are usually issued only in terms of the broad C, M, and X categories. Since x-ray bursts are observed as a full-Sun value, bursts below the x-ray background level are not discernible. The background drops to class A level during solar minimum; only bursts that exceed B1.0 are classified as x-ray events. During solar maximum the background is often at the class M level, therefore class A, B, or C x-ray bursts cannot be discerned. Data are measured by the NOAA GOES satellites, monitored in real time in Boulder (Grubb 1975).

-----  
The C is often referred to as « Common », M as « Medium (or moderate) », and X as « eXtreme »

# Solar flare classification: X-ray



Source: <http://iopscience.iop.org/article/10.1086/304521/fulltext/36016.text.html>

X-ray Background: The daily average background x-ray flux as measured by the GOES satellite. To better reflect mid day values, the average is the lower of (a) the average of 1-minute data between 0800UT to 1600UT, or (b) the average of the 0000UT to 0800UT and the 1600UT to 2400UT data. The value is given in terms of x-ray class (Donnelly 1982); (Bouwer, et al. 1982). X-ray flux values below the B1 level can be erroneous because of energetic electron contamination of the x-ray sensors. At times of high electron flux at geosynchronous altitude, the x-ray measurements in the low A-class range can be in error by 20-30 percent. Measurements taken during periods of low energetic electron fluxes are much more accurate.

Barbara Poppe—Sentinels of the Sun (2006)—pp. 120

First, in the mid-1960s Don Baker classified solar flares using x-ray data. The Naval Research Laboratory used German-made Vela V2 rockets, captured by the Americans after the war, to measure x-rays from the Sun. Baker, then working at the Space Disturbances Laboratory (SDL), used these data to identify the wavelengths, 1 to 8 angstroms, that best characterized a flare's intensity. He created NOAA's flare classification, labeled "CMX": C, M, and X stand for small, medium, and large flares, with a range within each category from 1 to 9 (e.g., an M1 flare is one step higher than a C9 flare). Having C represent the smallest flare left A and B open should there be observations smaller than those currently known. Similarly, Y and Z could follow X if scientists discovered extremely large flares. A and B flares can now in fact be seen with improved instrumentation and are categorized as such. Y and Z have never been used, despite the orderly progression that should have followed as scientists classified bigger and bigger flares (an X1 to X9 would be followed by Y1 to Y9, then Z1 to Z9). Instead we have now seen an X28 flare. This classification system replaced an older one that reported flux numbers; that is, the flare is an M5 rather than flux  $\Phi = 5 \times 10^{-5}$  watts/m<sup>2</sup>. The improvement was obvious.

# Solar flare classification: X-ray

- Frequency terminology
  - Solar (flaring) activity
  - For a 24 hour period

## Terms Used to Describe Solar Activity

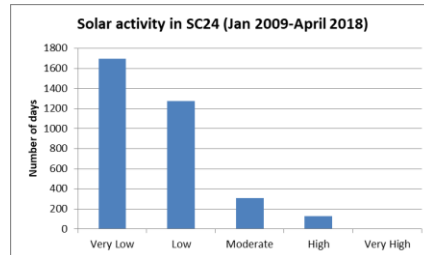
Very Low: x-ray events less than C-class.

Low: C-class x-ray events.

Moderate: isolated (one to four) M-class x-ray events.

High: several (5 or more) M-class x-ray events, or isolated (one to four) M5 or greater x-ray events.

Very High: several (5 or more) M5 or greater x-ray events.



PRF User Guide – August 2012

SWIC - Collaboration between STCE, Koninklijke Luchtmacht, KNMI

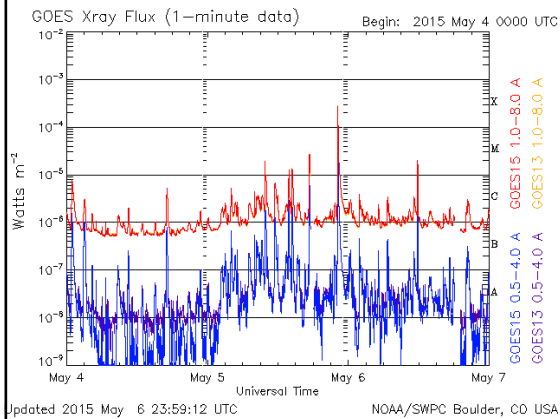


Source: [https://www.swpc.noaa.gov/sites/default/files/images/u2/Usr\\_guide.pdf](https://www.swpc.noaa.gov/sites/default/files/images/u2/Usr_guide.pdf)

Solar Activity in SC24 (Jan 2009 - Dec 2016)

Very Low 1291 Low 1214 Moderate 299 High 118 Very High 0

## Exercise: Solar flare classification in X-ray



- How would you classify solar activity on 4-5-6 May 2015?
  - Low-High-High
  - Low-High-Moderate
  - Low-High-Low
  - Low-Very high-High

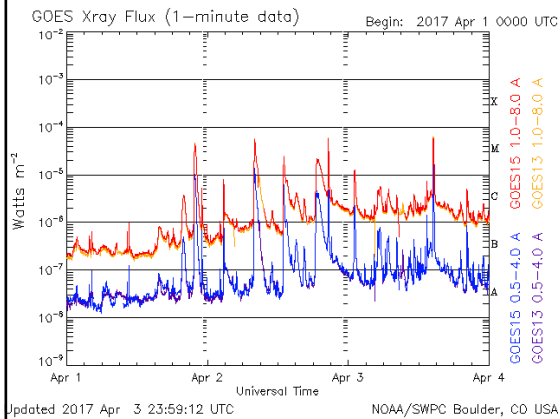
4 May: < M-class

5 May: M1.9, M1.2, M1.3, M2.6, X2.7

6 May: M1.9

SWIC - Collaboration between STCE, Koninklijke Luchtmacht, KNMI

## Exercise: Solar flare classification in X-ray



- How would you classify solar activity on 1-2-3 April 2017?
  - Low-High-High
  - Moderate-High-High
  - High-High-High
  - High-Very high-High

1 April: M4,4

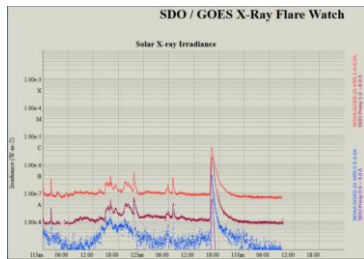
2 April: 4 M-class flares, incl. M5,7 and M5,8

3 April: M5,8

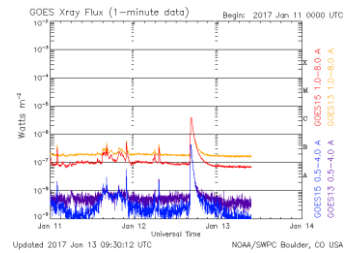
SWIC - Collaboration between STCE, Koninklijke Luchtmacht, KNMI

# Solar flare classification: X-ray

- Back-up for GOES x-ray
  - SDO/EVE
  - PROBA2/LYRA



SWIC - Collaboration between STCE, Koninklijke Luchtmacht, KNMI



# Solar flare classification: X-ray

- NOAA-scales: R-scale

| Scale | Description | Effect | Physical measure              | Average Frequency (1 cycle = 11 years) |
|-------|-------------|--------|-------------------------------|--|
| R 5   | Extreme     |        | X20<br>( $2 \times 10^{-3}$ ) | Less than 1 per cycle                  |
| R 4   | Severe      |        | X10<br>( $10^{-3}$ )          | 8 per cycle<br>(8 days per cycle)      |
| R 3   | Strong      |        | X1<br>( $10^{-4}$ )           | 175 per cycle<br>(140 days per cycle)  |
| R 2   | Moderate    |        | M5<br>( $5 \times 10^{-5}$ )  | 350 per cycle<br>(300 days per cycle)  |
| R 1   | Minor       |        | M1<br>( $10^{-5}$ )           | 2000 per cycle<br>(950 days per cycle) |

SWIC - Collaboration between STCE, Koninklijke Luchtmacht, KNMI



48

From the SWPC webpage:

## NOAA Space Weather Scales

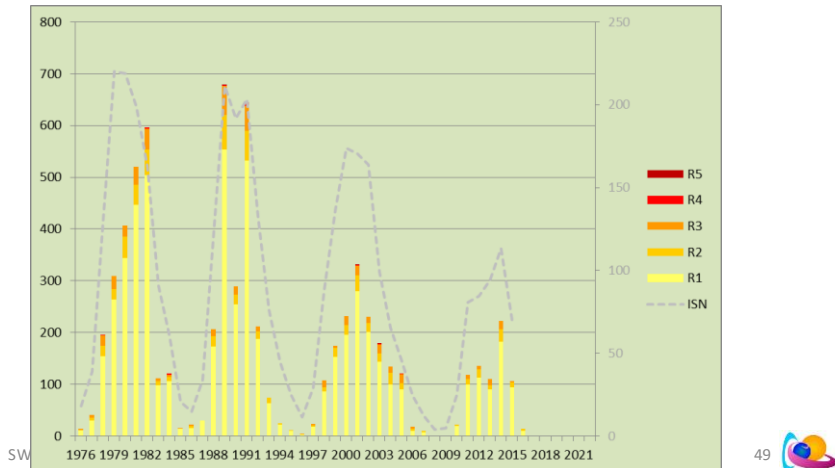
The NOAA Space Weather Scales were introduced as a way to communicate to the general public the current and future space weather conditions and their possible effects on people and systems. Many of the SWPC products describe the space environment, but few have described the effects that can be experienced as the result of environmental disturbances. These scales are useful to users of our products and those who are interested in space weather effects. The scales describe the environmental disturbances for three event types: geomagnetic storms, solar radiation storms, and radio blackouts. The scales have numbered levels, analogous to hurricanes, tornadoes, and earthquakes that convey severity. They list possible effects at each level. They also show how often such events happen, and give a measure of the intensity of the physical causes.

The « R » stands for Radio Blackout. Note it starts only from M1 class flares and higher.

More at <http://www.stce.be/news/366/welcome.html>

# Solar flare classification: X-ray

- NOAA-scales: R-scale



From the SWPC webpage:

## NOAA Space Weather Scales

The NOAA Space Weather Scales were introduced as a way to communicate to the general public the current and future space weather conditions and their possible effects on people and systems. Many of the SWPC products describe the space environment, but few have described the effects that can be experienced as the result of environmental disturbances. These scales are useful to users of our products and those who are interested in space weather effects. The scales describe the environmental disturbances for three event types: geomagnetic storms, solar radiation storms, and radio blackouts. The scales have numbered levels, analogous to hurricanes, tornadoes, and earthquakes that convey severity. They list possible effects at each level. They also show how often such events happen, and give a measure of the intensity of the physical causes.

The « R » stands for Radio Blackout. Note it starts only from M1 class flares and higher.

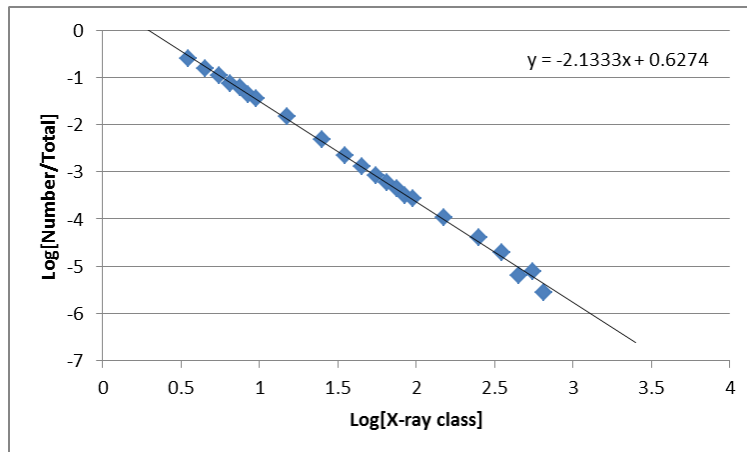
More at <http://www.stce.be/news/366/welcome.html>

Systematic satellite observations of the Sun started in 1976 with GOES. For each year and for each disturbance type, one can count for every level the number of events. E.g. so far for 2016, we've had only 10 R1 events (flares with intensity between M1 and M5) and 4 R2 events (intensity between M5 and X1). Data can be retrieved at resp. NGDC/NOAA, NASA/NOAA and WDC Kyoto, and run through mid-October 2016.

Each graph shows the yearly accumulation of the events, with the yearly International Sunspot Number (SILSO) superposed on it as the gray dashed line. E.g. in the chart above, for 2014 -the year of SC24 maximum-, the number of radio blackouts amounted to 222, consisting of 183 minor (R1), 23 moderate (R2), and 16 strong (R3) events. This is clearly less than during previous solar cycles such as e.g. in 1989 when there were no less than 679 radio blackouts including 59 strong or more intense events! Also, SC24 has not produced any severe or extreme event so far, i.e. X10 or stronger flare.

# Solar flare numbers

- X-ray



The above chart shows for each bin of solar flare intensity (C3-X6) the ratio of the number of flares for that bin vs. the total number of flares (25031 flares; January 1976–May 2016). Both axis are logarithmic in nature. The C2 and lower classes were omitted as these numbers are affected during high solar activity (high x-ray background). The X7 and higher intensities were omitted for not sufficient data.

The linear expression between these two quantities is  $y = 0.6274 - 2.1333x$

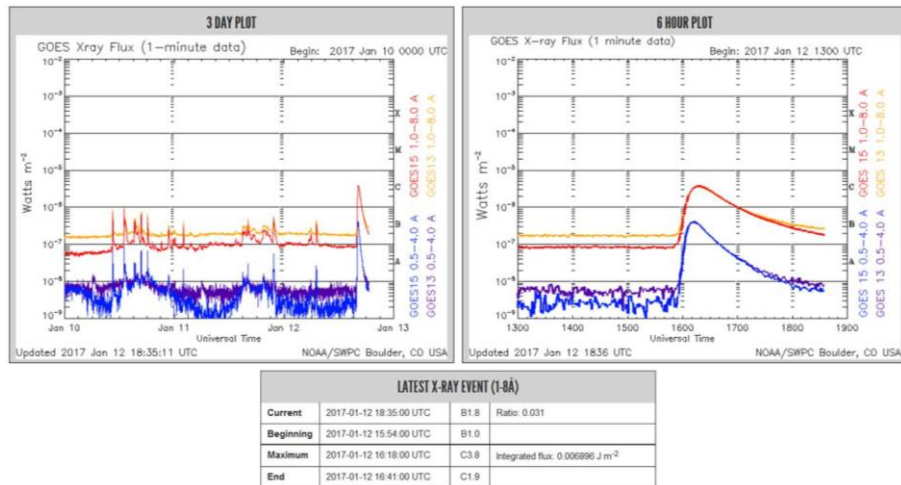
This means that the number of flares  $N$  for a bin can be calculated from a power law equation:  $N = 25031 \cdot \delta \cdot 4.24 \cdot I^{-2.13}$ , with  $\delta$  equalling 1, 10 or 100 for the resp. class C, M or X.

Another rule of thumb: Since 1976, there have been a total of 55000 x-ray flares. About 48000 were C-class flares, 6500 were M-class flares, and 500 were X-class flares.

Or in percentages: For every 100 solar flares, there are 87 C-class flares, 12 M-class flares, and 1 X-class flare.

More on this (for the period 1976-1993) is at the Australian SWS:  
<http://www.sws.bom.gov.au/Educational/2/4/5>

# Solar flare duration



SWIC - Collaboration between STCE, Koninklijke Luchtmacht, KNMI



From SWPC's « The Weekly » User guide

([https://www.swpc.noaa.gov/sites/default/files/images/u2/Usr\\_guide.pdf](https://www.swpc.noaa.gov/sites/default/files/images/u2/Usr_guide.pdf) ; page 15)

The start of an x-ray event is defined as the first minute in a sequence of 4 minutes of steep monotonic increase in 0.1-0.8 nm flux. The time of x-ray maximum is defined as the time tag of the peak 1-minute averaged value x-ray flux. The end time is the time when the flux level decays to a point halfway (1/2 peak) between the maximum flux and the pre-flare background level.

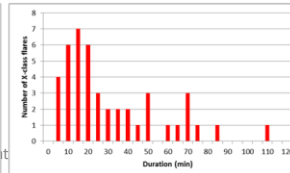
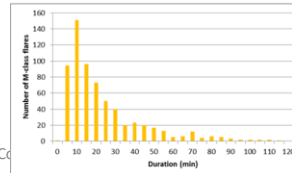
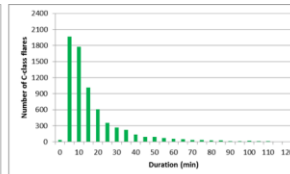
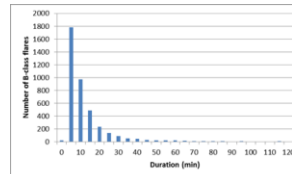
**\*\*Attention!!\*\***

A recent (to be published) paper by Swalwell et al. (2018: <https://arxiv.org/pdf/1805.10246.pdf>) indicates that the duration of flares prior to 1997 was determined from H-alpha observations, and thus much longer than for the post-1997 flares (x-ray):

« ...The effect is particularly clear for X and M-class flares: the mean duration of X-class flares in Cycles 21 and 22 was respectively 2.4 and 2.7 times as long as that for Cycle 23; for M-class flares the mean duration for Cycles 21 and 22 was respectively 1.6 and 1.7 times as long as that for Cycle 23. ... The table headed "GOES Solar X-ray Flares" in those books often has an "Editor's Note" at the bottom which reads "Please note that whenever optical flares are given, the times given are times of the optical flares and not the times of the X-ray flares". Our analysis indicates that this is the case for most, especially large, flares ...»

# Solar flare duration

| Jan 1976 - Dec 2000 |        |        | Jan 2009 - Nov 2015 |        |        |
|---------------------|--------|--------|---------------------|--------|--------|
| Class               | Number | Median | Class               | Number | Median |
| B                   | 8844   | 10     | B                   | 4041   | 10     |
| C                   | 16507  | 12     | C                   | 7015   | 14     |
| M                   | 1331   | 24     | M                   | 659    | 19     |
| X                   | 63     | 30     | X                   | 45     | 24     |
| T                   | 26745  | 12     | T                   | 11760  | 13     |



SWIC-C

52



From SWPC's « The Weekly » User guide

([https://www.swpc.noaa.gov/sites/default/files/images/u2/Usr\\_guide.pdf](https://www.swpc.noaa.gov/sites/default/files/images/u2/Usr_guide.pdf) ; page 15)

The start of an x-ray event is defined as the first minute in a sequence of 4 minutes of steep monotonic increase in 0.1-0.8 nm flux. The time of x-ray maximum is defined as the time tag of the peak 1-minute averaged value x-ray flux. The end time is the time when the flux level decays to a point halfway (1/2 peak) between the maximum flux and the pre-flare background level.

From **Temporal aspects and frequency distributions of solar soft X-ray flares**

Veronig et al. (2002): <https://www.aanda.org/articles/aa/pdf/2002/06/aa1910.pdf>

And from **The duration of solar flares**

<http://www.stce.be/news/332/welcome.html>

**\*\*Attention!!\*\***

A recent (to be published) paper by Swalwell et al. (2018: <https://arxiv.org/pdf/1805.10246.pdf>) indicates that the duration of flares prior to 1997 was determined from H-alpha observations, and thus much longer than for the post-1997 flares (x-ray):

« ...The effect is particularly clear for X and M-class flares: the mean duration of X-class flares in Cycles 21 and 22 was respectively 2.4 and 2.7 times as long as that for Cycle 23; for M-class flares the mean duration for Cycles 21 and 22 was respectively 1.6 and 1.7 times as long as that for Cycle 23. ... The table headed "GOES Solar X-ray Flares" in those books often has an "Editor's Note" at the bottom which reads "Please note that whenever optical flares are given, the times given are times of the optical flares and not the times of the X-ray flares". Our analysis indicates that this is the case for most, especially large, Flares ...»

# Solar flare duration

## Impulsive flare

- M- and X-class only
- Duration
  - Total duration < 10 minutes
- Usually NOT associated with CMEs
- Compact

## Long Duration Event

- All flare classes
- Duration
  - Total duration > 1 hour
  - Decay time > 30 minutes (SWPC)
- Association with CMEs increases with increased duration
  - But exceptions, e.g. NOAA 2192

SWIC - Collaboration between STCE, Koninklijke Luchtmacht, KNMI



From the SWPC glossary at <https://www.swpc.noaa.gov/content/space-weather-glossary#longduration> (operational definition)

long duration event (LDE) With reference to x-ray events, those events that are not impulsive in appearance. The exact time threshold separating impulsive from long-duration events is not well defined, but operationally, any event requiring 30 minutes or more to decay to one-half peak flux is regarded as an LDE. It has been shown that the likelihood of a coronal mass ejection increases with the duration of an x-ray event, and becomes virtually certain for durations of 6 hours or more.

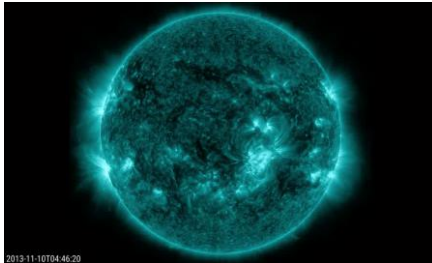
**\*\*Attention!!\*\***

A recent (to be published) paper by Swalwell et al. (2018: <https://arxiv.org/pdf/1805.10246.pdf>) indicates that the duration of flares prior to 1997 was determined from H-alpha observations, and thus much longer than for the post-1997 flares (x-ray):

« ...The effect is particularly clear for X and M-class flares: the mean duration of X-class flares in Cycles 21 and 22 was respectively 2.4 and 2.7 times as long as that for Cycle 23; for M-class flares the mean duration for Cycles 21 and 22 was respectively 1.6 and 1.7 times as long as that for Cycle 23. ... The table headed "GOES Solar X-ray Flares" in those books often has an "Editor's Note" at the bottom which reads "Please note that whenever optical flares are given, the times given are times of the optical flares and not the times of the X-ray flares". Our analysis indicates that this is the case for most, especially large, Flares ...»

# Solar flare duration

## Impulsive flare



2013-11-10T04:46:20

X1 - NOAA 1890 - 10 Nov 2013 (duration: 10 minutes)

## Long Duration Event



2012-07-12T15:15:45

X1 - NOAA 1520 - 12 July 2012 (duration: 113 minutes)

SWIC - Collaboration between STCE, Koninklijke Luchtmacht, KNMI



From the SWPC glossary at <https://www.swpc.noaa.gov/content/space-weather-glossary#longduration> (operational definition)

long duration event (LDE) With reference to x-ray events, those events that are not impulsive in appearance. The exact time threshold separating impulsive from long-duration events is not well defined, but operationally, any event requiring 30 minutes or more to decay to one-half peak flux is regarded as an LDE. It has been shown that the likelihood of a coronal mass ejection increases with the duration of an x-ray event, and becomes virtually certain for durations of 6 hours or more.

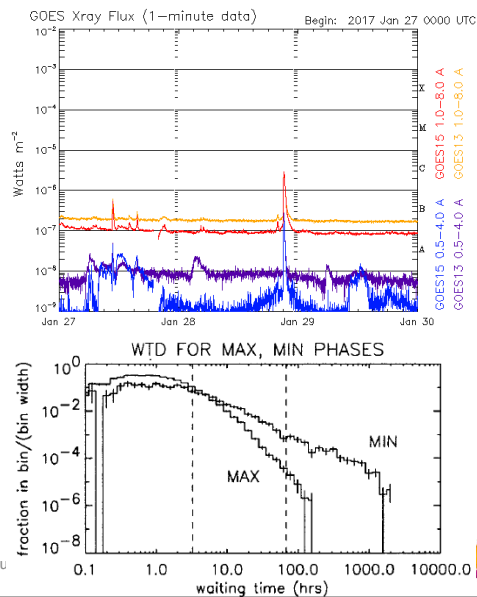
Imagery from STCE: <http://www.stce.be/news/332/welcome.html>

A short and a long duration X1 flaring event. These took place resp. in NOAA 11890 on 10 November 2013 (duration: 10 minutes) and in NOAA 11520 on 12 July 2012 (duration: 113 minutes or nearly 2 hours). The latter was accompanied by a full halo CME (no surprise), but also the 2013 X1 flare was associated with a partial halo CME.

# Solar flare frequency

- Isolated flare
  - Usually specified per class
    - B, C, M
  - From entire Sun
  - NOAA/SWPC:
    - 1-4 per day
  - In practice
    - 1 event in 24 hours
  - Avg. waiting time
    - 6.5 hours ( $\geq$  C1)
    - SCmax: 3 hours
    - SCmin: 3 days

SWIC - Collaboration between STCE, Koninklijke Lu



From SWPC's « The Weekly » User guide ([https://www.swpc.noaa.gov/sites/default/files/images/u2/Usr\\_guide.pdf](https://www.swpc.noaa.gov/sites/default/files/images/u2/Usr_guide.pdf); page 1)

## Terms Used to Describe Solar Activity

Very Low: x-ray events less than C-class.

Low: C-class x-ray events.

Moderate: isolated (one to four) M-class x-ray events.

High: several (5 or more) M-class x-ray events, or isolated (one to four) M5 or greater x-ray events.

Very High: several (5 or more) M5 or greater x-ray events.

Wheatland et al. (2002): Understanding solar flare waiting-time distributions  
[http://www.physics.usyd.edu.au/wheat/papers/pdfs/understanding\\_WTD.pdf](http://www.physics.usyd.edu.au/wheat/papers/pdfs/understanding_WTD.pdf)

Figure 2 shows the waiting-time distributions for the GOES events (greater than C1 class) for the maximum and minimum phases of the cycle as defined by

Figure 1. The upper panel shows the WTD for all years 1975–2001, and reproduces the power-law tail reported by Boffeta *et al.* (1999). The dashed vertical

line indicates the average waiting time, which is about 6.5 hours.

The lower panel shows the WTDs for the maximum and minimum phases of the cycle. The distribution for the maximum phase has a steeper distribution,

because the rate of flaring is higher around solar maximum, and so the average waiting time is less. The average waiting times for the two phases are indicated by the dashed vertical lines. The maximum and minimum

distributions both exhibit approximate power-law tails.

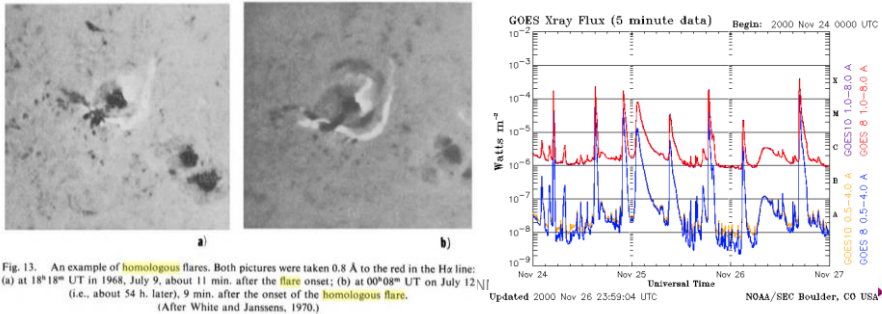
From <http://users.telenet.be/j.janssens/Archives/Archives.html#021109>

The longest stretch without C-class flares was from 3 April till 3 November 2008, that's 214 consecutive days of very low activity.

Since the start of systematic GOES observations, there have been only 9 periods with more than 60 consecutive days with no C-class flares, 6 of those happened during the most recent SC23-SC24 minimum... The longest stretch without M-class flares was from 25 March 2008 till 19 January 2010 (665 days). ... The longest stretch without X-class flares was from 14 Dec 2006 till 15 February 2011 (1524 days).

# Different types of solar flares

- Homologous flares
  - Same region
  - Almost identical location & shape
  - Occurring repeatedly
  - Often similar strength & time interval



More info at <http://www.stce.be/news/244/welcome.html>

And in Ranns et al., 2000, Emerging flux as a driver for homologous flares

<http://adsabs.harvard.edu/abs/2000A%26A...360.1163R>

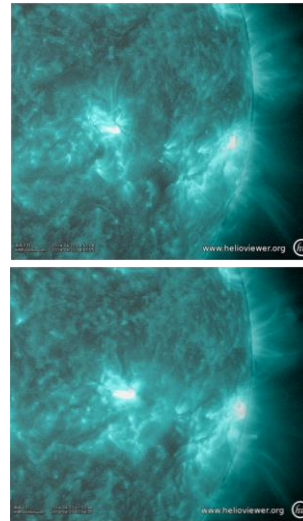
And in Zirin, Astrophysics of the Sun, 1988 pp. 353

Homologous flares are the solar equivalent of identical twins. They concern a series of solar flares taking place repetitively in the same active region with essentially the same position and with a common pattern of development, i.e. having the same main footpoints and general shape in the main phase as defined in H-alpha or EUV-imagery. Though not a requirement, homologous flares often have similar strength, and if there are more than two, they sometimes occur within similar time intervals.

Image source: **Solar Flares**, Zdenek Svestka, 1976, chapter II, page 24

# Different types of solar flares

- Simultaneous flares
  - In different active regions
  - At nearly the same time
    - Difficult to attribute flare source
- Sympathetic flares
  - Simultaneous flares
  - Physically connected
    - Statistical evidence
    - Observational evidence
      - 1 August 2010 event



SWIC - Collaboration between STCE, Koninklijke Luchtmacht, KNMI

57



More at <http://www.stce.be/news/249/welcome.html>

Last week, scientists got a few additional simultaneous flares requiring further investigation. No less than 8 flare events had coinciding brightenings in two or even three well separated sunspot regions. Half of these occurred between NOAA 2035 and 2038. This **movie** shows two examples on 22 and 23 April. It concerns a C2 and C4 flare peaking resp. at 18:41UT and 01:04UT (images underneath). In both cases, the brightening peaked almost at the same moment in the sunspot groups.

Also Moon et al. (2002): Statistical Evidence for Sympathetic Flares  
<http://iopscience.iop.org/article/10.1086/340945/fulltext/55477.text.html>

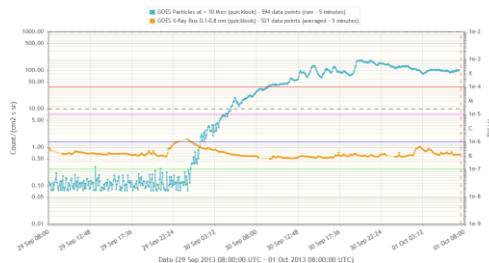
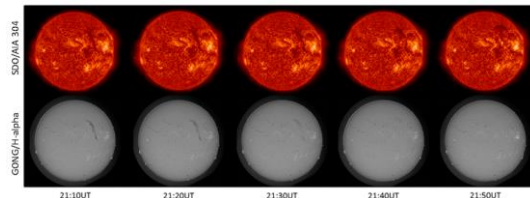
Global connection:

1 August 2010 event:

[https://science.nasa.gov/science-news/science-at-nasa/2010/13dec\\_globaleruption/](https://science.nasa.gov/science-news/science-at-nasa/2010/13dec_globaleruption/)

# Different types of solar flares

- Spotless flares
  - Waldmeier (1938)
    - H-alpha
  - Filament eruptions
    - Hyder flares (1967)
      - “Disparitions brusques”
      - Can occur all over the solar disk
  - In (nearly) spotless regions
    - NOT from behind the limb!



SWIC - Collaboration between STCE, Koninklijke Luchtmacht, KNMI



Imagery from STCE: <http://www.stce.be/news/218/welcome.html>

In contrast to the eruption 5 days earlier, the 29 September event resulted in a minor C-class x-ray flare (a so-called Hyder flare, albeit a weak one). It concerned a long duration event that started at 21:43UT, so about 15 minutes after the first visible signs of the eruption in H-alpha and EUV. The flare reached its maximum at 23:39UT and lasted 200 minutes (over 3 hours!). Numerous post-flare coronal loops were visible. Another difference was that this eruption was also associated to a moderate proton event. This was only the fifth such event this year.

Info at STCE: <http://www.stce.be/news/281/welcome.html>

And at Australian SWS: <http://www.sws.bom.gov.au/Educational/2/4/1>

Another example at <http://www.stce.be/news/203/welcome.html>

Two seminal papers by C. Hyder (theory not entirely correct!)

A Phenomenological Model for Disparitions Brusques followed by Flarelike Chromospheric Brightenings, I: The Model, its Consequences, and Observations in Quiet Solar Regions

<http://adsabs.harvard.edu/abs/1967SoPh...2...49H> (1967)

A Phenomenological Model for disparitions brusques followed by Flarelike Chromospheric Brightenings, II: Observations in Active Regions

<http://adsabs.harvard.edu/abs/1967SoPh...2...267H> (1967)

Luo (1982): The flares of spotless regions

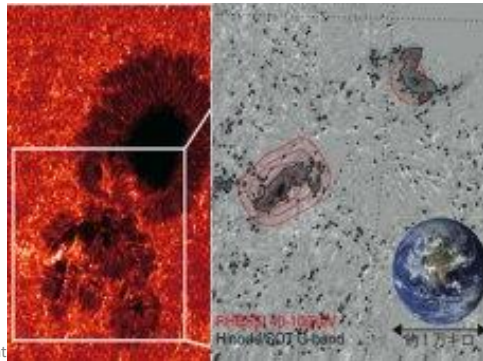
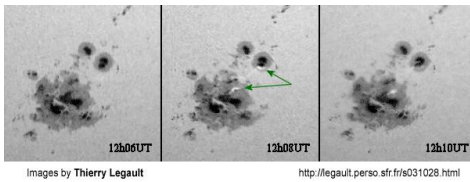
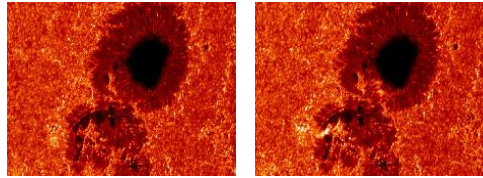
<http://adsabs.harvard.edu/abs/1982AcASn..23...95L>

The 20 flares of sunspotless regions observed at Yunnan Observatory in cycle 21 are analyzed. It is found that the natural productivity of spotless flares is about three percent, that the distribution of the Carrington longitudes tends to shift eastwards, that most of the spotless region flares are those at low energy, and that the background conditions of producing spotless region flares are the same as those of producing spot region flares. Thus, there must be a magnetic field structure with opposite polarity in the solar atmosphere of a flare region. The change in inclination of a filament to a fibril in a spotless region from a large angle to a small one indicates that the force exerted on the spotless active region transforms gradually from pressure to shearing force, meaning that the activity changes gradually from energy storage to sudden energy release.

# Different types of solar flares

## White-light flare

- WLF
  - Flare visible in white light
  - Carrington, 1 September 1859
- Acceleration of huge amounts of particles to the solar “surface”
  - Hinode (2010)
    - Match of HXR location and WL location



NASA: Hinode Discovers the Origin of White Light Flare (2010)

<https://www.nasa.gov/centers/marshall/news/news/releases/2010/10-052.html>

White light emissions were observed by the Solar Optical Telescope during an X-class flare that occurred at 22:09 UT on Dec. 14, 2006 (see Fig. 1). The RHESSI satellite simultaneously recorded hard X-ray emissions, an indicator of non-thermal electrons accelerated by solar flares. The team found that the spatial location and temporal change of white light emissions are correlated with those of hard X-ray emissions (see Fig. 2). Moreover, the energy of white light emissions is equivalent to the energy supplied by all the electrons accelerated to above 40 keV (~40 percent of the light speed). This finding strongly suggests that highly accelerated electrons are responsible for producing white light emissions. Hard X-rays are emitted when accelerated electrons impact the dense atmosphere near the solar surface. Normally, white light emissions primarily come from the solar surface, whereas 40 keV electrons can penetrate into the atmosphere about 1,000 km above the solar surface, i.e., the chromosphere.

Fig. 1, above, White light images of solar surface observed by the Hinode Solar Optical Telescope at 22:07 UT, before the flare, and below, at 22:09 UT, during the flare on Dec. 14, 2006. Image Credit: NASA/JAXA

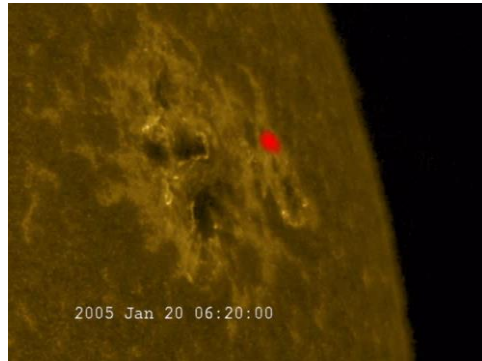
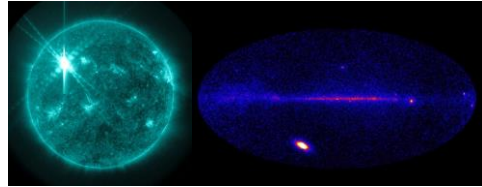
Fig.2: White light emission, left, taken by Hinode/SOT, and the difference image of white light emission and RHESSI hard X-ray contours at 22:09 UT. The background image is the differential white light image (the average of the images taken at 22:07 UT and 22:17 UT is subtracted). Blue contours show 40-100 keV emission. Image credit: NASA/JAXA

An overview of WLFs is at <http://users.telenet.be/j.janssens/WLF/Whitelightflare.html> (last update: August 2012).

# Different types of solar flares

## Gamma-ray flare

- Not a gamma-ray burst
  - Can also impact Ionosphere!
    - 27 December 2004
- (most likely) Continuous acceleration of protons in the solar corona that penetrate the lower solar atmosphere and produce pions that decay into gamma rays
  - « Nuclear » radiation
  - Fermi
    - 07 March 2012 (X5.4 in NOAA 1429)
  - TRACE & RHESSI
    - 20 January 2005



SWIC - Collaboration between STCE, Koninklijke Luchtmacht, KNMI

60

## Gamma-ray Burst Effects on the Ionosphere

<http://vlf.stanford.edu/research/gamma-ray-burst-effects-ionosphere>

<http://news.stanford.edu/news/2006/march1/ainansr-030106.html>

Inan et al. (2007): Massive disturbance of the daytime lower ionosphere by the giant g-ray flare from magnetar SGR 1806-20

<http://adsabs.harvard.edu/abs/2007GeoRL..34.8103I>

Wiki: The intense radiation of most observed GRBs is believed to be released during a supernova or hypernova as a rapidly rotating, high-mass star collapses to form a neutron star, quark star, or black hole.

Gamma-ray flares:

### NASA's Fermi Detects the Highest-Energy Light from a Solar Flare

<https://svs.gsfc.nasa.gov/vis/a010000/a011000/a011000/index.html>

Solar flares produce gamma rays by several processes, one of which is illustrated here. The energy released in a solar flare rapidly accelerates charged particles. When a high-energy proton strikes matter in the sun's atmosphere and visible surface, the result may be a short-lived particle — a pion — that emits gamma rays when it decays.

This image from Fermi's Large Area Telescope (LAT) shows how the entire sky looked on March 7 in the light of gamma rays with energies beyond 100 MeV. Although the Vela pulsar is the brightest continuous LAT source, it was outmatched this day by the X5.4 solar flare, which brightened the sun by 1,000 times.

Nuclear radiation: <http://www.world-nuclear.org/information-library/safety-and-security/radiation-and-health/nuclear-radiation-and-health-effects.aspx>

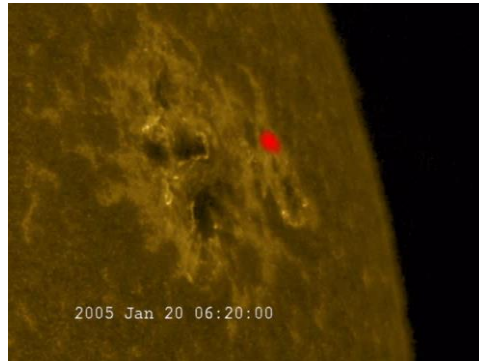
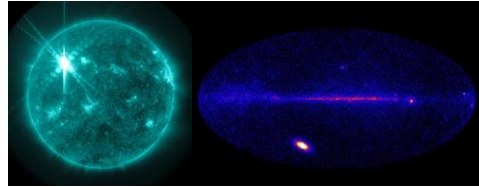
Nuclear radiation arises from hundreds of different kinds of unstable atoms. While many exist in nature, the majority are created in nuclear reactions. Ionizing radiation which can damage living tissue is emitted as the unstable atoms (radionuclides) change ('decay') spontaneously to become different kinds of atoms.

Gamma ray event lists and plots can be found at [https://hesperia.gsfc.nasa.gov/fermi\\_solar/](https://hesperia.gsfc.nasa.gov/fermi_solar/)

# Different types of solar flares

## Gamma-ray flare

- Not a gamma-ray burst
  - Can also impact Ionosphere!
    - 27 December 2004
- (most likely) Continuous acceleration of protons in the solar corona that penetrate the lower solar atmosphere and produce pions that decay into gamma rays
  - « Nuclear » radiation
  - Fermi
    - 07 March 2012 (X5.4 in NOAA 1429)
  - TRACE & RHESSI
    - 20 January 2005



SWIC - Collaboration between STCE, Koninklijke Luchtmacht, KNMI

61

Ajello et al. (2014): Impulsive and Long Duration High-energy Gamma-Ray Emission from the Very Bright 2012 March 7 Solar Flares

<http://adsabs.harvard.edu/abs/2014ApJ...789...20A>

Another example of a gamma flare (20 January 2005)

[https://www.nasa.gov/vision/universe/solarsystem/solar\\_fireworks.html](https://www.nasa.gov/vision/universe/solarsystem/solar_fireworks.html)

[https://www.nasa.gov/home/hqnews/2005/may/HQ\\_05132\\_solar\\_fireworks.html](https://www.nasa.gov/home/hqnews/2005/may/HQ_05132_solar_fireworks.html)

Movies at <https://svs.gsfc.nasa.gov/3162>

"This flare produced the largest solar radiation signal on the ground in nearly 50 years," said Dr. Richard Mewaldt of the California Institute of Technology in Pasadena. Normally it takes two or more hours for a dangerous proton shower to reach maximum intensity at Earth after a solar flare, but the particles from the January 20 flare peaked about 15 minutes after the first sign. That's important," said Mewaldt, "because it's too fast to respond with much warning to astronauts or spacecraft that might be outside Earth's protective magnetosphere. In addition to monitoring the Sun, we need to develop the ability to predict flares in advance if we are going to send humans to explore our solar system."

The event also shakes current theory about the origin of proton storms at Earth. "Since about 1990, we've believed that proton storms at Earth are caused by shock waves in the inner solar system as coronal mass ejections plow through interplanetary space," says Professor Robert Lin of the University of California at Berkeley, principal investigator for the Reuven Ramaty High Energy Solar Spectroscopic Imager (RHESSI). "But the protons from this event may have come from the Sun itself, which is very confusing."

TRACE website: <http://www.lmsal.com/TRACE/> ;

<http://www.lmsal.com/TRACE/POD/TRACEpodarchive21.html#case03>

Active region NOAA 10720 is one of the most flare-productive regions of the last few years, with 10 M-class and 5 X-class flares in a week. The largest flare (to date) from the region was an X7.9 on 20-Jan-2005, starting at 06:36 UT. The 53 min. movie (11MB) showing the UV evolution of the flare (C IV 1600Å band). Movie courtesy of Dawn Myers (GSFC).

The proton storm associated with this flare impacted many spacecraft. Not only those orbiting Earth were affected: the NASA Deep Impact mission en route to comet Tempel 1, even went into a safehold until the electronics could be restarted after the storm passed.

:Issued: 2014 Apr 17 1325 UTC  
 :Product: documentation at http://www.sidc.be/product/s/ot  
 #-----#  
 # DAILY BULLETIN ON SOLAR AND GEOMAGNETIC ACTIVITY from the SIDC #  
 #-----#  
 SIDCURSIGRAM 40417  
 SIDCSOLAR BULLETIN 17 Apr 2014, 1304UT



SIDCFORCAST (valid from 1220UT, 17 Apr 2014 until 19 Apr 2014)

**SOLAR FLARES - Active (M-class flares expected, probability >=50%)**  
 GEOMAGNETISM : Quiet (A<20 and K<4)  
 SOLAR PROTONS : Quiet

PREDICTIONS FOR 17 Apr 2014 10CM FLUX: 180 / AP: 013  
 PREDICTIONS FOR 18 Apr 2014 10CM FLUX: 184 / AP: 007  
 PREDICTIONS FOR 19 Apr 2014 10CM FLUX: 188 / AP: 005

COMMENT: Eleven sunspot groups were reported by NOAA today. NOAA ARs 2035, 2036, and 2037 (Catania numbers 24, 25, and 26 respectively) maintain the beta-gamma configuration of the photospheric magnetic field. The strongest flare of the past 24 hours was the M1.0 flare peaking at 19:59 UT yesterday in the NOAA AR 2035 (Catania number 24). The flare was associated with an EIT wave and a weak coronal dimming, but the associated CME was narrow and is not expected to arrive at the Earth.  
 We expect further flaring activity on the C-level, especially in the NOAA ARs 2035 and 2037 (Catania numbers 24 and 26 respectively) as well as in the NOAA AR 2042 (no Catania number yet) that yesterday appeared from behind the east solar limb, with a good chance for an M-class event.

Since yesterday evening the Earth is situated inside a solar wind structure with an elevated interplanetary magnetic field magnitude (occasionally up to 10 nT). It may be a weak ICME or the compression region on the flank of an ICME that missed the Earth. The solar origin of this structure is not clear. The north-south magnetic field component Bz was not strong, so no significant geomagnetic disturbance resulted (Kindex stayed below 4). Currently the solar wind speed is around 380 km/s and the IMF magnitude is around 8 nT.

We expect quiet to unsettled (K index up to 3) geomagnetic conditions, with active geomagnetic conditions (K=4) possible, but unlikely.

TODAY'S ESTIMATED ISN : 145, BASED ON 17 STATIONS.  
 99999

SOLAR INDICES FOR 16 Apr 2014  
 WOLF NUMBER CATANIA : ///  
 10CM SOLAR FLUX : 184  
 AK CHAMBON LA FORET : 012  
 AK WINGST : 004  
 ESTIMATED AP : 004  
 ESTIMATED ISN : 139, BASED ON 29 STATIONS.

## Flare classification

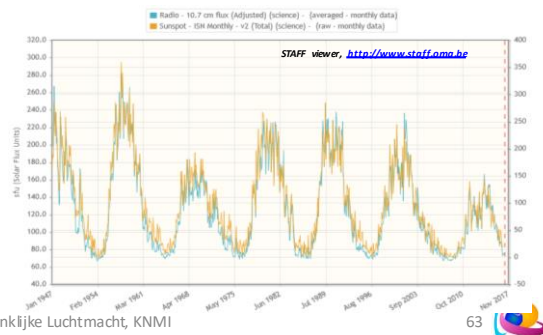
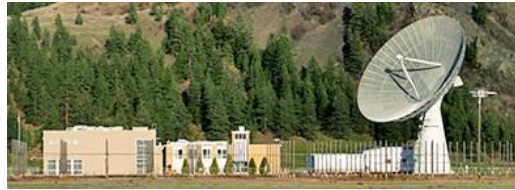
**NOTICEABLE EVENTS SUMMARY**

| DAY | BEGIN | MAX  | END  | LOC    | XRAY | OP | 10CM | Catania/NOAA | RADIO_BURST_TYPES |
|-----|-------|------|------|--------|------|----|------|--------------|-------------------|
| 16  | 1954  | 1959 | 2004 | S14E09 | M1.0 | 1N |      | 24/2035      | I/2               |

END

# The 10.7cm radio flux

- Measured at Penticton, CA
  - 2800 MHz
    - 2750-2850 MHz
  - 17UT, 20UT, 23UT
    - Official daily value: 20UT
    - Observed flux
      - Also values adjusted to 1AU
  - 3 components
    - Affected by flares
  - Good correlation with sunspot number



SWIC - Collaboration between STCE, Koninklijke Luchtmacht, KNMI

63

See notes at:

STCE news item: <http://www.stce.be/news/374/welcome.html>

SWS: <http://www.sws.bom.gov.au/Educational/2/2/5>

SWS: <http://www.sws.bom.gov.au/Educational/2/2/6>

Tapping, K. (2013): The 10.7 cm solar radio flux ( $F_{10.7}$ )

<http://adsabs.harvard.edu/abs/2013SpWea..11..394T>

The connection between sunspots and solar centimetric emissions was discovered independently by Covington [1947, 1948], Lehaney and Yabsley [1949], and through a statistical study, Denisse [1948]. Covington [1947] used the edge of the Moon during a solar eclipse to identify a significant emission contribution associated with a large active region. The utility of what became known as  $F_{10.7}$  as an indicator of the level of solar activity led to the continuation of measurement to the present day and to the program becoming a data service.

A 10.7 cm solar flux measurement is a determination of the strength of solar radio emission in a 100 MHz-wide band centered on 2800 MHz (a wavelength of 10.7 cm), averaged over an hour. It is expressed in solar flux units (sfu), where  $1 \text{ sfu} = 10^{-22} \text{ W m}^{-2} \text{ Hz}^{-1}$ .

This data filtering procedure has been discontinued for two reasons: one was the staffing issue mentioned earlier.

Second, many applications require the measured flux value, not a value that has been modified. Subsequently, practice has been to distribute the data as measured and to provide auxiliary data so that users could apply whatever data modification procedures they require.

Three flux determinations are made each day, at 1700, 2000, and 2300 UT, except during the winter months, where the low elevation of the Sun (DRAO lies at  $+50^\circ$  latitude) and the hilly terrain, forces the times to be changed to 1800, 2000, and 2200 UT. Each flux determination takes 1 h and takes no account of the solar radio emissions recorded outside the intervals covered by the measurements. Since the active region emissions contributing to the slowly varying emission (and  $F_{10.7}$ ) may vary over hours or less, there may be a significant degree of undersampling. In addition, there could be a contribution by a burst. The undersampling means there is a possible error if one uses a flux value in an application involving a different time from that at which the flux measurement is made.

# Radio bursts

- Tenflare
  - Compared to pre-flare background levels, the 10.7cm (2800 MHz) radio flux suddenly increases by at least 100%
  - Example:
    - 17 May 2013
      - M3 flare in NOAA 1748
      - From +/- 140 sfu to >400 sfu
  - May affect daily 10.7cm radio flux values (20UT)
  - Radio flares also observed at other wavelengths



SWIC - Collaboration between STCE, Koninklijke Luchtmacht, KN

$$1 \text{ sfu} = 10^{-22} \text{ Wm}^{-2} \text{ Hz}^{-1}$$

Tapping(2013): The 10.7 cm solar radio flux (F10.7)  
<http://onlinelibrary.wiley.com/doi/10.1002/swe.20064/epdf>

A 10.7 cm solar flux measurement is a determination of the strength of solar radio emission in a 100 MHz-wide band centered on 2800 MHz (a wavelength of 10.7 cm), averaged over an hour. It is expressed in solar flux units (sfu), where  $1 \text{ sfu} = 10^{-22} \text{ Wm}^{-2} \text{ Hz}^{-1}$ . It is daily measured at Penticton, British Columbia, Canada (DRAO: Dominion Radio Astrophysical Observatory). Measurements are taken at 17UT, 20UT and 23UT (winter period: 18-20-22UT), with the local noon value (20UT) as the value for that day. It is uncorrected for any flare influence. The daily values are at <http://www.spaceweather.ca/solarflux/sx-4a-en.php>

The 10.7cm radio flux consists of three identifiable components: a rapidly varying or R component, comprising emissions varying over timescales in the second-minute range, perhaps as long as an hour. Slower variations were lumped into a slowly varying or S component. Extrapolation to zero activity suggested an underlying constant, base level, which became called the quiet sun, or Q component. The terms R and Q have fallen out of use, and these components are now known, respectively, as bursts and the quiet sun background emission. The slowly varying component originates primarily in active regions; its intensity is a measure of the overall level of solar magnetic activity and has a broad spectral peak at about 10 cm wavelength. The F10.7 values comprise contributions from the S component and the quiet sun background, and sometimes from radio bursts.

From SWPC Glossary at <https://www.swpc.noaa.gov/content/space-weather-glossary#>  
 Tenflare: A solar flare accompanied by a 10cm radio burst of intensity greater than 100% of the pre-burst value.

# Radio bursts

- Tenflare
  - Compared to pre-flare background levels, the 10.7cm (2800 MHz) radio flux suddenly doubles
  - Example:
    - 17 May 2013
      - M3 flare in NOAA 1748
      - From +/- 140 sfu to > 400 sfu
  - May affect daily 10.7cm radio flux values (20UT)
  - Radio flares also observed at other wavelengths



SWIC - Collaboration between STCE, Koninklijke Luchtmacht, KN



An example of a radio flare (17 May 2013)

<http://link.springer.com/article/10.1007/s11038-008-9265-8>

<http://www.spaceweather.org/ISES/code/aaf/ugeoi.html>

<https://www.swpc.noaa.gov/content/space-weather-glossary#>

<http://www.solarham.net/tenflare.htm>

|        |       |       |       |     |   |     |                          |      |         |      |
|--------|-------|-------|-------|-----|---|-----|--------------------------|------|---------|------|
| 5490   | 0843  | 0857  | 0919  | G15 | 5 | XRA | 1-8A                     | M3.2 | 4.4E-02 | 1748 |
| 5490 + | 0847  | 0853  | 0913  | SVI | G | RBR | 4995                     | 800  |         | 1748 |
| 5490 + | 0848  | 0857  | 0912  | SVI | G | RBR | 2695                     | 450  |         | 1748 |
| 5490 + | 0848  | 0848  | 0848  | SVI | G | RBR | 410                      | 100  |         | 1748 |
| 5490 + | 0848  | 0853  | 0912  | SVI | G | RBR | 8800                     | 620  |         | 1748 |
| 5490 + | 0850  | ////  | 1120  | SVI | C | RSP | 025-180                  | IV/2 |         | 1748 |
| 5490 + | 0850  | ////  | 0918  | SVI | U | RSP | 025-180                  | II/2 | 376     | 1748 |
| 5490 + | 0850  | 0855  | 0912  | SVI | G | RBR | 15400                    | 410  |         | 1748 |
| 5490 + | 0850  | 0858  | 0912  | SVI | G | RBR | 1415                     | 190  |         | 1748 |
| 5490 + | 0851  | 0852  | 0907  | SVI | G | RBR | 245                      | 1500 |         | 1748 |
| 5490   | 0853  | 0855  | 0857  | LEA | G | RBR | 610                      | 210  |         | 1748 |
| 5490 + | B0854 | U0854 | 1056  | SVI | 3 | FLA | N12E57                   | 2B   | PRB     | 1748 |
| 5490   | B0912 | ////  | A1319 | SOH | 4 | CME | XUV,EUV,UV061-060/FS1436 |      |         | 1748 |

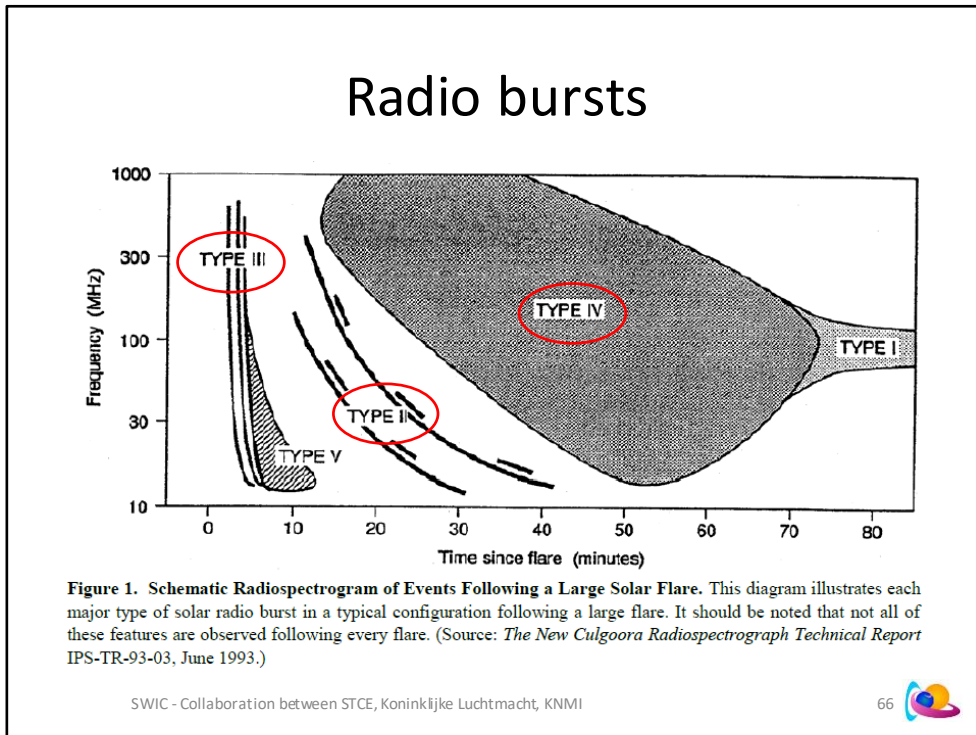
This flare occurred around 09UT, and had little influence on the official radio flux for that day (20UT):

| Date Time           | Julian day  | Carrington | rotation | Observed Flux | Adjusted Flux | URSI Flux |
|---------------------|-------------|------------|----------|---------------|---------------|-----------|
| 2013-05-17 17:00:00 | 2456430.197 | 2137.106   | 137.9    |               | 141.1         | 127.0     |
| 2013-05-17 20:00:00 | 2456430.322 | 2137.111   | 136.4    |               | 139.6         | 125.6     |
| 2013-05-17 23:00:00 | 2456430.447 | 2137.115   | 135.7    |               | 138.8         | 125.0     |

Data from RNCAN: <http://www.spaceweather.ca/solarflux/sx-5-flux-en.php?year=2013>

From the SWPC's "Solar Events" User guide (<ftp://ftp.swpc.noaa.gov/pub/indices/events/README>):

RBR: The peak value above pre-burst background of associated radio bursts at frequencies 245, 410, 610, 1415, 2695, 4995, 8800 and 15400 MHz: 1 flux unit =  $10^{-22}$  Wm<sup>-2</sup> Hz<sup>-1</sup>



Source of Figure: SWPC's « The Weekly » User guide  
[https://www.swpc.noaa.gov/sites/default/files/images/u2/Usr\\_guide.pdf](https://www.swpc.noaa.gov/sites/default/files/images/u2/Usr_guide.pdf); page 5)

Mind the orientation of the vertical axis! Other figures may have a reversed direction. As the frequency is proportional to the square root of the density, and the density decreases with increasing distance from the Sun, a decreasing frequency means locations higher up in the solar atmosphere.

The ionospheric cut-off frequency is around 15MHz (due to too low frequency and so reflected by ionosphere). In order to observe radio disturbances below this frequency, one has to use satellites (above the earth atmosphere) such as STEREO/SWAVES or WIND. Radio bursts at low frequencies (< 15 MHz) are of particular interest because they are associated with energetic CMEs that travel far into the interplanetary (IP) medium and affect Earth's space environment if Earth-directed. Low frequency radio emission needs to be observed from space because of the ionospheric cutoff.

Example: <https://stereo-ssc.nascom.nasa.gov/browse/2017/01/16/insitu.shtml>

Solar Radio Bursts and Space Weather, S.M. White

[https://www.nrao.edu/astrores/gbsrbs/Pubs/AJP\\_07.pdf](https://www.nrao.edu/astrores/gbsrbs/Pubs/AJP_07.pdf)

White: Solar radio bursts at frequencies below a few hundred MHz were classified into 5 types in the 1960s (Wild et al., 1963).

Coronal Mass Ejections and solar radio emissions, N. Gopalswamy

<http://cites.eerx.ist.psu.edu/viewdoc/download?doi=10.1.1.708.626&rep=rep1&type=pdf>

Gopalswamy: The three most relevant to space weather radio burst types are type II, III, and IV. Three types of low-frequency non-thermal radio bursts are associated with coronal mass ejections (CMEs): Type III bursts due to accelerated electrons propagating along open magnetic field lines, type II bursts due to electrons accelerated in shocks, and type IV bursts due to electrons trapped in post-eruption arcades behind CMEs.

[Radio burst type II, III, and IV are also the only ones that ever get mentioned in the Ursigrams.]

# Radio bursts

## Solar Radio Burst Classifications

| TYPE | CHARACTERISTICS   | DURATION  | FREQUENCY RANGE              | ASSOCIATED PHENOMENA                                     |
|------|---|---|------------------------------|--|
| I    | Short, narrow-bandwidth bursts. Usually occur in large numbers with underlying continuum.   | Single burst: ~ 1 second<br>Storm: hours - days                               | 80 – 200 MHz                 | Active regions, flares, eruptive prominences.            |
| II   | Slow frequency drift bursts. Usually accompanied by a (usually stronger intensity) second harmonic.   | 3- 30 minutes   | Fundamental:<br>20 – 150 MHz | Flares, proton emission, magnetohydrodynamic shockwaves. |
| III  | Fast frequency drift bursts. Can occur singularly, in groups, or storms (often with underlying continuum). Can be accompanied by a second harmonic. | Single burst: 1 - 3 seconds<br>Group: 1 - 5 minutes<br>Storm: minutes - hours | 10 kHz – 1 GHz               | Active regions, flares.                                  |
| IV   | Stationary Type IV:<br>Broadband continuum with fine structure  | Hours - days  | 20 MHz – 2 GHz               | Flares, proton emission.                                 |
|      | Moving Type IV:<br>Broadband, slow frequency drift, smooth continuum.   | 30 – 2 hours  | 20 – 400 MHz                 | Eruptive prominences, magnetohydrodynamic shockwaves.    |
| V    | Flare Continua:<br>Broadband, smooth continuum.   | 3 – 45 minutes  | 25 – 200 MHz                 | Flares, proton emission.                                 |
|      | Smooth, short-lived continuum. Follows some type III bursts. Never occur in isolation.  | 1-3 minutes   | 10 - 200 MHz                 | Same as type III bursts.                                 |

NOTES: In nearly all cases, drifting bursts drift from high to low frequencies.  
The Frequency Range is the typical range in which the bursts appear – not their bandwidth.  
The sub-types of type IV are not universally agreed upon and are thus open to debate.

@Copyright IPS AUSTRALIA

SWIC - Collaboration between STCE, Koninklijke Luchtmacht, KNMI

67



Source - Table taken from the Australian SWS:

<http://www.sws.bom.gov.au/Category/World%20Data%20Centre/Data%20Display%20and%20Download/Spectrograph/Solar%20Radio%20Burst%20Classifications.pdf>

From the SWPC's "Solar Events" User guide (<ftp://ftp.swpc.noaa.gov/pub/indices/events/README>):  
RSP:

Type/Intensity

Type II: Slow drift burst

Type III: Fast drift burst

Type IV: Broadband smooth continuum burst

Type V: Brief continuum burst, generally associated with Type III bursts

Type VI: Series of Type III bursts over a period of 10 minutes or more, with no period longer than 30 minutes without a activity

Type VII: Series of Type III and Type V bursts over a period of 10 minutes or more, with no period longer than 30 minutes without a activity

Type CTM: Broadband, long-lived, decametric continuum

Intensity is a relative scale 1=Minor, 2=Significant, 3=Major

Shock speed in km/s

Note from Dr Christophe Marqué (ROB): Types VI and VII are not used outside NOAA reports. They are not "official" within the radio community.

# Radio bands

<sup>1</sup> In the application of the [ITU Radio Regulations](#), the [Radiocommunication Bureau](#) uses the following units:

kHz: For frequencies up to 28 000 kHz inclusive;

MHz: For frequencies above 28 000 kHz up to 10 500 MHz inclusive; and

GHz: For frequencies above 10 500 MHz.

| Band number | Symbols | Frequency range (lower limit exclusive, upper limit inclusive) | Corresponding metric subdivision | Metric abbreviations for the bands |
|-------------|---------|--|----------------------------------|------------------------------------|
| 4           | VLF     | 3 to 30 kHz  | Myriametric waves                | B.Mam                              |
| 5           | LF      | 30 to 300 kHz  | Kilometric waves                 | B.km                               |
| 6           | MF      | 300 to 3 000 kHz   | Hectometric waves                | B.hm                               |
| 7           | HF      | 3 to 30 MHz  | Decametric waves                 | B.dam                              |
| 8           | VHF     | 30 to 300 MHz  | Metric waves                     | B.m                                |
| 9           | UHF     | 300 to 3 000 MHz   | Decimetric waves                 | B.dm                               |
| 10          | SHF     | 3 to 30 GHz  | Centimetric waves                | B.cm                               |
| 11          | EHF     | 30 to 300 GHz  | Millimetric waves                | B.mm                               |
| 12          |         | 300 to 3 000 GHz   | Decimillimetric waves            |                                    |

**Note 1:** "Band N" (N = band number) extends from  $0.3 \times 10^N$  Hz to  $3 \times 10^N$  Hz.

**Note 2:** Prefix: k = kilo ( $10^3$ ), M = mega ( $10^6$ ), G = giga ( $10^9$ ).

SWIC - Collaboration between STCE, Koninklijke Luchtmacht, KNMI

68

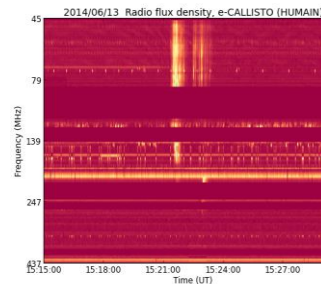
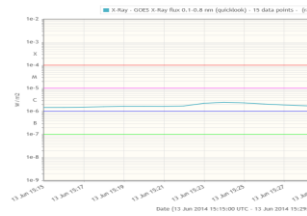


Source: <https://www.law.cornell.edu/cfr/text/47/2.101>

Question: The 10.7cm radio flux belongs to which metric subdivision?

# Radio bursts

- Type III
  - Source:
    - accelerated electrons propagating along open magnetic field lines
  - During impulsive phase of flares
    - Exceptions...
  - Duration
    - Seconds (isolated) to minutes (groups)
  - Frequency
    - 10 kHz-1GHz



SWIC - Collaboration between STCE, Koninklijke Luchtmacht, KNMI



Image courtesy:

GOES-curve: STAFF viewer, <http://www.staff.oma.be>

Radio plot: ROB/Humain Radio Observatory, <http://www.sidc.be/humain/>

13 June 2014

|       |      |      |      |     |   |     |         |       |         |      |
|-------|------|------|------|-----|---|-----|---------|-------|---------|------|
| 3940  | 1521 | 1524 | 1527 | G15 | 5 | XRA | 1-8A    | C2.4  | 5.2E-04 | 2087 |
| 3940+ | 1521 | 1522 | 1523 | SAG | G | RBR | 245     | 290   |         | 2087 |
| 3940+ | 1521 | //// | 1523 | SAG | C | RSP | 025-180 | III/2 |         | 2087 |
| 3940+ | 1522 | 1522 | 1525 | HOL | 3 | FLA | S19E38  | SF    |         | 2087 |

Solar Radio Bursts and Space Weather, S.M. White

[https://www.nrao.edu/astrores/gbsrbs/Pubs/AJP\\_07.pdf](https://www.nrao.edu/astrores/gbsrbs/Pubs/AJP_07.pdf)

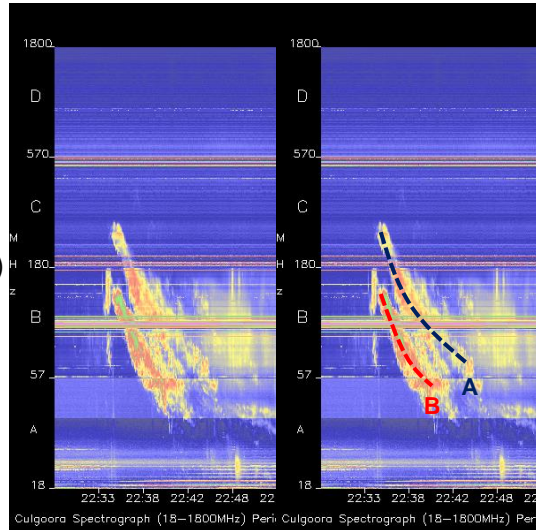
White: Type III bursts are brief radio bursts that drift very rapidly in frequency versus time (Fig. 1). For example, it can drift from 50 to 20 MHz in about 3 seconds, or 10 MHz s<sup>-1</sup>. Type IIIs are commonly seen in the impulsive phase of solar flares, and the connection they imply between the acceleration region in solar flares and open field lines that reach the solar wind makes them important for understanding field line connectivity in flares and the access of flare-accelerated particles to the Earth.

Coronal Mass Ejections and solar radio emissions, N. Gopalswamy

<http://citeseerx.ist.psu.edu/viewdoc/download?doi=10.1.1.708.626&rep=rep1&type=pdf>

# Radio bursts

- Type II
  - Source:
    - electrons accelerated in shocks
    - Indicates CME
    - Shock speed can be derived from fundamental band (B)
  - Start at peak SXR flux of flare
    - Exceptions...
  - Duration
    - 3-30 minutes
  - Frequency
    - 20-150 MHz



SWIC - Collaboration between STCE, Koninklijke Luchtmacht, KNMI

70

Culgoora spectrograph at 01 Nov 2003 - <http://www.sws.bom.gov.au/Solar/2/2/1> (Type II/2 , 1079 km/s)

Solar Radio Bursts and Space Weather, S.M. White  
[https://www.nrao.edu/astrores/gbsrbs/Pubs/AJP\\_07.pdf](https://www.nrao.edu/astrores/gbsrbs/Pubs/AJP_07.pdf)

Type II bursts typically occur at around the time of the soft X-ray peak in a solar flare and are identified by a slow drift to lower frequencies with time in dynamic spectra, the frequent presence of both fundamental and second-harmonic bands (with a frequency ratio of 2), and splitting of each of these bands into two traces. The frequency drift rate is typically two orders of magnitude slower than that of the ("fast-drift") Type III bursts, so the two burst types are readily distinguished.

Hillan et al. (2012): Type II solar radio bursts: Modeling and extraction of shock parameters  
<http://onlinelibrary.wiley.com/doi/10.1029/2011JA016754/full>

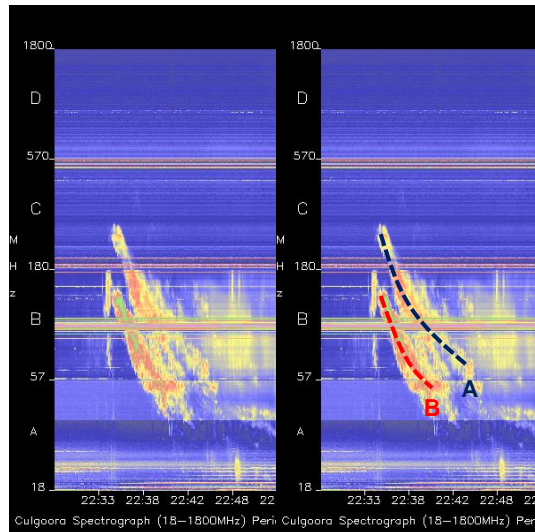
Coronal mass ejections (CME) driving shocks through the corona and into the heliosphere have long been associated with interplanetary type II bursts in the kilometric range [Wild et al., 1963; Cane et al., 1982; Cane, 1985; Nelson and Melrose, 1985; Reiner et al., 2001]. Blast waves have long been discussed as potential shock drivers in the metric type II burst range [Cliver et al., 1999; Claßen and Aurass, 1999], but are not usually thought to persist into the interplanetary medium to drive kilometric emission [Cane et al., 1987]. Similarly, it is not clear that all metric type IIs are associated with CMEs, since the metric emission does not routinely (if ever) continue smoothly to the kilometric emission of an interplanetary type II [Cane and Erickson, 2005]. In the foregoing type II theories, it is the presence and characteristics of the shock that are important, not the mechanism which produced it.

[The fundamental band is the one provoked by the shock of the CME and is the one that reaches the lowest frequencies first (track « B » in the image). It is the fundamental track that is used to calculate the (true) speed of the shock as it moves through the corona and away from the Sun (density decrease => frequency decrease).]

[The particles from the solar eruption disturb the environment of the particles already present in the higher-up corona. These particles start to oscillate, creating Langmuir waves in the process. These waves generated by both populations of particles, can interact with each other in different ways, as the particles don't move together and more or less stay at the same place. From these wave interactions, the fundamental and harmonic radio emissions are produced, i.e. at the local plasma frequency and multiples from it.]

# Radio bursts

- Type II
  - Source:
    - electrons accelerated in shocks
    - Indicates CME
    - Shock speed can be derived from fundamental band
  - Start at peak SXR flux of flare
    - Exceptions...
  - Duration
    - 3-30 minutes
  - Frequency
    - 20-150 MHz



SWIC - Collaboration between STCE, Koninklijke Luchtmacht, KNMI

71

[Jasmina Magdalenic PhD:

Plasma emission is the dominant coherent emission process for the majority of solar radio bursts at decimeter and longer wavelengths.

The plasma emission may be defined as an emission process in which the energy of the Langmuir turbulence is partly converted into the escaping radiation. The plasma emission is a multi-stage process, including:

- Formation of an unstable beam distribution by the velocity dispersion.
- Generation of the Langmuir turbulence as a consequence of plasma instabilities.
- Nonlinear evolution and conversion into escaping electromagnetic radiation.

Two steps can be distinguished:

a) conversion into fundamental transverse radiation - fundamental plasma emission.

The fundamental plasma emission at the frequency  $f_p \sim \omega_p/2$ , is due to conversion into escaping radiation with only small changes in frequency. This conversion could be:

- 1) scattering of Langmuir waves into transverse waves of thermal ions,
- 2) coalescence of Langmuir waves and low-frequency waves, such as ion-acoustic waves, into transverse waves, and
- 3) sort of "direct" conversion due to plasma inhomogeneities.

b) production of secondary Langmuir waves and generation of second-harmonic transverse radiation - second harmonic emission.

Coalescence of two Langmuir waves results in escaping radiation at the sum of their frequencies ( $f \sim 2f_p$ ), named the harmonic emission.

Roberts (1959): Solar Radio Bursts of Spectral Type II :

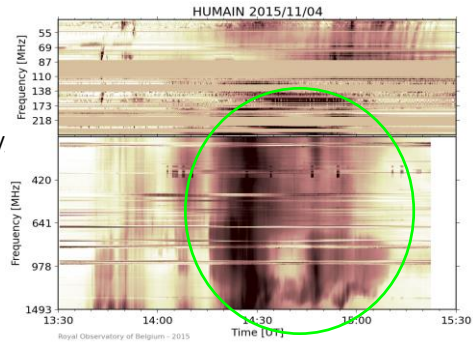
<http://adsabs.harvard.edu/abs/1959AuJPh..12..327R>

Gopalswamy: Coronal Mass Ejections and solar radio emissions :

<http://citeserx.ist.psu.edu/viewdoc/download?doi=10.1.1.708.626&rep=rep1&type=pdf>

# Radio bursts

- Type IV
  - Source
    - e<sup>-</sup> trapped in post-eruption arcades behind CMEs
    - Related to very energetic CMEs
      - average speed: 1200 km/
  - During decay phase of solar flares
    - Connection with SEPs
  - Duration
    - Hours (to days)
  - Frequency
    - 20 to >1000 MHz
    - **Lowest: 8 +/- 5 MHz**



SWIC - Collaboration between STCE, Koninklijke Luchtmacht, KNMI



Gopalswamy: Coronal Mass Ejections and solar radio emissions

<http://citeseerx.ist.psu.edu/viewdoc/download?doi=10.1.1.708.626&rep=rep1&type=pdf>

The type IV bursts are associated with very energetic CMEs (average speed 1200 km/s), confirming the earlier finding by Robinson [1986] for the continuum events at metric wavelengths. The radio emission should originate from a heliocentric distance 3.5 to 4.5 Rs, depending on whether the radio emission occurs at the fundamental or harmonic of the plasma frequency. When the type IV burst attains the lowest frequency, the IP type II burst occurs at frequencies well below 1 MHz, which means the shock is much farther away. This suggests that the energetic electrons responsible for the type IV burst might come from the continued reconnection occurring beneath the CME.

*[Comment by Dr Christophe Marqué (ROB): The height of type IV reported by Gopalswamy concerns the low frequency ones. The one for example observed in Humain (04 Nov 2015) is really taking place in the post flare loops close to the flare site.]*

Solar Radio Bursts and Space Weather, S.M. White

[https://www.nrao.edu/astrores/gbsrbs/Pubs/AJP\\_07.pdf](https://www.nrao.edu/astrores/gbsrbs/Pubs/AJP_07.pdf)

Type IV bursts are broadband quasi-continuum features associated with the decay phase of solar flares. They are attributed to electrons trapped in closed field lines in the post-flare arcades produced by flares; their presence implies ongoing acceleration somewhere in these arcades, possibly at the tops of the loops in a "helmet-streamer" configuration. Type IV bursts have long been of interest in Space Weather studies because they have a high degree of association with solar energetic particle events.

Example: 04 Nov 2015: <http://www.stce.be/news/326/welcome.html>

2340B1327 U1339 A1348 SVI 2 FLA N09W04 2B ERU 2443  
 2340 + 1331 1352 1413 G15 5 XRA 1-8A M3.7 5.9E-02 2443  
 2340 + 1336 1341 1438 SVI G RBR 4995 740 2443  
 2340 + 1337 1341 1442 SVI G RBR 2695 340 2443  
 2340 + 1337 1341 1429 SVI G RBR 8800 560 2443  
 2340 + 1338 1341 1414 SVI G RBR 15400 210 2443  
 2340 + 1343 //// 1358 SAG C RSP 048-180 II/2 955 2443  
 2340 + 1351 //// 1531 SVI C RSP 025-171 IV/1 2443  
 2340 + 1404 1426 1502 SAG G RBR 410 1400 2443  
 2340 + 1405 1433 1507 SAG G RBR 245 1400 2443  
 2340 + 1406 1427 1456 SAG G RBR 1415 5800 2443  
 2340 + 1406 1427 1458 SAG G RBR 610 1000 2443

:Issued: 2014 Apr 17 1325 UTC  
 :Product: documentation at http://www.sidc.be/product/sft/ot  
 #-----#  
 # DAILY BULLETIN ON SOLAR AND GEOMAGNETIC ACTIVITY from the SIDC #  
 #-----#  
 SIDCURSIGRAM 40417  
 SIDCSOLAR BULLETIN 17 Apr 2014, 1304UT



SIDC FORECAST (valid from 1230UT, 17 Apr 2014 until 19 Apr 2014)  
 SOLAR FLARES : Active (M-class flares expected, probability >=50%)  
 GEOMAGNETISM : Quiet (A<20 and K<4)  
 SOLAR PROTONS : Quiet

PREDICTIONS FOR 17 Apr 2014 10CM FLUX: 180 / AP: 013  
 PREDICTIONS FOR 18 Apr 2014 10CM FLUX: 184 / AP: 007  
 PREDICTIONS FOR 19 Apr 2014 10CM FLUX: 188 / AP: 005

COMMENT: Eleven sunspot groups were reported by NOAA today. NOAA ARs 2035, 2036, and 2037 (Catania numbers 24, 25, and 26 respectively) maintain the beta-gamma configuration of the photospheric magnetic field. The strongest flare of the past 24 hours was the M1.0 flare peaking at 19:59 UT yesterday in the NOAA AR 2035 (Catania number 24). The flare was associated with an EIT wave and a weak coronal dimming, but the associated CME was narrow and is not expected to arrive at the Earth.  
 We expect further flaring activity on the C-level, especially in the NOAA ARs 2035 and 2037 (Catania numbers 24 and 26 respectively) as well as in the NOAA AR 2042 (no Catania number yet) that yesterday appeared from behind the east solar limb, with a good chance for an M-class event.

Since yesterday evening the Earth is situated inside a solar wind structure with an elevated interplanetary magnetic field magnitude (occasionally up to 10 nT). It may be a weak ICME or the compression region on the flank of an ICME that missed the Earth. The solar origin of this structure is not clear. The north-south magnetic field component Bz was not strong, so no significant geomagnetic disturbance resulted (Kindex stayed below 4). Currently the solar wind speed is around 380 km/s and the IMF magnitude is around 8 nT.  
 We expect quiet to unsettled (K index up to 3) geomagnetic conditions, with active geomagnetic conditions (K=4) possible, but unlikely.

TODAY'S ESTIMATED ISN : 145, BASED ON 17 STATIONS.  
 99999

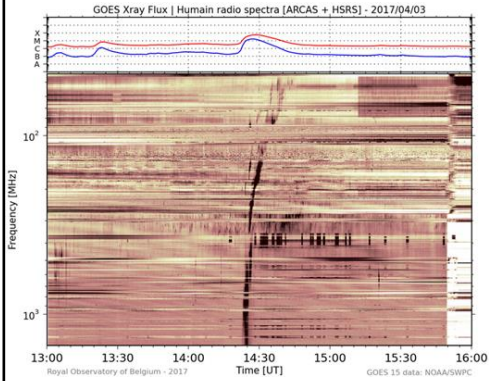


SOLAR INDICES FOR 16 Apr 2014  
 WOLF NUMBER CATANIA : ///  
 10CM SOLAR FLUX : 184  
 AK CHAMBON LA FORET : 012  
 AK WINGST : 004  
 ESTIMATED AP : 004  
 ESTIMATED ISN : 139, BASED ON 29 STATIONS.

NOTICEABLE EVENTS SUMMARY

| DAY | BEGIN | MAX  | END  | LOC    | XRAY | OP | 10CM | Catania/NOAA | RADIO_BURST_TYPES |
|-----|-------|------|------|--------|------|----|------|--------------|-------------------|
| 16  | 1954  | 1959 | 2004 | S14E09 | M1.0 | 1N |      | 24/2035      | 11/2              |

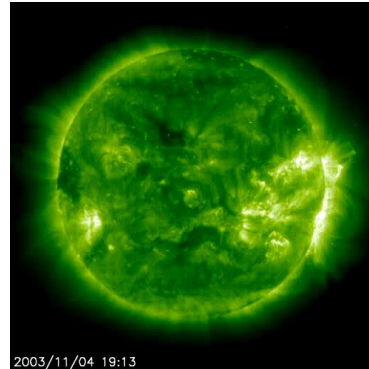
## Exercise: Radio burst classification



- Which obvious radio burst can be recognized in this radiogram by the Human Radio Solar Observatory?
  - Type II
  - Type III
  - Type IV

# Solar flares - Contents

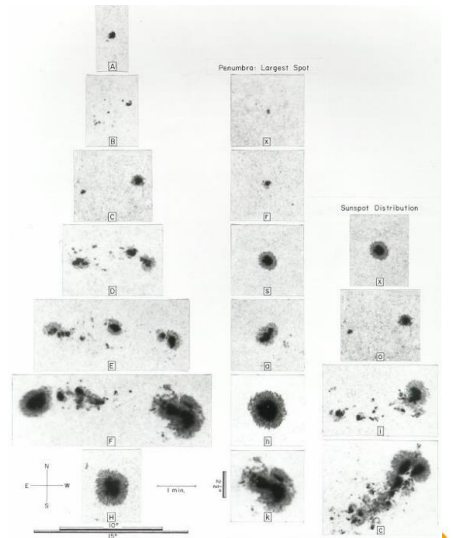
- **Characteristics**
  - Definition
  - Standard model
  - Flare triggers
  - Flare features
- **Classification**
  - H-alpha
  - X-ray
    - Intensity, duration, frequency
  - Types of solar flares
  - Radio bursts
- **Flare predictions**
  - **McIntosh**
  - **Hale**
  - **Filament eruptions**



SWIC - Collaboration between STCE, Koninklijke Luchtmacht, KNMI

# Flare predictions

- McIntosh classification
  - 1990
    - Patrick S. McIntosh<sup>+</sup>
  - Zpc (3-letter code)
    - Z - Modified Zürich classification
    - p - Penumbra largest spot
    - c - Interior sunspot distribution
  - 60 possible combinations
    - Linked to flare intensity
    - Rather large uncertainties
  - Used worldwide

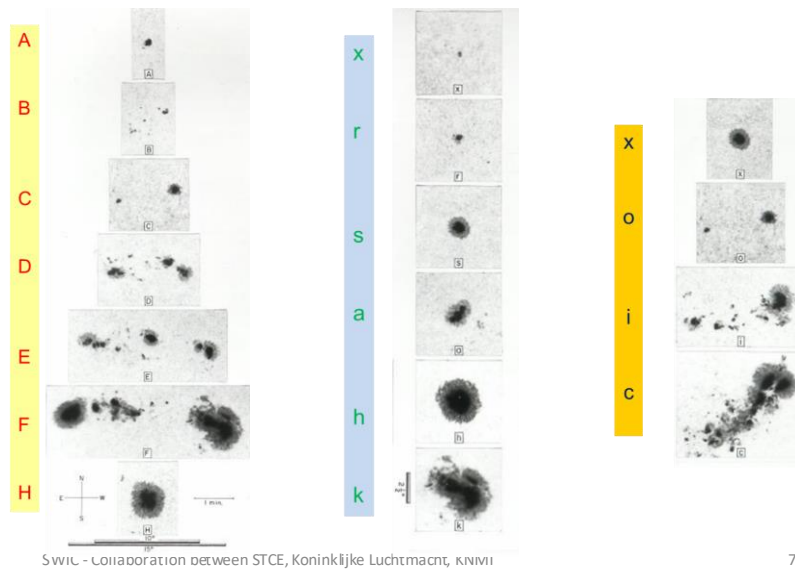


SWIC - Collaboration between STCE, Koninklijke Luchtmacht, KNMI

76

McIntosh, P.S. (1990): The classification of sunspot groups  
<http://adsabs.harvard.edu/abs/1990SoPh..125..251M>

# Flare predictions



77

McIntosh, P.S. (1990): The classification of sunspot groups  
<http://adsabs.harvard.edu/abs/1990SoPh..125..251M>

Questions to ask (Table 1 from McIntosh paper)

Z – General outlook of the sunspot group:

- => Unipolar or bipolar group?
- => Penumbra or no penumbra?
- => Penumbra on one or both sides of the group?
- => Length of the group ( $>10^\circ$ ?  $>15^\circ$ ?)
- \* 7 options: A, B, C, D, E, F, H

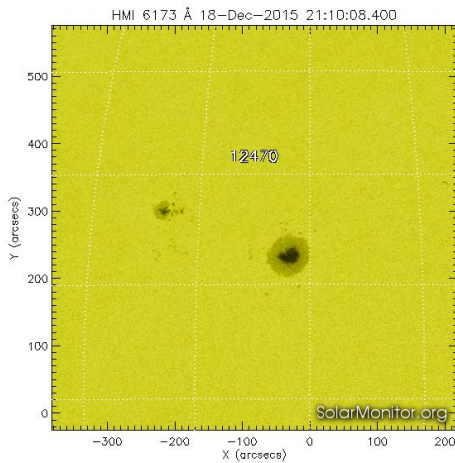
p – Penumbra largest spot

- => Rudimentary or mature penumbra?
- => Symmetric or asymmetric penumbra main spot?
- => N-S-diameter of the largest spot ( $>2,5^\circ$ ?)
- \* 6 options: x, r, s, a, h, k

c – Sunspot distribution interior (“compactness”)

- => Several spots between leading and trailing main spot?
- => Internally, is there at least one spot with a mature penumbra?
- \* 4 options: x, o, i, c (open, intermediate, compact)

## Exercise: McIntosh classification



- What would be the McIntosh classification of active region NOAA 12470 on 18 Dec 2015?
  - Cso
  - Cho
  - Eso
  - Eho
  - Esi
  - Ehi

SWIC - Collaboration between STCE, Koninklijke Luchtmacht, KNMI



In case of doubt: zoom out! Back in the 80s and 90s, McIntosh did not have those crisp high-resolution images at his disposal as we have with e.g. SDO!

# Flare predictions

THE ASTROPHYSICAL JOURNAL LETTERS, 747:L41 (7pp), 2012 March 10

BLOOMFIELD ET AL.

**Table 2**  
McIntosh Classification Flare Statistics

| McIntosh<br>Classes <sup>a</sup> | SWPC (1988–1996) |              |     | Kildahl (1969–1976) <sup>b</sup> |        |              | Combined Flare Rate (24 hr <sup>-1</sup> ) |                |               |      | Poisson Flare Probability (%) |      |               |    |    |    |    |
|----------------------------------|------------------|--------------|-----|----------------------------------|--------|--------------|--|----------------|---------------|------|-------------------------------|------|---------------|----|----|----|----|
|                                  | Region           | Total Flares |     |                                  | Region | Total Flares |  |                | In GOES Class |      |                               |      | In GOES Class |    |    |    |    |
|                                  |                  | Count        | C   | M                                |        | X            | Count                                      | C <sup>c</sup> | M             | X    | C                             | M    | X             | ±σ | C  | M  | X  |
| AXX                              | 2748             | 82           | 10  | 0                                | 2517   | 75.1         | 31   | 3              | 0.03          | 0.01 | 0.00                          | 0.01 | 3             | 1  | 0  | 1  | 4  |
| BXO                              | 3342             | 217          | 18  | 1                                | 1906   | 123.8        | 41   | 2              | 0.06          | 0.01 | 0.00                          | 0.01 | 6             | 1  | 0  | 1  | 7  |
| BXI                              | 0                | 0            | 0   | 0                                | 334    | 0.0          | 20   | 0              | 0.00          | 0.06 | 0.00                          | 0.05 | 0             | 6  | 0  | 6  | 6  |
| HRX                              | 336              | 21           | 1   | 0                                | 211    | 13.2         | 7  | 1              | 0.06          | 0.01 | 0.00                          | 0.04 | 6             | 1  | 0  | 2  | 8  |
| HSX                              | 1968             | 94           | 21  | 0                                | 1963   | 93.8         | 99   | 6              | 0.05          | 0.03 | 0.00                          | 0.02 | 5             | 3  | 0  | 3  | 8  |
| HAX                              | 598              | 49           | 13  | 0                                | 222    | 18.2         | 14   | 0              | 0.08          | 0.03 | 0.00                          | 0.03 | 8             | 3  | 0  | 3  | 11 |
| HHX                              | 53               | 3            | 1   | 0                                | 150    | 8.5          | 16   | 2              | 0.06          | 0.08 | 0.01                          | 0.07 | 6             | 8  | 1  | 9  | 14 |
| HXX                              | 49               | 11           | 2   | 0                                | 38     | 8.5          | 7  | 0              | 0.22          | 0.10 | 0.00                          | 0.11 | 20            | 10 | 0  | 10 | 28 |
| CRO                              | 745              | 102          | 3   | 0                                | 368    | 50.4         | 20   | 2              | 0.14          | 0.02 | 0.00                          | 0.03 | 13            | 2  | 0  | 2  | 15 |
| CRI                              | 6                | 2            | 0   | 0                                | 152    | 50.7         | 7  | 0              | 0.33          | 0.04 | 0.00                          | 0.08 | 28            | 4  | 0  | 4  | 31 |
| CSO                              | 1504             | 284          | 27  | 0                                | 1020   | 192.6        | 40   | 1              | 0.19          | 0.03 | 0.00                          | 0.02 | 17            | 3  | 0  | 3  | 19 |
| CSI                              | 14               | 8            | 2   | 0                                | 211    | 120.6        | 16   | 2              | 0.57          | 0.08 | 0.01                          | 0.07 | 44            | 8  | 1  | 9  | 48 |
| CAO                              | 1455             | 361          | 38  | 2                                | 232    | 57.6         | 18   | 1              | 0.25          | 0.03 | 0.00                          | 0.02 | 22            | 3  | 0  | 3  | 25 |
| CAI                              | 27               | 14           | 6   | 0                                | 166    | 86.1         | 19   | 0              | 0.52          | 0.13 | 0.00                          | 0.07 | 40            | 12 | 0  | 12 | 48 |
| CHO                              | 88               | 21           | 2   | 1                                | 112    | 26.7         | 8  | 1              | 0.24          | 0.05 | 0.01                          | 0.07 | 21            | 5  | 1  | 6  | 26 |
| CHI                              | 2                | 1            | 0   | 0                                | 29     | 14.5         | 6  | 0              | 0.50          | 0.19 | 0.00                          | 0.18 | 39            | 18 | 0  | 18 | 50 |
| CKO                              | 135              | 59           | 11  | 0                                | 52     | 22.7         | 13   | 2              | 0.44          | 0.13 | 0.01                          | 0.07 | 35            | 12 | 1  | 13 | 44 |
| CKI                              | 17               | 14           | 6   | 0                                | 28     | 23.1         | 6  | 2              | 0.82          | 0.27 | 0.04                          | 0.15 | 56            | 23 | 4  | 27 | 68 |
| DRO                              | 63               | 12           | 3   | 0                                | 75     | 14.3         | 6  | 0              | 0.19          | 0.07 | 0.00                          | 0.09 | 17            | 6  | 0  | 6  | 23 |
| DRI                              | 2                | 7            | 0   | 0                                | 54     | 189.0        | 7  | 1              | 3.50          | 0.12 | 0.02                          | 0.13 | 97            | 12 | 2  | 13 | 97 |
| DSO                              | 546              | 198          | 26  | 1                                | 553    | 200.5        | 51   | 6              | 0.36          | 0.07 | 0.01                          | 0.03 | 30            | 7  | 1  | 7  | 36 |
| DSI                              | 39               | 34           | 6   | 0                                | 246    | 214.5        | 31   | 1              | 0.87          | 0.13 | 0.00                          | 0.06 | 58            | 12 | 0  | 12 | 63 |
| DSC                              | 0                | 0            | 0   | 0                                | 20     | 0.0          | 5  | 2              | 0.00          | 0.25 | 0.10                          | 0.22 | 0             | 22 | 10 | 30 | 30 |
| DAO                              | 1775             | 784          | 124 | 4                                | 288    | 127.2        | 28   | 2              | 0.44          | 0.07 | 0.00                          | 0.02 | 36            | 7  | 0  | 7  | 40 |
| DAI                              | 391              | 419          | 70  | 6                                | 324    | 347.2        | 58   | 7              | 1.07          | 0.18 | 0.02                          | 0.04 | 66            | 16 | 2  | 18 | 72 |
| DAC                              | 8                | 5            | 3   | 0                                | 46     | 28.8         | 12   | 1              | 0.62          | 0.28 | 0.02                          | 0.14 | 46            | 24 | 2  | 26 | 60 |
| DHO                              | 46               | 26           | 1   | 1                                | 43     | 24.3         | 11   | 0              | 0.57          | 0.13 | 0.01                          | 0.11 | 43            | 13 | 1  | 14 | 51 |
| DHI                              | 11               | 14           | 1   | 0                                | 41     | 52.2         | 3  | 0              | 1.27          | 0.08 | 0.00                          | 0.14 | 72            | 7  | 0  | 7  | 74 |
| DHC                              | 0                | 0            | 0   | 0                                | 6      | 0.0          | 2  | 0              | 0.00          | 0.33 | 0.00                          | 0.41 | 0             | 28 | 0  | 28 | 28 |
| DKO                              | 217              | 178          | 55  | 5                                | 43     | 35.3         | 14   | 2              | 0.82          | 0.27 | 0.03                          | 0.06 | 56            | 23 | 3  | 25 | 67 |
| DKI                              | 223              | 288          | 69  | 6                                | 88     | 113.7        | 42   | 6              | 1.29          | 0.36 | 0.04                          | 0.06 | 73            | 30 | 4  | 33 | 81 |
| DKC                              | 57               | 93           | 35  | 5                                | 100    | 163.2        | 72   | 10             | 1.63          | 0.68 | 0.10                          | 0.08 | 80            | 49 | 9  | 54 | 91 |



Bloomfield S. et al. (2012): Toward Reliable Benchmarking of Solar Flare Forecasting Methods  
<http://adsabs.harvard.edu/abs/2012ApJ...747L..41B>

# Flare predictions

THE ASTROPHYSICAL JOURNAL LETTERS, 747:L41 (7pp), 2012 March 10

BLOOMFIELD ET AL.

**Table 2**  
McIntosh Classification Flare Statistics

| McIntosh<br>Classes <sup>a</sup> | SWPC (1988–1996) |              |     | Kildahl (1969–1976) <sup>b</sup> |        |              | Combined Flare Rate (24 hr <sup>-1</sup> ) |                |               |      | Poisson Flare Probability (%) |      |               |    |    |                         |     |
|----------------------------------|------------------|--------------|-----|----------------------------------|--------|--------------|--|----------------|---------------|------|-------------------------------|------|---------------|----|----|-------------------------|-----|
|                                  | Region           | Total Flares |     |                                  | Region | Total Flares |  |                | In GOES Class |      |                               |      | In GOES Class |    |    | Above GOES <sup>d</sup> |     |
|                                  |                  | Count        | C   | M                                |        | X            | Count                                      | C <sup>c</sup> | M             | X    | C                             | M    | X             | ±σ | C  | M                       | X   |
| ESO                              | 95               | 37           | 6   | 0                                | 82     | 31.9         | 14   | 0              | 0.39          | 0.11 | 0.00                          | 0.08 | 32            | 11 | 0  | 11                      | 39  |
| ESL                              | 18               | 33           | 1   | 0                                | 78     | 143.0        | 22   | 2              | 1.83          | 0.24 | 0.02                          | 0.10 | 84            | 21 | 2  | 23                      | 88  |
| EAO                              | 459              | 267          | 61  | 0                                | 47     | 27.3         | 10   | 4              | 0.58          | 0.14 | 0.01                          | 0.04 | 44            | 13 | 1  | 14                      | 52  |
| EAI                              | 295              | 370          | 83  | 2                                | 82     | 102.8        | 48   | 1              | 1.25          | 0.35 | 0.01                          | 0.05 | 71            | 29 | 1  | 30                      | 80  |
| EAC                              | 3                | 5            | 1   | 0                                | 17     | 28.3         | 6  | 3              | 1.67          | 0.35 | 0.15                          | 0.22 | 81            | 30 | 14 | 39                      | 89  |
| EHO                              | 42               | 31           | 6   | 0                                | 39     | 28.8         | 6  | 0              | 0.74          | 0.15 | 0.00                          | 0.11 | 52            | 14 | 0  | 14                      | 59  |
| EHI                              | 15               | 24           | 6   | 0                                | 45     | 72.0         | 28   | 4              | 1.60          | 0.57 | 0.07                          | 0.13 | 80            | 43 | 6  | 47                      | 89  |
| EHC                              | 2                | 9            | 0   | 0                                | 4      | 18.0         | 8  | 0              | 4.50          | 1.33 | 0.00                          | 0.41 | 99            | 74 | 0  | 74                      | 100 |
| EKO                              | 185              | 173          | 35  | 3                                | 52     | 48.6         | 20   | 1              | 0.94          | 0.23 | 0.02                          | 0.06 | 61            | 21 | 2  | 22                      | 69  |
| EKI                              | 423              | 703          | 173 | 23                               | 81     | 134.6        | 103  | 11             | 1.66          | 0.55 | 0.07                          | 0.04 | 81            | 42 | 7  | 46                      | 90  |
| EKC                              | 103              | 278          | 132 | 17                               | 63     | 170.0        | 149  | 21             | 2.70          | 1.69 | 0.23                          | 0.08 | 93            | 82 | 20 | 85                      | 99  |
| FRI                              | 0                | 0            | 0   | 0                                | 2      | 0.0          | 1  | 0              | 0.00          | 0.50 | 0.00                          | 0.71 | 0             | 39 | 0  | 39                      | 39  |
| FSO                              | 14               | 9            | 3   | 0                                | 13     | 8.4          | 6  | 1              | 0.64          | 0.33 | 0.04                          | 0.19 | 47            | 28 | 4  | 31                      | 64  |
| FSI                              | 6                | 12           | 0   | 0                                | 8      | 16.0         | 15   | 0              | 2.00          | 1.07 | 0.00                          | 0.27 | 86            | 66 | 0  | 66                      | 95  |
| FACD                             | 73               | 63           | 16  | 0                                | 3      | 2.6          | 0  | 0              | 0.86          | 0.21 | 0.00                          | 0.11 | 58            | 19 | 0  | 19                      | 66  |
| FAI                              | 91               | 106          | 35  | 3                                | 12     | 14.0         | 8  | 0              | 1.16          | 0.42 | 0.03                          | 0.10 | 69            | 34 | 3  | 36                      | 80  |
| FHO                              | 9                | 5            | 1   | 0                                | 10     | 5.6          | 0  | 0              | 0.56          | 0.05 | 0.00                          | 0.23 | 43            | 5  | 0  | 5                       | 46  |
| FHI                              | 10               | 17           | 9   | 0                                | 18     | 30.6         | 15   | 0              | 1.70          | 0.86 | 0.00                          | 0.19 | 82            | 58 | 0  | 58                      | 92  |
| FHC                              | 0                | 0            | 0   | 0                                | 5      | 0.0          | 4  | 0              | 0.00          | 0.80 | 0.00                          | 0.45 | 0             | 55 | 0  | 55                      | 55  |
| FKO                              | 97               | 165          | 29  | 1                                | 19     | 32.3         | 6  | 0              | 1.70          | 0.30 | 0.01                          | 0.09 | 82            | 26 | 1  | 27                      | 87  |
| FKI                              | 235              | 517          | 161 | 17                               | 47     | 103.4        | 106  | 17             | 2.20          | 0.95 | 0.12                          | 0.06 | 89            | 61 | 11 | 66                      | 96  |
| FKC                              | 93               | 233          | 146 | 24                               | 27     | 67.6         | 39   | 13             | 2.51          | 1.54 | 0.31                          | 0.09 | 92            | 79 | 27 | 84                      | 99  |

**Notes.**

<sup>a</sup> Only includes classifications producing  $\geq 1$  C-, M-, or X-class flare in either time range.

<sup>b</sup> From Kildahl (1980).

<sup>c</sup> Non-integer flare numbers result from use of observed C-class rates from SWPC (1988–1996).

<sup>d</sup> "Above GOES X1.0" is equivalent to "In GOES Class X".

SWIC - Collaboration between STCE, Koninklijke Luchtmacht, KNMI



Bloomfield S. et al. (2012): Toward Reliable Benchmarking of Solar Flare Forecasting Methods  
<http://adsabs.harvard.edu/abs/2012ApJ...747L..41B>

# Flare predictions

- Likelihood (terminology)

| Descriptive phrase | Mean minimum | All data mean | Mean maximum |
|--------------------|--------------|---------------|--------------|
| Definite           | 76.6         | 80.1          | 83.5         |
| Almost certain     | 73.6         | 78.9          | 84.1         |
| Highly probable    | 64.2         | 71.4          | 78.3         |
| A good chance      | 54.3         | 64.5          | 74.3         |
| Likely             | 49.9         | 59.3          | 68.4         |
| Quite likely       | 51.8         | 59.2          | 66.4         |
| Probable           | 47.5         | 57.2          | 66.7         |
| Better than even   | 47.1         | 56.5          | 65.6         |
| Possible           | 28.8         | 43.3          | 57.5         |
| Improbable         | 10.6         | 18.0          | 25.3         |
| Highly unlikely    | 9.8          | 16.6          | 23.3         |
| Unlikely           | 6.6          | 13.6          | 20.4         |
| Seldom             | 6.2          | 11.7          | 17.1         |
| Impossible         | 5.5          | 8.5           | 11.4         |
| Rare               | 3.9          | 8.1           | 12.2         |

SWH Exhibit 3: Research results for probability-related terms (values as percentages)



The figure was taken from D. A. Hillson: **Describing probability: The limitations of natural language**  
<http://www.risk-doctor.com/pdf-files/emeamay05.pdf>

Other (nearly equivalent) terms are used in SWx (SWPC, SIDC):

**Probability (%) Terminology**

|        |                       |
|--------|-----------------------|
| 0-10   | Unlikely              |
| 10-25  | Small chance          |
| 25-50  | A chance; Possible    |
| 50-75  | Likely                |
| 75-100 | Very likely; Expected |

As far as we know, there's no clear terminology consistently applied internal or between the SWx prediction services.

# Flare predictions

- Likelihood (terminology)

**RWC Belgium: Decision on use of scales and wording**

Flare forecast

| ISES   |   |
|--|---|
| 0 = Quiet (<50% probability of C-class flares)                         |   |
| 1 = Eruptive (C-class flares expected, probability >=50%)              |   |
| 2 = Active (M-class flares expected, probability >=50%)                |   |
| 3 = Major flares expected (X-class flares expected, probability >=50%) |   |
| Activity level   | wording for bulletin  |
| <50% probability of C-class flares                                     | Quiet solar conditions  |
| C-class flares expected, probability >=50%                             | C-class flaring activity/conditions expected<br>we expect solar active conditions ([C,M,X]-class flares)<br>with a high/small probability for a [C, M, X]-flare |
| M-class flares expected, probability >=50%                             | M-class flares expected / idem as above   |
| X-class flares expected, probability >=50%                             | X-class flares expected / idem as above   |

Unofficial terminology deduced from various SWx reports/services



| Probability (%) | Terminology           |
|-----------------|-----------------------|
| 0-10            | Unlikely              |
| 10-25           | Small chance          |
| 25-50           | A chance; Possible    |
| 50-75           | Likely                |
| 75-100          | Very likely; Expected |

**This is a topic under continued improvement / discussion....**

SWIC - Collaboration between STCE, Koninklijke Luchtmacht, KNMI



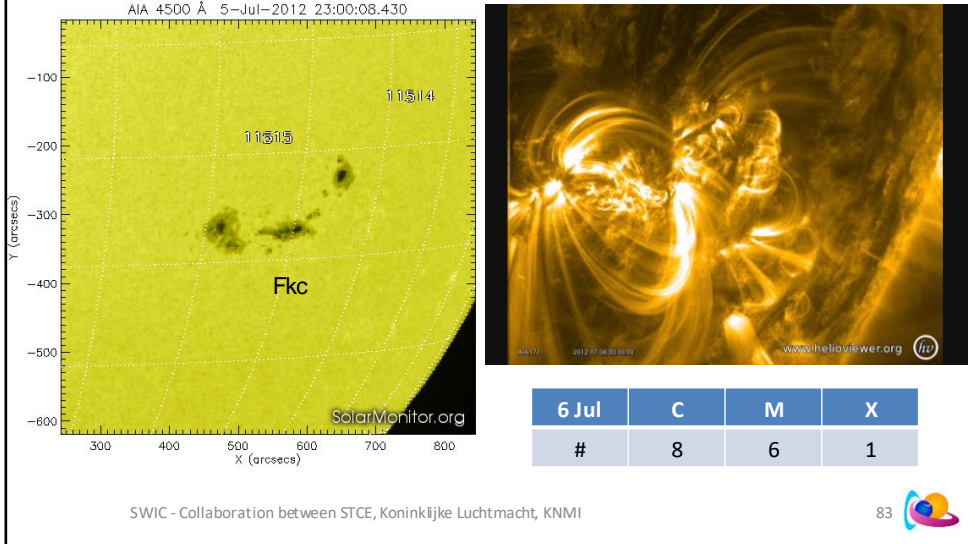
The figure was taken from D. A. Hillson: **Describing probability: The limitations of natural language**  
<http://www.risk-doctor.com/pdf-files/emeamay05.pdf>

Other (nearly equivalent) terms are used in SWx (SWPC, SIDC,...):

| Probability (%) | Terminology           |
|-----------------|-----------------------|
| 0-10            | Unlikely              |
| 10-25           | Small chance          |
| 25-50           | A chance; Possible    |
| 50-75           | Likely                |
| 75-100          | Very likely; Expected |

As far as we know, there's no clear terminology consistently applied internal or between the SWx prediction services.

# Flare predictions: an example

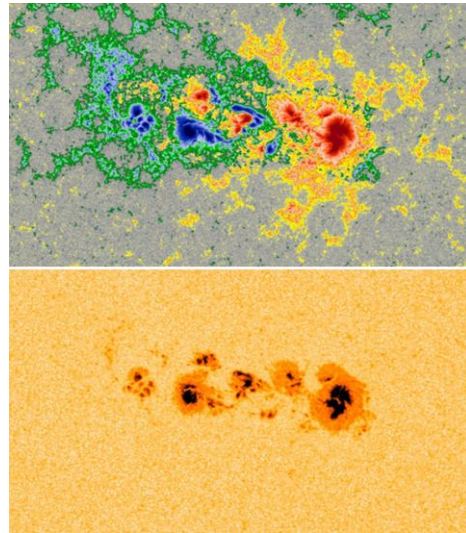


McIntosh, P.S. (1990): The classification of sunspot groups  
<http://adsabs.harvard.edu/abs/1990SoPh..125..251M>

6 July 2012: 8 C, 6 M, X (X1)

# Flare predictions

- Mount Wilson (Hale) classification
  - Hale (1919)
  - Kunzel (1965)
    - Delta spots
- Based on the magnetic properties of a sunspot group
- 7 options:
  - A ( $\alpha$ )
  - B ( $\beta$ ), BG ( $\beta\gamma$ ), G ( $\gamma$ )
  - BD ( $\beta\delta$ ), BGD ( $\beta\gamma\delta$ ), GD ( $\gamma\delta$ )



SWIC - Collaboration between STCE, Koninklijke Luchtmacht, KNMI

84



Jaeggli and Norton (2016): The Magnetic Classification of Solar Active Regions 1992-2015  
<http://adsabs.harvard.edu/abs/2016ApJ...820L..11J>  
<http://iopscience.iop.org/article/10.3847/2041-8205/820/1/L11/pdf>

Magnetic classifications provide a simple way to describe the configuration of the magnetic flux and sunspots in a solar active region (AR). The Mount Wilson (or Hale) classification system for sunspot groups put forward by Hale et al. (1919) has been used for nearly a century. In the original Hale classification scheme, the designation (**alpha**) is given to regions that contain a single sunspot or sunspot group all having the same polarity. Generally, these also have a weaker opposite polarity counterpart that is not strong or concentrated enough to produce sunspots. (**beta**) is assigned to regions that have two sunspots or sunspot groups of opposite polarity. The classification (**gamma**) is appended to the above classes to indicate the AR has a complex region of sunspots with intermixed polarity. This classification can also be used individually to describe an AR that has no organized magnetic behavior. As an addendum to the original scheme, Kunzel (1965) proposed an additional classification to modify the existing three. (**delta**) indicates that at least one sunspot in the region contains opposite magnetic polarities inside of a common penumbra separated by no more than  $2^\circ$  in heliographic distance (24 Mm or 33" at disk center).

Also at STCE: <http://www.stce.be/news/222/welcome.html>

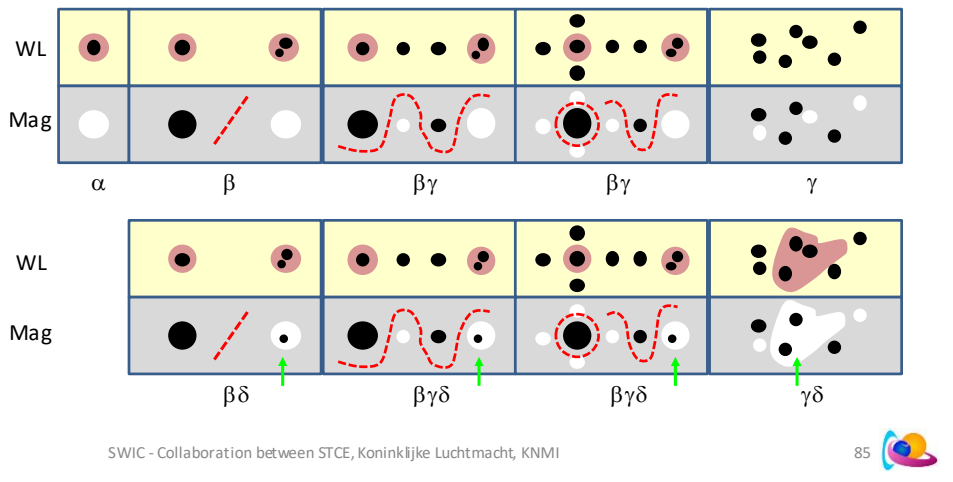
Make sure to avoid classifying too quickly a sunspot group as a delta or a gamma type when this sunspot group is still very close to the limb. Indeed, line-of-sight may come into play that show an unipolar spot as if it would have a delta structure.

See STCE: <http://www.stce.be/news/188/welcome.html>

The pictures to the right are from SDO/HMI and show a magnetogram and a white light image of NOAA 1875 on 23 October 2013.

# Flare predictions

- Mount Wilson (Hale) classification - Sketches



See STCE: <http://www.stce.be/news/188/welcome.html>

Text underneath based on SWPCUser Guide, SWPCGlossary (<https://www.swpc.noaa.gov/content/space-weather-glossary#m>), Mount Wilson (<http://obs.astro.ucla.edu/spotlgn.html>) and SIDC old webpages (<http://sidc.oma.be/educational/classification.php#magnetic>).

Alpha - Unipolar group; that is, all plus or all minus magnetic field

Beta - A bipolar group; that is a mix of plus and minus magnetic polarities exist, with the plus well divided from the minus with one polarity in each end (E-W) of the group, i.e. "easily divided by a simple line".

Beta-Gamma - A group which is generally bipolar but which is lacking a well marked dividing line between the opposite polarity regions ("you need to lift your pencil to divide the polarities" or "no single, continuous line can be drawn between spots of opposite polarities").

Gamma - a group in which the polarities are so completely mixed that no bipolar structure can obviously be recognized.

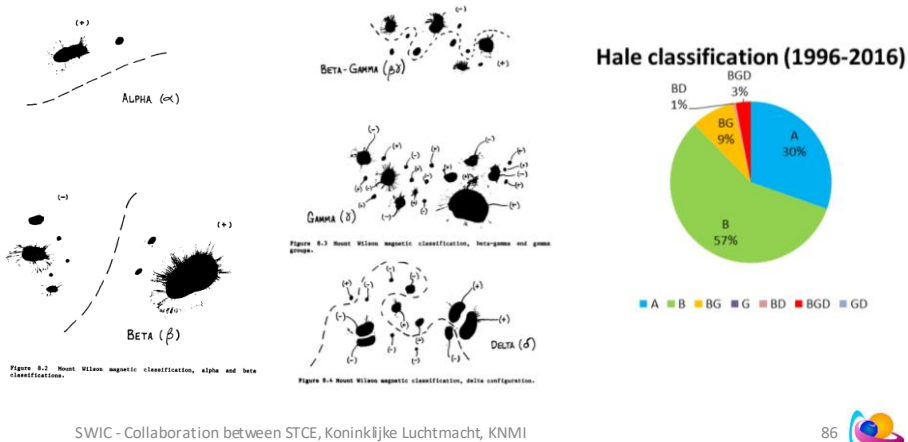
Delta - This is a sub-classification for non-unipolar regions. It means at least two opposing polarity umbrae are within two heliographic degrees of each other and share the same penumbra.

The chart with the % of Hale classification was based on the NOAA reports at <https://solarscience.msfc.nasa.gov/greenwch.shtml> for the period Jan 1996-September 2016. A total of 32965 classifications were made. The percentage of reported delta's in the sunspot groups is 3.5%.

[The determination of the Hale class is done on the (magnetic polarity of the) sunspots, NOT the magnetograms!]

# Flare predictions

- Mount Wilson (Hale) classification - Examples



Figures from Townsend et al. (1982): A source book of the solar-geophysical environment <http://www.dtic.mil/dtic/tr/fulltext/u2/a138682.pdf>

See STCE: <http://www.stce.be/news/188/welcome.html>

Text underneath based on SWPC User Guide, SWPC Glossary (<https://www.swpc.noaa.gov/content/space-weather-glossary#m>), Mount Wilson (<http://obs.astro.ucla.edu/spotlgn.html>) and SIDC old webpages (<http://sidc.oma.be/educational/classification.php#magnetic>).

Alpha - Unipolar group; that is, all plus or all minus magnetic field

Beta - A bipolar group; that is a mix of plus and minus magnetic polarities exist, with the plus well divided from the minus with one polarity in each end (E-W) of the group, i.e. "easily divided by a simple line".

Beta-Gamma - A group which is generally bipolar but which is lacking a well marked dividing line between the opposite polarity regions ("you need to lift your pencil to divide the polarities" or "no single, continuous line can be drawn between spots of opposite polarities").

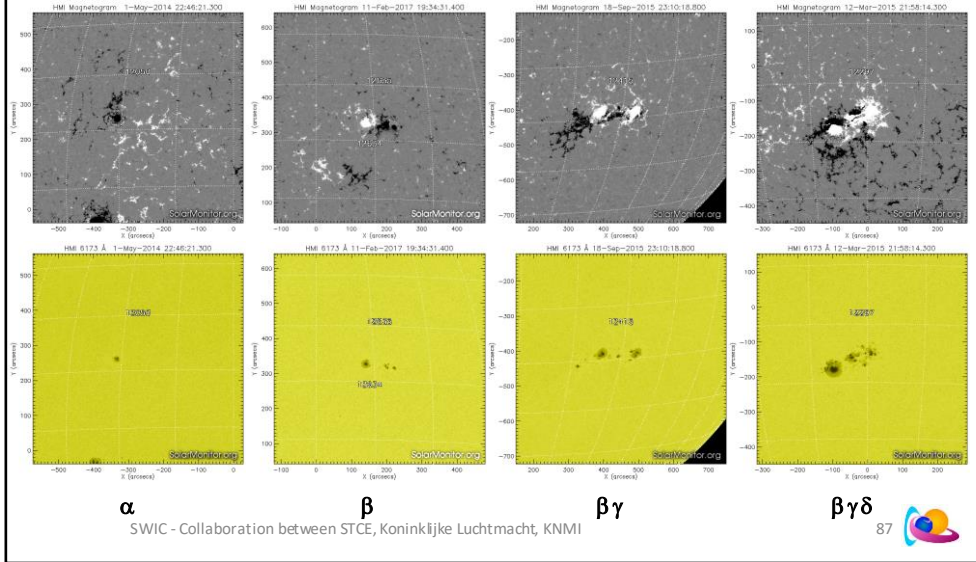
Gamma - a group in which the polarities are so completely mixed that no bipolar structure can obviously be recognized.

Delta - This is a sub-classification for non-unipolar regions. It means at least two opposing polarity umbrae are within two heliographic degrees of each other and share the same penumbra.

The chart with the % of Hale classification was based on the NOAA reports at <https://solarscience.msfc.nasa.gov/greenwch.shtml> for the period Jan 1996-September 2016. A total of 32965 classifications were made. The percentage of reported delta's in the sunspot groups is 3.5%.

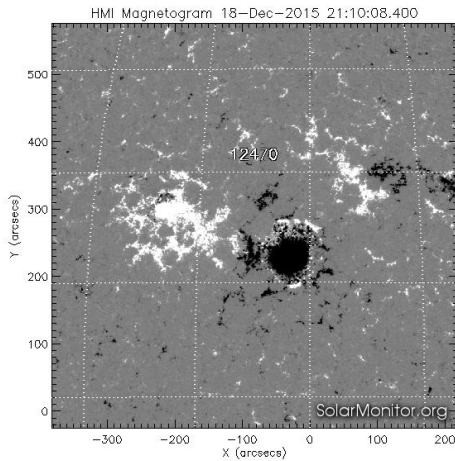
[The determination of the Hale class is done on the (magnetic polarity of the) sunspots, NOT the magnetograms!]

# Examples of Hale classification



Examples from <https://www.solarmonitor.org/index.php>

## Exercise: Hale classification



- What would be the Hale classification of active region NOAA 12470?
  - $\beta$
  - $\beta\delta$
  - $\beta\gamma$
  - $\beta\gamma\delta$

SWIC - Collaboration between STCE, Koninklijke Luchtmacht, KNMI

# Flare predictions

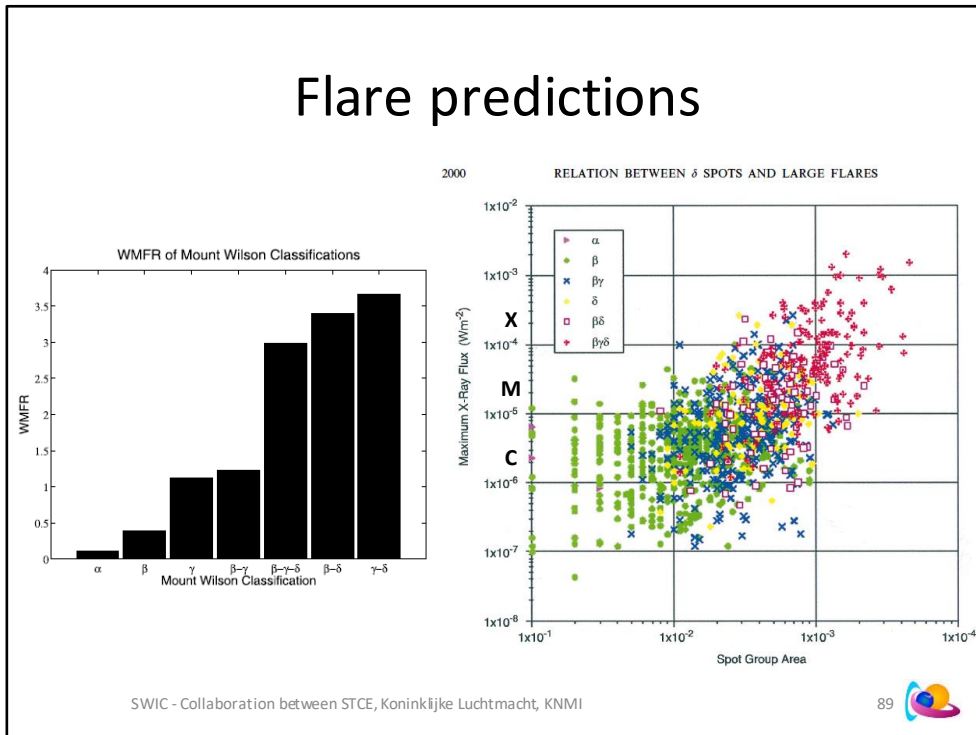


Figure left: Shin et al. (2016): Development of Daily Maximum Flare-Flux Forecast Models for Strong Solar Flares - <http://adsabs.harvard.edu/abs/2016SoPh..291..897S>

Most of the complex sunspots of the Mount Wilson magnetic classification that are characterized by *gamma* and/or *delta* show higher WMFR values (WMFR: weighted mean flare rate).

Figure right: Sammis et al. (2000): The Dependence of Large Flare Occurrence on the Magnetic Structure of Sunspots

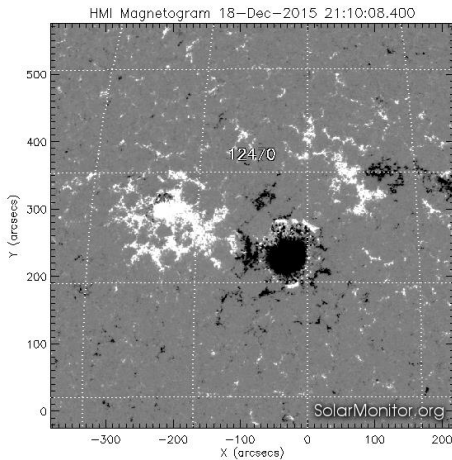
<http://adsabs.harvard.edu/abs/2000ApJ...540..583S>  
<http://iopscience.iop.org/article/10.1086/309303/pdf>

In Figure 2, we plot the largest flare from each active region against the largest reported area from that region, for each magnetic class. This shows a roughly linear connection between the logs of SXR flux and active region maximum areas. But the dependence on magnetic class is much stronger. All flares above X4 ( $4 \cdot 10^{-4} \text{ Wm}^{-2}$ ) come from 11 bgd regions of area greater than 1000 MH. Thus, these two conditions constitute a necessary, but not sufficient, condition for an X4 flare. ... The general slope of Figure 2, upward and to the right, confirms the well-known fact that large active regions have more large flares than small ones and also tend to be more complex.

The probability of a bgd spot group larger than 1000 MH producing an X1 or greater event is only 40%, accounting for about 60% of those events. However, 82% of X1 flares and 100% of the more important X4 events occur in delta spots. By comparison, only 24% of all regions greater than 1000 MH produce X1.

The increase in flare size with spot size shows that although the sharp gradient and currents of the delta configuration provide the appropriate situation for flare occurrence, the scale offered by a large spot is important in producing great flares. All large flares (X4 or higher) occur in spot groups of area greater than 1000 MH classified bgd. Predictions that X1 flares will occur for such a class will enjoy a 41% probability of success with no other considerations. Adding some of the considerations mentioned by Zirin & Liggett (1987) and Zirin & Marquette (1991), particularly H-alpha brightness and flux emergence, should improve these predictions considerably.

## Exercise: Flare likelihood based on McIntosh and Hale classification



SWIC - Collaboration between STCE, Koninklijke Luchtmacht, KNMI



- Judging the McIntosh and Hale classification of active region NOAA 12470 and knowing its area is 690 MH, what would be its likelihood to produce an M-class flare?
  - Unlikely
  - Small chance
  - Possible
  - Likely
  - Very likely

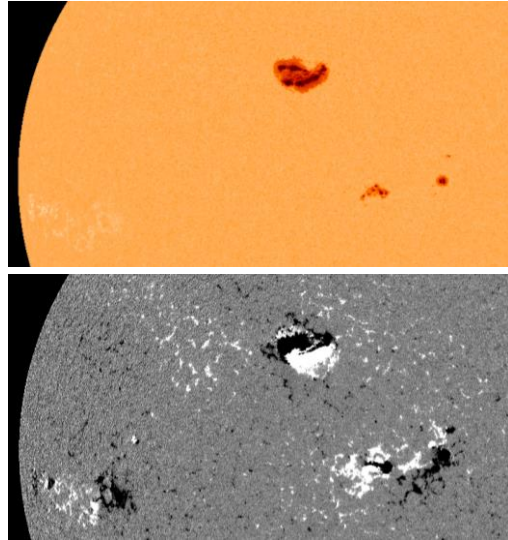
NOAA 12470

- McIntosh
  - Eho: C/M/X = 52/14/0% => A small chance on an M-class flare
- Hale
  - Beta + 690 MH => produces mostly C-class flares => A small chance on an M-class flare

NOAA 12470 would only produce one low-level C-class flare.

# Flare predictions

- Magnetic shear
- Magnetic helicity
- Group filament
  - E.g. 7 June 2011
- Flaring history
- Evolution stage of group
  - Increase, mature, decay
- Size of the spots
- Superactive regions
  - In SC21-23, 45 SARs produced 44% of all X-class flares...



SWIC - Collaboration between STCE, Koninklijke Luchtmacht, KNMI



Massi et al.: <http://www3.mpifr-bonn.mpg.de/staff/mmassi/c4-Model.pdf>

⇒ Magnetic shear: the vector magnetic field is oriented parallel to the neutral line than perpendicular to it. Another example of magnetic shear is at MSFC: <https://solarscience.msfc.nasa.gov/flares.shtml>

From <https://solarscience.msfc.nasa.gov/flares.shtml>

Stable sunspots tend to be fairly symmetrical unless there is extensive magnetic shear nearby from emerging magnetic flux or the passing of an area of opposite magnetic polarity. Magnetic shearing can cause large portions of sunspot penumbras to distort or vanish.

Lee et al. (2012): Solar Flare Occurrence Rate and Probability in Terms of the Sunspot Classification Supplemented with Sunspot Area and Its Changes

<http://adsabs.harvard.edu/abs/2012SoPh..281..639L>

We used sunspot data from 1996 to 2010. We noted that sunspot area and its changes can be a proxy of magnetic flux and its emergence/cancellation, respectively. We classify each sunspot group into the following sub-groups: “Large” and “Small” according to its area and “Decrease”, “Steady”, and “Increase” according to its area changes. Major results from this study can be summarized as follows.

i) In the McIntosh sunspot group classification (60 classes in total), the most flare-productive 11 sunspot groups are ‘Dai’, ‘Eai’, ‘Fai’, ‘Dko’, ‘Eko’, ‘Dki’, ‘Dkc’, ‘Eki’, ‘Ekc’, ‘Fki’, and ‘Fkc’.

ii) In case of large and compact groups, the flare probabilities noticeably increase with sunspot area.

iii) When the sunspot area increases, the flare occurrence rates and probabilities noticeably increase, especially for major flares.

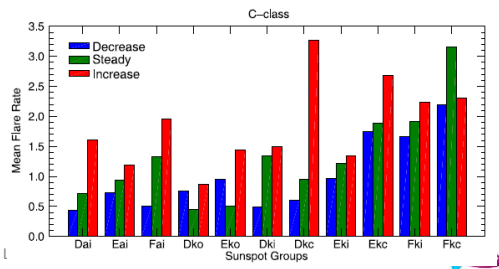
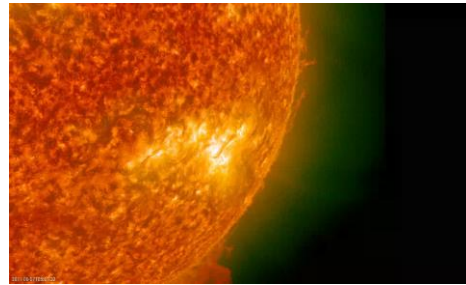
Our results show that the sunspot classes having the top five flare occurrence rates are ‘Fkc’, ‘Ekc’, ‘Dkc’, ‘Fki’, and ‘Eki’, ... We note that ‘Fkc’ and ‘Ekc’ sunspot groups are included in all three studies. This fact may imply that large, asymmetric penumbra sunspot groups should be most flare productive.

From the relationship between flare probability and sunspot group area, in the case of large and compact groups, the solar flare probabilities are higher than those of other groups.

In the case of “Increase” sub-groups, the flare occurrence rates and probabilities are higher than other sub-groups. This means that when the sunspot area is larger, then the flare probability becomes higher. This is statistical evidence that magnetic flux emergence is an important mechanism for triggering solar flares, because sunspot area can be a good proxy of magnetic flux (Zharkov and Zharkova, 2006). ...

# Flare predictions

- Magnetic shear
- Magnetic helicity
- Group filament
  - E.g. 7 June 2011
- Flaring history
- Evolution stage of group
  - Increase, mature, decay
- Size of the spots
- Superactive regions
  - In SC21-23, 45 SARs produced 44% of all X-class flares...



SWIC - Collaboration between STCE, Koninklijke I

7 June 2011 event:

STCE: <http://www.stce.be/news/353/welcome.html>

STCE: <http://www.stce.be/news/x137x/welcome.html>

Science at NASA: [https://science.nasa.gov/science-news/science-at-nasa/2011/11jul\\_darkfireworks](https://science.nasa.gov/science-news/science-at-nasa/2011/11jul_darkfireworks)

## Superactive regions

Chen et al. (2011): Statistical properties of superactive regions during solar cycles 19-23

<http://adsabs.harvard.edu/abs/2011A%26A...534A..47C>

<https://www.aanda.org/articles/aa/pdf/2011/10/aa16790-11.pdf>

Our results indicate that these 45 SARs produced 44% of all the X class X-ray flares during solar cycles 21–23, and that all the SARs are likely to produce a very fast CME. The latitudinal distributions of SARs display the Maunder butterfly diagrams and SARs occur preferentially in the maximum period of each solar cycle. Northern hemisphere SARs dominated in solar cycles 19 and 20 and southern hemisphere SARs dominated in solar cycles 21 and 22. In solar cycle 23, however, SARs occurred about equally in each hemisphere. There are two active longitudes in both the northern and southern hemispheres, about 160°–200° apart and with half-widths of 45°.

Criteria to be considered as a SAR:

We refer to an AR as a SAR, if three of the four criterion conditions listed in Table 1 are fulfilled. The soft X-ray flare index is the sum of the numerical

multipliers of M and X class X-ray flares for the disk transit of the AR. When applying all four criterion conditions, there are 45 SARs selected in solar cycles 21–23.

**Table 1.** The four criterion conditions used to parameterize a SAR.

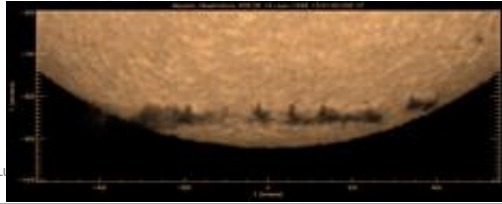
| Criterion condition  | Value     |
|----------------------|-----------|
| Maximum sunspot area | >1000 MH  |
| Flare index          | >10.0     |
| 10.7 cm peak flux    | >1000 sfu |
| $\Delta TSI$         | <-0.1%    |

# Filaments & prominences

- Chromospheric features
  - Protruding into corona
  - H-alpha and EUV
  - Relatively cool (10.000K)
- Prominences at limb, filaments on solar disk
  - Same features!
- Mark the transition between positive and negative magnetic areas
  - Appear all over solar disk
- Location
  - In active region
    - Group filament
  - Outside active region
    - Quiescent filament
  - **Polar crown filament**



Large NE Solar Filament (Filament and Prominence) by Jeff Agarwal, 01-45 UTC, April 26, 2015, Quezon City, Philippines  
Lent 100 cm ST-100 H-alpha telescope, 2.5x Televue Powermate, DMCH10003 Camera



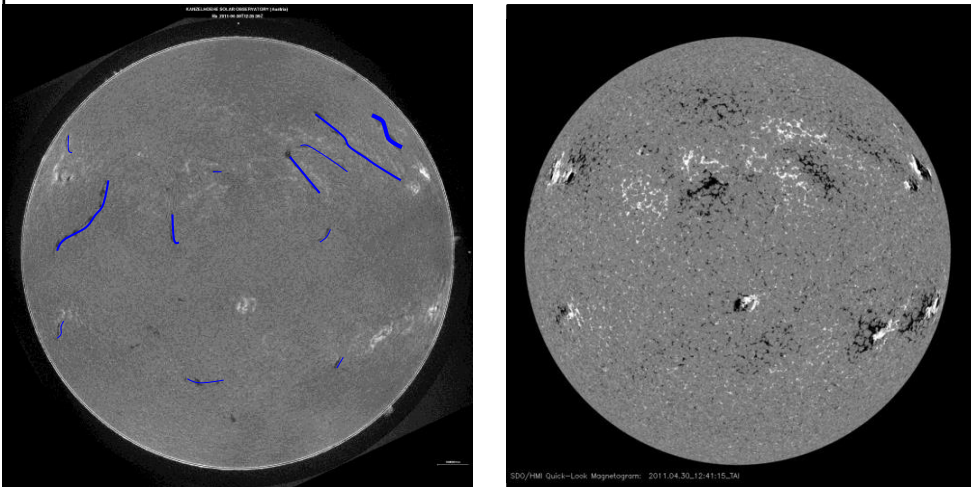
SWIC - Collaboration between STCE, Koninklijke L

More info on filaments at <http://www.stce.be/news/219/welcome.html>

More info on polar crown filaments at:

- <http://solar.physics.montana.edu/wood/99Prom.html>
- [https://science.nasa.gov/science-news/science-at-nasa/2008/17sep\\_polarcrown](https://science.nasa.gov/science-news/science-at-nasa/2008/17sep_polarcrown)

# Filaments & prominences



SWIC - Collaboration between STCE, Koninklijke Luchtmacht, KNMI



Parenti S. (2014): Solar Prominences: Observations  
<http://link.springer.com/article/10.12942/lrsp-2014-1>

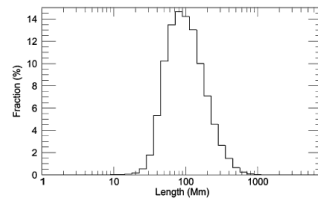
# Filament/Prominence eruptions

- Quiescent
  - Not associated to AR
  - Weeks to months
- Length
  - Long filaments ( $> 15^\circ$ )
    - About 18%
  - More prone to instabilities
    - Near (emerging) AR
    - From Moreton/EIT waves
    - Near CH
  - Flaring
    - 38% result in at least 1 flare
    - Intensity : C1-M1

1120

A.G. Tlatov et al.

Figure 4. Distribution of the filament length in a logarithmic scale. The relative number of filaments is given as a function of their length in Mm.



R. Mawad et al. *Advances in Space Research* 55 (2015) 696–704

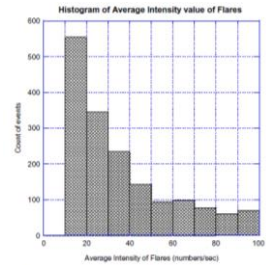


Fig. 6. Histogram of intensity of solar flares which are occurred during duration time of filament disappearance event during 1996–2010.

SWIC - Collaboration between STCE, Koninklijke Luchtmacht, KNMI

Tlatov et al. (2016): Tilt Angles of Solar Filaments over the Period of 1919 – 2014  
<http://adsabs.harvard.edu/abs/2016SoPh..291.1115T>

Mawad et al. (2014): Filaments disappearances in relation to solar flares during the solar cycle 23  
<http://adsabs.harvard.edu/abs/2015AdSpR..55..696M>

Hao et al. (2015): Statistical Analysis of Filament Features Based on the H $\alpha$  Solar Images from 1988 to 2013 by Computer Automated Detection Method  
<http://adsabs.harvard.edu/abs/2015ApJS..221...33H>

# Filament/Prominence eruptions

- Height
  - Zirin (1988)
    - If  $> 50.000$  km, eruption likely within next 48 hours
  - Filippov (2008)
    - Height cannot exceed critical height
      - Related to strength of and change in magnetic field
- Other signs
  - Darkening filament
  - Change in tilt or length

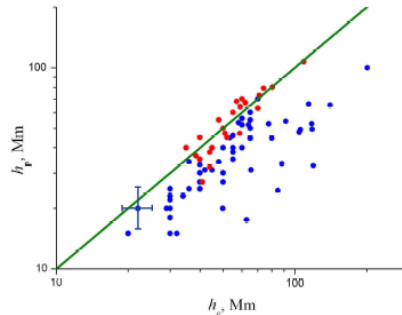


Fig. 7. The observed filament height above the chromosphere  $h_p$  versus the critical height of stable filament equilibrium  $h_c$ . The blue circles correspond to the filaments which safely passed the west limb. The red circles correspond to the filaments which disappeared from the disk. The straight green line corresponding to an equality of these quantities is the stability boundary.

SWIC - Collaboration between STCE, Koninklijke Luchtmacht, KNMI



Data taken from:

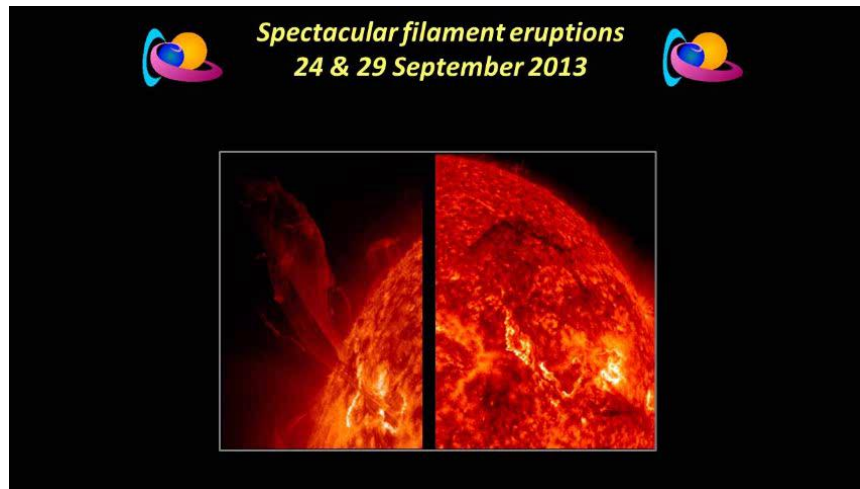
Filippov et al. (2008): Causal relationships between eruptive prominences and coronal mass ejections

<http://adsabs.harvard.edu/abs/2008AnGeo..26.3025F>

<http://www.ann-geophys.net/26/3025/2008/angeo-26-3025-2008.pdf>

Zirin (1988): Astrophysics of the Sun

# Filament/Prominence eruptions



SWIC - Collaboration between STCE, Koninklijke Luchtmacht, KNMI

97

From STCE: **Two spectacular filament eruptions**

<http://www.stce.be/news/218/welcome.html>

Some information on material falling back to the solar surface:

STCE: **A gorgeous filament eruption**

<http://www.stce.be/news/297/welcome.html>

Later in the event, some of the filament material is seen to fall back down to the surface of the Sun (see image above on the left). These parcels of filament material are trapped on dips in the magnetic field. When the field expands during the eruption, some of the field stretches and the dips disappear. If a magnetic flux tube straightens out, but remains connected to the Sun, the plasma on that tube may slide back to the Sun, and this is what we see in the movie. The filament plasma then causes localized brightenings where it hits the surface, as indicated by an arrow in the image above on the right.

:Issued: 2014 Apr 17 1325 UTC  
 :Product: documentation at http://www.sidc.be/product/sft/ot  
 #-----#  
 # DAILY BULLETIN ON SOLAR AND GEOMAGNETIC ACTIVITY from the SIDC #  
 #-----#  
 SIDCURSIGRAM 40417  
 SIDCSOLAR BULLETIN 17 Apr 2014, 1304UT



SIDCFORCAST (valid from 1220UT, 17 Apr 2014 until 19 Apr 2014)

**SOLAR FLARES - Active (M-class flares expected, probability >=50%)**

GEOMAGNETISM : Quiet (A<20 and K<4)

SOLAR PROTONS : Quiet

PREDICTIONS FOR 17 Apr 2014 10CM FLUX: 180 / AP: 013

PREDICTIONS FOR 18 Apr 2014 10CM FLUX: 184 / AP: 007

PREDICTIONS FOR 19 Apr 2014 10CM FLUX: 188 / AP: 005

COMMENT: Eleven sunspot groups were reported by NOAA today. NOAA ARs 2035, 2036, and 2037 (Catania numbers 24, 25, and 26 respectively) maintain the beta-gamma configuration of the photospheric magnetic field. The strongest flare of the past 24 hours was the M1.0 flare peaking at 19:59 UT yesterday in the NOAA AR 2035 (Catania number 24). The flare was associated with an EIT wave and a weak coronal dimming, but the associated CME was narrow and is not expected to arrive at the Earth.

We expect further flaring activity on the C-level, especially in the NOAA ARs 2035 and 2037 (Catania numbers 24 and 26 respectively) as well as in the NOAA AR 2042 (no Catania number yet) that yesterday appeared from behind the east solar limb, with a good chance for an M-class event.

Since yesterday evening the Earth is situated inside a solar wind structure with an elevated interplanetary magnetic field magnitude (occasionally up to 10 nT). It may be a weak ICME or the compression region on the flank of an ICME that missed the Earth. The solar origin of this structure is not clear. The north-south magnetic field component Bz was not strong, so no significant geomagnetic disturbance resulted (Kindex stayed below 4). Currently the solar wind speed is around 380 km/s and the IMF magnitude is around 8 nT.

We expect quiet to unsettled (K index up to 3) geomagnetic conditions, with active geomagnetic conditions (K=4) possible, but unlikely.

TODAY'S ESTIMATED ISN : 145, BASED ON 17 STATIONS.  
 99999

SOLAR INDICES FOR 16 Apr 2014

WOLF NUMBER CATANIA : ///

10CM SOLAR FLUX : 184

AK CHAMBON LA FORET : 012

AK WINGST : 004

ESTIMATED AP : 004

ESTIMATED ISN : 139, BASED ON 29 STATIONS.

*Active region classification  
& filaments / prominences*

*Flare prediction*

NOTICEABLE EVENTS SUMMARY

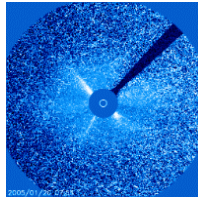
| DAY | BEGIN | MAX  | END  | LOC    | XRAY | OP | 10CM    | Catania/NOAA | RADIO_BURST_TYPES |
|-----|-------|------|------|--------|------|----|---------|--------------|-------------------|
| 16  | 1954  | 1959 | 2004 | S14E09 | M1.0 | 1N | 24/2035 |              | I/2               |
| END |       |      |      |        |      |    |         |              |                   |

# Solar eruptions

**Magnetic Reconnection**

**Particles**

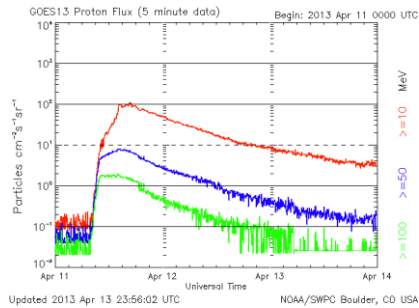
**Proton events**



SWIC - Collaboration between STCE, Koninklijke Luchtmacht, KNMI

# Proton events

- Proton event
  - > 10MeV proton flux
    - 5 min. average
  - Start:  $\geq 10$  pfu
    - Need at least 3 data points
  - Peak: maximum value
    - May take hours to days
  - End: < 10 pfu
    - NO new events as long as flux > 10 pfu
- Proton enhancement
  - Increased flux, but below 10 pfu
- Solar Energetic Particles
  - High energy (keV to GeV) protons, electrons and ions which come from the Sun



| SWPC Alert thresholds  |               |
|--|---------------|
| $\geq 10$ MeV proton flux  | $\geq 10$ pfu |
| $\geq 100$ MeV proton flux   | $\geq 1$ pfu  |
| 1 pfu = 1 particle / cm <sup>2</sup> s sr  |               |
| Time of maximum is the time tag of the 5 minute averaged flux value that has the greatest value. |               |

SWPC - Collaboration between STCE, Koninklijke Luchtmacht, KNIWI

100

SWPC's « The Weekly » User guide ([https://www.swpc.noaa.gov/sites/default/files/images/u2/Usr\\_guide.pdf](https://www.swpc.noaa.gov/sites/default/files/images/u2/Usr_guide.pdf) ; page 15) *Proton Events*

A proton event starts when the integrated proton flux (5-minute average) rises above a specific threshold for at least three points.

The two alert thresholds are (1 pfu = particle / cm<sup>2</sup>s-1sr-1):

- >10 MeV:  $\geq 10$  pfu
- >100 MeV:  $\geq 1$  pfu

The time of maximum is the time tag of the 5 minute averaged flux value that has the greatest value.

The term « **proton flare** » is also commonly used. According to the SWPC glossary at <https://www.swpc.noaa.gov/content/space-weather-glossary> , a proton flare is « Any flare producing significant counts of protons with energies exceeding 10 MeV in the vicinity of the Earth. »

Because proton events can originate from eruptions on the Sun's farside, i.e. without a flare recorded by GOES, proton flares are a subset of proton events.

From: <http://www.stce.be/news/232/welcome.html>

The issue here is that proton flares are not considered as separate events if the proton flux (particle energies larger than 10 MeV) at the time of the event is still above the threshold of 10 protons per flux unit (pfu). Example: 6 January 2014 X1 proton flare.

From: SESC: <https://umbra.nascom.nasa.gov/SEP/> (contains list of all proton events since 1976)

**Please Note:** Proton fluxes are integral 5-minute averages for energies >10 MeV, given in Particle Flux Units (pfu), measured by GOES spacecraft at Geosynchronous orbit: 1 pfu = 1 p / cm<sup>2</sup> sr<sup>1</sup> s<sup>-1</sup>. SESC defines the start of a proton event to be the first of 3 consecutive data points with fluxes greater than or equal to 10 pfu. The end of an event is the last time the flux was greater than or equal to 10 pfu. This definition, motivated by SESC customer needs, allows multiple proton flares and/or interplanetary shock proton increases to occur within one SESC proton event. Additional data may be necessary to more completely resolve any individual proton event.

**SEP** definition: from SWPC's glossary

<https://www.swpc.noaa.gov/content/space-weather-glossary#Solar%20Energetic%20Particles>

Solar Energetic Particles are high energy (keV to GeV) protons, electrons and ions which come from the Sun.

# Proton event classification

(exceptions abound...)

## Impulsive

- Associated with impulsive solar flares
  - Electron rich
- The onsets are not necessarily fast, but the events are rather of short duration
  - Hours
- Rather narrow propagation cones
  - Events from eastern hemisphere may not be observed

## Gradual

- Associated with CME-driven shocks
  - Gradual solar flares (LDE)
  - Wide and fast shocks
  - Type II and IV radio bursts
  - Usually proton rich
- The onsets are not necessarily gradual, but the events are of long duration
  - Days
  - Partly due to continuing acceleration of shock

SWIC - Collaboration between STCE, Koninklijke Luchtmacht, KNMI



101

A very good site on the characteristics between gradual and impulsive events is at SEPTEM: [http://dev.sepem.oma.be/help/sep\\_intro.html](http://dev.sepem.oma.be/help/sep_intro.html) (alternate: [http://sepem.eu/help/index\\_intro.html](http://sepem.eu/help/index_intro.html) )

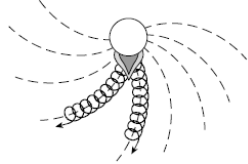
Papaioannou et al. (2016): Solar flares, coronal mass ejections and solar energetic particle event characteristics <https://www.swsc-journal.org/articles/swsc/pdf/2016/01/swsc150076.pdf>

Reames, 2013: The Two Sources of Solar Energetic Particles <http://adsabs.harvard.edu/abs/2013SSRv..175...53R>

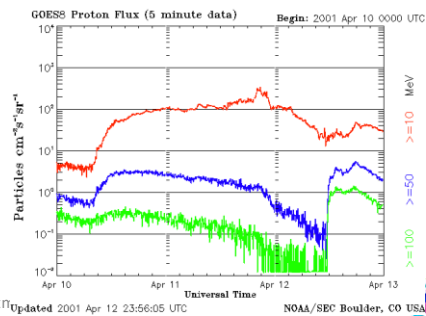
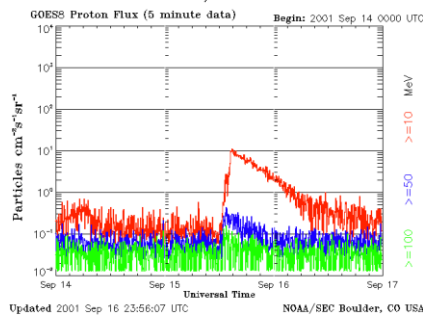
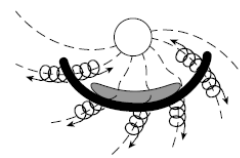
Park et al. , 2015: Study of Solar Energetic Particle Associations with Coronal Extreme-ultraviolet Waves <http://iopscience.iop.org/article/10.1088/0004-637X/808/1/3/pdf>  
Impulsive SEP events, having short durations of several hours, are associated with impulsive flares. They are electron rich and have enhanced  $3\text{He}/4\text{He}$  and  $\text{Fe}/\text{O}$  ratios in contrast to nominal coronal values. Also, they are generally distributed within a narrow propagation cone. Gradual SEP events are associated with gradual X-ray flares and type II and type IV radio emission. They are produced by wide and fast CME-driven shocks (Gopalswamy 2003) and have a broad range of source longitudes (Kahler 1994; Reames 1999). Gradual events show typical coronal abundances and are proton rich in contrast to impulsive events. Many events have characteristics of both gradual and impulsive events due to a combination of both flare- and shock-associated particles (Cane et al. 2006). Surprisingly, some of these appear to have poor magnetic connection to the associated flare sites, suggesting that flare-accelerated particles can be distributed over wide angles in interplanetary space either by efficient cross-field transport in interplanetary space or by ejection of flare particles into an expanding source, for example, a CME shock, near the Sun (Wiedenbeck et al. 2013; Dresing et al. 2014).

# Proton event classification

## Impulsive



## Gradual



A very good site on the characteristics between gradual and impulsive events (with more examples) is at

SEPEM: [http://dev.sepem.oma.be/help/sep\\_intro.html](http://dev.sepem.oma.be/help/sep_intro.html)

The cartoons were taken from:

Reames (1999): Particle acceleration at the Sun and in the heliosphere

<http://adsabs.harvard.edu/abs/1999SSRv...90..413R>

The 15 Sep 2001 event (11 pfu) resulted from an M1 (1N) flare on 11:28UT

The 10 Apr 2001 event (355 pfu) resulted from an X2 (3B) flare on 05:26UT. The (halo) CME arrived on 11 April around 15UT, hence the maximum proton flux (near 21UT) coincides with the passage of the ICME.

From Reames, 1999: Particle acceleration at the Sun and in the Heliosphere

<http://link.springer.com/content/pdf/10.1023%2FA%3A1005105831781.pdf>

Meanwhile, the evidence for two types of events grew. Pallavicini et al. (1977) distinguished impulsive and long-duration (gradual) soft X-ray events; the latter were associated with CMEs (Sheeley et al., 1975). Kahler (1992) has reviewed such differences between flares and CMEs. The connection between these two phenomena and energetic particles in space was made when Cane et al. (1986) found that SEPs associated with the two classes of X-ray events had different proton/electron ratios. The terms 'gradual' and 'impulsive' have stuck, even though time scales, especially X-ray time scales, poorly resolve those acceleration mechanisms we wish to distinguish.

# On the SEP origin

THE ASTROPHYSICAL JOURNAL, 830:28 (14pp), 2016 October 10

PETROSIAN

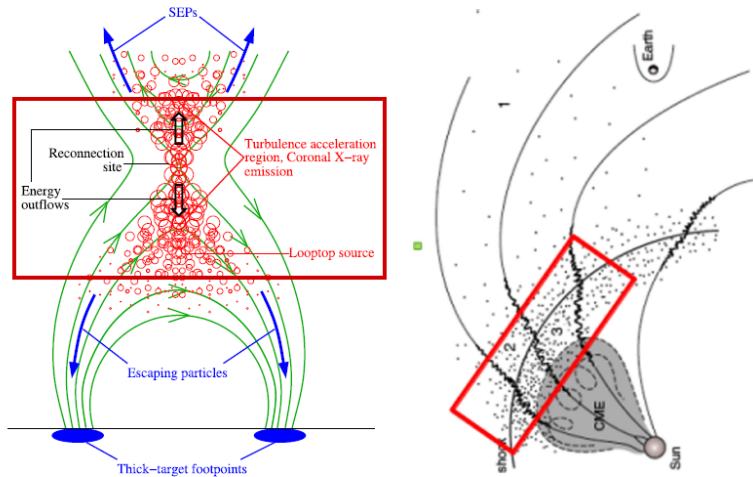


Figure 1. Left: schematic representation of the reconnecting field (solid green) forming closed coronal loops and open field lines presumably extending into higher up in the corona and the solar wind. The red beam represents turbulence. Acceleration probably takes place in the outflow regions above and below the X-point. Particles (temporarily) trapped here produce the radiation seen above the closed loops and particles escaping these regions up and down (blue arrows) are observed at 1 au as SEPs and produce the nonthermal radiation (mainly at the two footpoints; blue ovals), respectively (from Liu et al. 2013). Right: similar schematic joining the flare site field lines to the CME, the shock, and beyond (from Lee 2005). The rectangles define the boundary of the acceleration sites and represent the leaky box.

Additional (technical) information on the acceleration process is in Petrosian (2016): Particle acceleration in solar flares and associated CME shocks

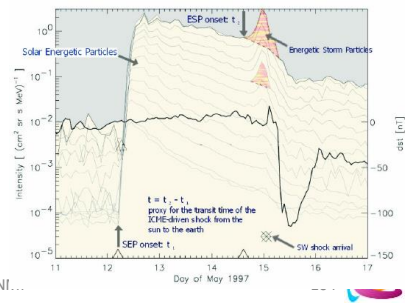
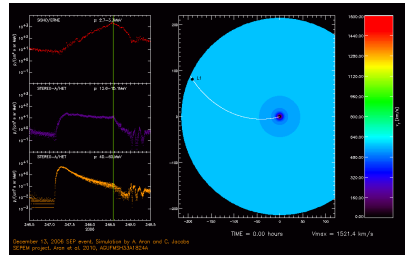
<http://adsabs.harvard.edu/abs/2016ApJ...830...28P>

In one group, referred to as “prompt” events, the SEPs appear to originate almost simultaneously with the radiations from the flare site located in the lower corona near the tops of reconnecting magnetic loops. The second group, referred to as “delayed” events, shows a complex temporal relation, often with the deduced time of emission of SEPs at the Sun coming after that of HXR or type III radio. A similar dichotomy seems to be present in the observations of SEP ions. Shorter, weaker events, often referred to as “impulsive,” appear to have higher enrichment of  $^3\text{He}$  and heavier than CNO ions and softer spectra with an unusual convex spectral shape for enriched ions, while longer-duration and stronger events show near-normal abundances and harder broken power-law spectra. Both the delayed-electron and gradual-normal abundance ion events are more likely to be associated with a fast CME.

Here we consider an alternative model where seed particles come from the downstream region. Because of the strong temporal relation, the weak spectral correlation, and consistently harder spectra of the delayed events, we are led to consider a scenario where the SEP spectra result from reacceleration of flare site electrons. This reacceleration is the cause of the harder SEP than HXR-producing electron spectra in these events. An important assumption here is that the CME launch and acceleration of the electrons at the reconnection are almost simultaneous, and/or the upward-escaping accelerated electrons are trapped by turbulence (or other means) in the downstream region of the shock. As described in Section 3.2, we need only a small fraction of these electrons to be trapped and reaccelerated, which renders this assumption reasonable.

# The difference between SEP and ESP

- SEP
  - Solar Energetic Particles
  - Accelerated:
    - in solar flare processes (low corona)
    - by fast ICME-driven shocks (high corona)
  - Fast rise (location!), starting at time of flare or CME lift-off
  - Energies up to GeV range
  
- ESP
  - Energetic Storm Particles
  - Accelerated by fast ICME-driven shocks in IP space
  - Gradual rise, starting hours before shock arrival
  - Energies: prominent in MeV range

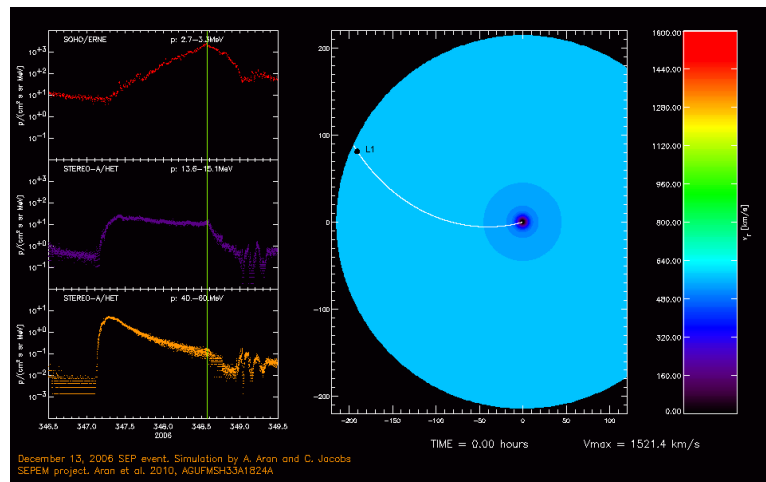


SWIC - Collaboration between STCE, Koninklijke Luchtmacht, KNI...

Animation source: SPACECAST: <http://fp7-spacecast.eu/index.php?page=seps>  
 Aran A., N. Agueda, C. Jacobs et al. 2011, American Geophysical Union, Fall Meeting 2011, abstract #SH33B-2051A.

Valtonen et al. (2005; poster at EWWW2):  
[http://swe.ssa.esa.int/TECEES/spweather/workshops/eswwII/proc/Session1/esww2\\_poster\\_valtonen.pdf](http://swe.ssa.esa.int/TECEES/spweather/workshops/eswwII/proc/Session1/esww2_poster_valtonen.pdf)

# On the SEP origin



December 13, 2006 SEP event. Simulation by A. Aran and C. Jacobs  
SEPEM project. Aran et al. 2010, AGUPMH33A1924A  
Aran A., N. Agueda, C. Jacobs et al. 2011, American Geophysical Union, Fall Meeting 2011, abstract #SH33B-2051A

SWIC - Collaboration between STCE, Koninklijke Luchtmacht, KNMI

105 

Animation source: SPACECAST: <http://fp7-spacecast.eu/index.php?page=seps>

Aran A., N. Agueda, C. Jacobs et al. 2011, American Geophysical Union, Fall Meeting 2011, abstract #SH33B-2051A.

## Solar energetic particles - Modelling of gradual SEP events: an example

The movie below shows the modelling of the evolution of the interplanetary shock and the cobpoint (= the point of the shock front that is magnetically connected to the observer), and the fitting to the proton intensity-time profiles measured at 1.0 AU during the gradual proton event on 13 December 2006.

The left panel shows:

- Three measured proton intensity-time profiles (coloured dots) at L1, the lower energy channel is from the SOHO/ERNE instrument and the other two from the STEREO-A/HET telescope.
- The vertical green line marks the shock passage at L1.
- The white lines represent the synthetic flux profiles obtained from the fitting using the shock-and-particle model. This model assumes that the shock-accelerated particles are injected onto the interplanetary magnetic field line connecting with the observer at the cobpoint.

In this event, high-energy particles are observed shortly after the first cobpoint is established, thus the first injection of shock accelerated particles occurs when the shock is still close to the Sun. The lower energy profiles start increasing later than that because of the presence of a background population of particles, but mainly due to their smaller velocity and due to particle propagation effects along the interplanetary magnetic field.

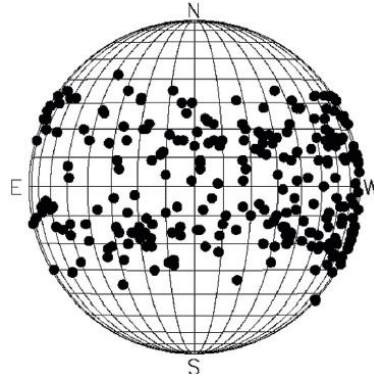
Note that the high energy proton flux peaks a few hours after the onset of the event, while the low energy intensity peaks at the shock arrival. Thus, indicating that the shock is efficient at accelerating high energy protons when it is close to the Sun, but as it propagates away, it becomes only efficient at accelerating low energy particles.

The >10MeV proton flux as measured by GOES for this event is at

[ftp://ftp.swpc.noaa.gov/pub/warehouse/2015/2015\\_plots/proton/20151030\\_proton.gif](ftp://ftp.swpc.noaa.gov/pub/warehouse/2015/2015_plots/proton/20151030_proton.gif)

# Effects from location SEP source

- There's a higher likelihood for SEP events from the western hemisphere
  - Does not exclude SEPs from the eastern hemisphere or even from the Sun's backside!
    - E.g. Major flare on 23 July 2012
    - Mechanism?
  - Eastern SEPs: slower rise



SWIC - Collaboration between STCE, Koninklijke Luchtmacht, KNMI

106 

Papaioannou et al. (2016): Solar flares, coronal mass ejections and solar energetic particle event characteristics <https://www.swsc-journal.org/articles/swsc/pdf/2016/01/swsc150076.pdf>

Image taken from their Figure 5 (D).

Major farside flare from 23 July 2012: <http://www.stce.be/news/152/welcome.html>

Example from 29 October 2015 event: <http://www.stce.be/news/325/welcome.html>

It is believed that the coronal waves associated to strong CMEs widen the access possibilities of the energetic particles to earth coronal Parker spiral magnetic field lines. This would allow some of the backside events still to create a proton event at Earth. But even then, there's still a problem of the eastern hemisphere events, in particular e.g. at locations E120.

Alternative mechanism for proton events with farside source:

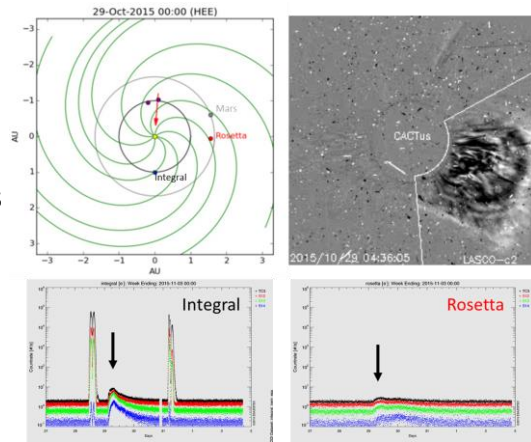
Laitinen et al., 2016: Solar energetic particle access to distant longitudes through turbulent field-line meandering <https://www.aanda.org/articles/aa/pdf/2016/07/aa27801-15.pdf>

We developed a new SEP transport model that takes the non-diffusive propagation of SEPs early in the event history into account for a Parker spiral geometry. We showed that the early onset of SEPs over a wide range of longitudes can be explained by field-line random walk and requires an SEP transport model that properly describes the non-diffusive early phase of SEP cross-field propagation. Our FP+FLRW model is the first model that is capable of reproducing the observed fast access of SEPs to distant longitudes, when the particle and field-line diffusion coefficients are consistently derived from an interplanetary turbulence model. When the FLRW is not included (in the FP model), a much narrower cross-field extent of the SEP event is produced. We conclude that introducing field-line wandering into SEP modelling has the potential of resolving the problem of fast access of SEPs to a wide range of longitudes.

(FP: Fokker-Planck; FLRW: Field Lines Random Walk)

# Effects from location SEP source

- There's a higher likelihood for SEP events from the western hemisphere
  - Does not exclude SEPs from the eastern hemisphere or even from the Sun's backside!
    - E.g. Major flare on 23 July 2012
    - Mechanism?



SWIC - Collaboration between STCE, Koninklijke Luchtmacht, KNMI



Papaioannou et al. (2016): Solar flares, coronal mass ejections and solar energetic particle event characteristics  
<https://www.swsc-journal.org/articles/swsc/pdf/2016/01/swsc150076.pdf>

- Major farside flare from 23 July 2012: <http://www.stce.be/news/152/welcome.html>

- Example from 29 October 2015 event: <http://www.stce.be/news/325/welcome.html> The likely source of the proton event (NOAA 2434) was 39 degrees behind the west limb as seen from Earth.

Mechanism for proton events with farside source:

Laitinen et al., 2016: Solar energetic particle access to distant longitudes through turbulent field-line meandering  
<https://www.aanda.org/articles/aa/pdf/2016/07/aa27801-15.pdf>

We developed a new SEP transport model that takes the non-diffusive propagation of SEPs early in the event history into account for a Parker spiral geometry. We showed that the early onset of SEPs over a wide range of longitudes can be explained by field-line random walk and requires an SEP transport model that properly describes the non-diffusive early phase of SEP cross-field propagation. Our FP+FLRW model is the first model that is capable of reproducing the observed fast access of SEPs to distant longitudes, when the particle and field-line diffusion coefficients are consistently derived from an interplanetary turbulence model. When the FLRW is not included (in the FP model), a much narrower cross-field extent of the SEP event is produced. We conclude that introducing field-line wandering into SEP modelling has the potential of resolving the problem of fast access of SEPs to a wide range of longitudes. (FP: Fokker-Planck; FLRW: Field Lines Random Walk)

Aside GOES, there are other satellites equipped with SREM that also measure proton fluxes:

[http://space-env.esa.int/index.php/SREM\\_Plots.html](http://space-env.esa.int/index.php/SREM_Plots.html)

Currently (2017), only the Integral satellite has an operational SREM.

Finally, STEREO and SOHO also measure proton fluxes:

ACE: <https://services.swpc.noaa.gov/images/ace-sis-3-day.gif>

STEREO: [https://stereo-ssc.nascom.nasa.gov/beacon/beacon\\_insitu.shtml](https://stereo-ssc.nascom.nasa.gov/beacon/beacon_insitu.shtml) (click plots, scroll down to « IMPACT »).

# Effects from location SEP source

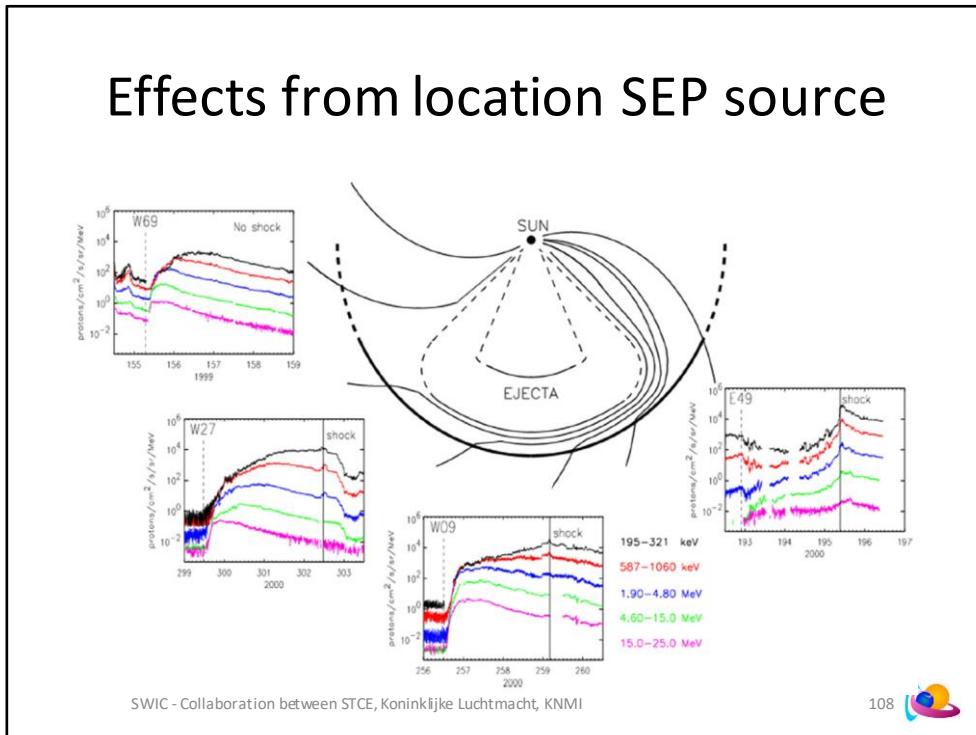


Figure taken and slightly modified from Lavraud et al. (2016): A small mission concept to the Sun-Earth Lagrangian L5 point for innovative solar, heliospheric and space weather science <http://adsabs.harvard.edu/abs/2016JASTP.146..171L>

It is likely to have a much faster increase from SEP events from a source on the western hemisphere.

When a shock from the associated CME passes the observer (earth), the proton flux will peak (again).

For Earth, the solar magnetic footpoint of the Parker spiral associated with a nominal solar wind speed of 400 km/s corresponds to a longitude of about W60. See the graph at [http://solar.physics.montana.edu/ypop/Nuggets/2002/021004/parker\\_spiral.png](http://solar.physics.montana.edu/ypop/Nuggets/2002/021004/parker_spiral.png) in the Yohkoh Science nugget at <http://solar.physics.montana.edu/ypop/Nuggets/2002/021004/021004.html>

# Proton event classification

- NOAA-scales: S-scale

| Scale | Description | Effect | Physical measure<br>(Flux level<br>of $>= 10$<br>MeV<br>particles) | Average Frequency<br>(1 cycle = 11 years) |
|-------|-------------|--------|--|---|
| S 5   | Extreme     |        | $10^5$   | Fewer than 1 per cycle                    |
| S 4   | Severe      |        | $10^4$   | 3 per cycle                               |
| S 3   | Strong      |        | $10^3$   | 10 per cycle                              |
| S 2   | Moderate    |        | $10^2$   | 25 per cycle                              |
| S 1   | Minor       |        | 10   | 50 per cycle                              |

From the SWPC webpage (<https://www.swpc.noaa.gov/noaa-scales-explanation>)

## NOAA Space Weather Scales

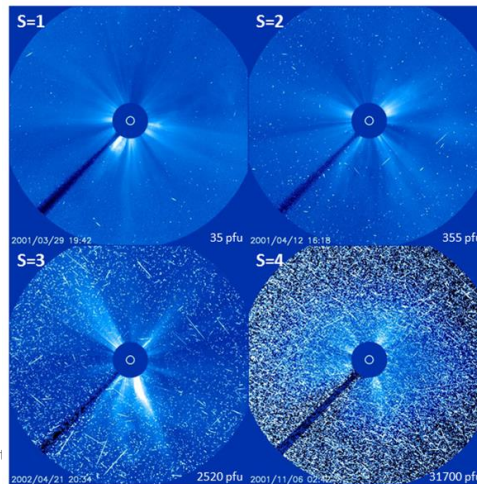
The NOAA Space Weather Scales were introduced as a way to communicate to the general public the current and future space weather conditions and their possible effects on people and systems. Many of the SWPC products describe the space environment, but few have described the effects that can be experienced as the result of environmental disturbances. These scales are useful to users of our products and those who are interested in space weather effects. The scales describe the environmental disturbances for three event types: geomagnetic storms, solar radiation storms, and radio blackouts. The scales have numbered levels, analogous to hurricanes, tornadoes, and earthquakes that convey severity. They list possible effects at each level. They also show how often such events happen, and give a measure of the intensity of the physical causes.

The « S » stands for Solar radiation Storm. Since observations started in 1976, no S5 event has been recorded.

More at <http://www.stce.be/news/366/welcome.html>

# Proton event classification

- NOAA-scales: S-scale



From the SWPC webpage (<https://www.swpc.noaa.gov/noaa-scales-explanation>):

## **NOAA Space Weather Scales**

The NOAA Space Weather Scales were introduced as a way to communicate to the general public the current and future space weather conditions and their possible effects on people and systems. Many of the SWPC products describe the space environment, but few have described the effects that can be experienced as the result of environmental disturbances. These scales are useful to users of our products and those who are interested in space weather effects. The scales describe the environmental disturbances for three event types: geomagnetic storms, solar radiation storms, and radio blackouts. The scales have numbered levels, analogous to hurricanes, tornadoes, and earthquakes that convey severity. They list possible effects at each level. They also show how often such events happen, and give a measure of the intensity of the physical causes.

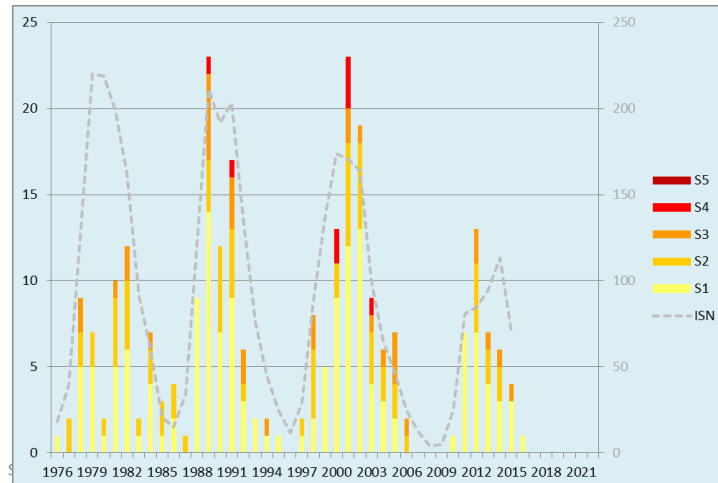
The « S » stands for Solar radiation Storm. Since observations started in 1976, no S5 event has been recorded.

More on NOAA scales at <http://www.stce.be/news/366/welcome.html>

More on proton intensity at <http://www.stce.be/news/233/welcome.html>

# Proton event classification

- NOAA-scales: S-scale



111

From the SWPC webpage (<https://www.swpc.noaa.gov/noaa-scales-explanation>)

## **NOAA Space Weather Scales**

The NOAA Space Weather Scales were introduced as a way to communicate to the general public the current and future space weather conditions and their possible effects on people and systems. Many of the SWPC products describe the space environment, but few have described the effects that can be experienced as the result of environmental disturbances. These scales are useful to users of our products and those who are interested in space weather effects. The scales describe the environmental disturbances for three event types: geomagnetic storms, solar radiation storms, and radio blackouts. The scales have numbered levels, analogous to hurricanes, tornadoes, and earthquakes that convey severity. They list possible effects at each level. They also show how often such events happen, and give a measure of the intensity of the physical causes.

The « S » stands for Solar radiation Storm. Since observations started in 1976, no S5 event has been recorded.

More at <http://www.stce.be/news/366/welcome.html>

# Forecasting proton events

K. Bronarska, G. Michalek / *Advances in Space Research* 59 (2017) 384–392

387

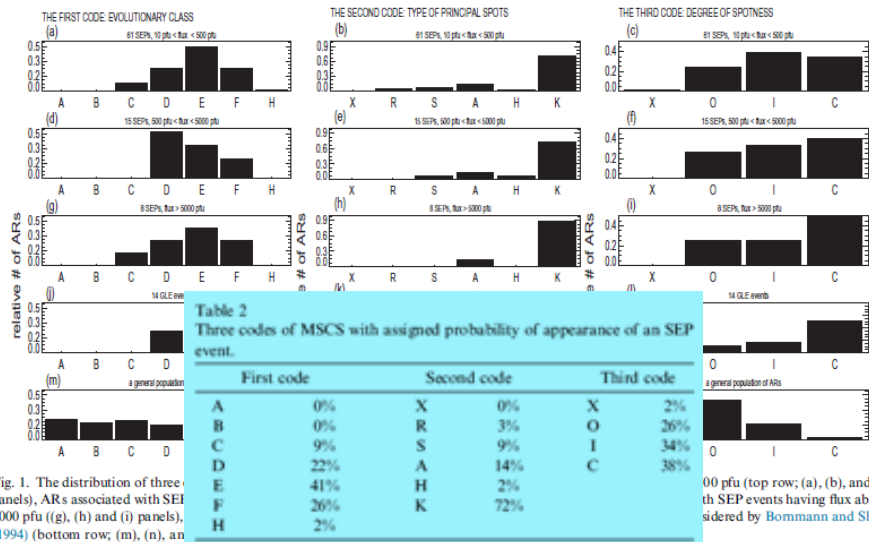


Fig. 1. The distribution of three panels), ARs associated with SEP 5000 pfu (g), (h) and (i) panels), (1994) (bottom row; (m), (n), an

Bronarska et al. (2017): Characteristics of active regions associated to large solar energetic proton events

<http://adsabs.harvard.edu/abs/2017AdSpR...59..384B>

Papaioannou et al. (2016): Solar flares, coronal mass ejections and solar energetic particle event characteristics

<https://www.swsc-journal.org/articles/swsc/pdf/2016/01/swsc150076.pdf>

Dierckxsens et al. (2015): Relationship between Solar Energetic Particles and Properties of Flares and CMEs: Statistical Analysis of Solar Cycle 23 Events

<http://link.springer.com/content/pdf/10.1007%2F11207-014-0641-4.pdf>

Posner et al. (2009): A New Trend in Forecasting Solar Radiation Hazards

<http://adsabs.harvard.edu/abs/2009SpWea...7.5001P>

Monitoring of relativistic electrons, which arrive a few to tens of minutes before the actual high-energetic ions.

Also in <https://arxiv.org/pdf/1210.4475.pdf>

Example: Bastille day event: [https://soho.nascom.nasa.gov/hotshots/2000\\_07\\_14/costep\\_000714.gif](https://soho.nascom.nasa.gov/hotshots/2000_07_14/costep_000714.gif)

# Forecasting proton events

848

M. Dierckxsens *et al.*

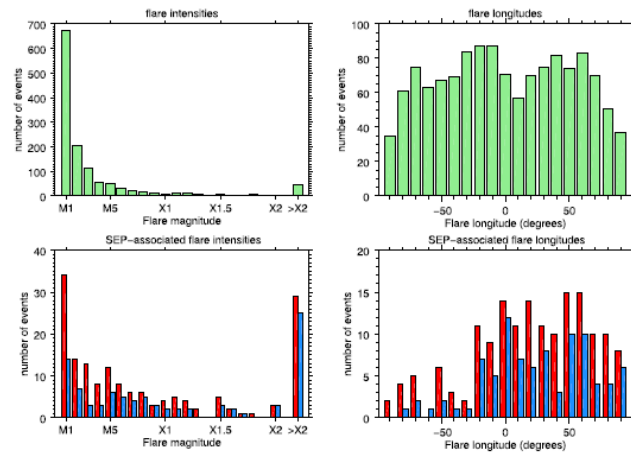


**Figure 3** Top row: distributions of flare magnitude (left) and flare longitude (right) in the sample of 1298 flares used for the analysis in Section 4.1.1. Bottom row: distributions of the respective parameters of the flares associated with the events in the CRR2010 list (red bars) and in the SSE list (blue bars).

SWIC -

113 

Papioannou *et al.* (2016): Solar flares, coronal mass ejections and solar energetic particle event characteristics

<https://www.swsc-journal.org/articles/swsc/pdf/2016/01/swsc150076.pdf>

Dierckxsens *et al.*, 2015: Relationship between Solar Energetic Particles and Properties of Flares and CMEs: Statistical Analysis of Solar Cycle 23 Events

<http://link.springer.com/content/pdf/10.1007%2Fs11207-014-0641-4.pdf>

# Forecasting proton events

A. Papaioannou et al.: SEP events and their parent solar sources

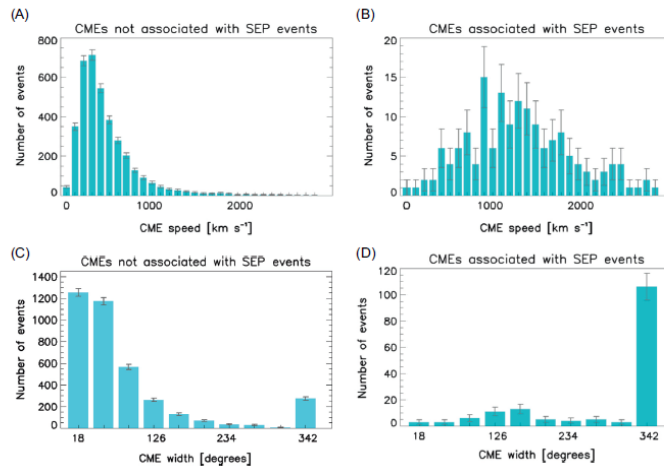


Fig. 6. Distribution of the CME velocity (in  $\text{km s}^{-1}$ ) for all 3535 CMEs not associated with SEP events in our sample from 1997–2013 (A) and for the 158 SEP events, within the same time period (B). Distribution of the CME width (in degrees) for all 3535 CMEs not associated with SEP events in our sample from 1997–2013 (C) and for the 158 SEP events, within the same time period (D). The error bars denote the statistical error.



Papaioannou et al. (2016): Solar flares, coronal mass ejections and solar energetic particle event characteristics

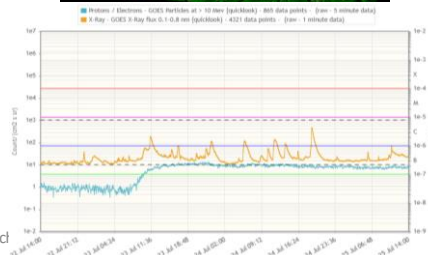
<https://www.swsc-journal.org/articles/swsc/pdf/2016/01/swsc150076.pdf>

Dierckxsens et al., 2015: Relationship between Solar Energetic Particles and Properties of Flares and CMEs: Statistical Analysis of Solar Cycle 23 Events

<http://link.springer.com/content/pdf/10.1007%2Fs11207-014-0641-4.pdf>

# Forecasting proton events

- Look for active regions & filaments that can:
  - Produce strong x-ray flares
  - Fast CMEs ( $\sim 1000$  km/s or more)
  - Wide CMEs (partial or full halo CMEs)
  - Preferably on the western solar hemisphere
- Finetune from history on farside/eastern hemisphere
  - Proton flux enhancements,...
  - Observations by STEREO spacecraft



Source: <http://www.stce.koninklijke-luchtvaart.nl>

Probabilities and intensities for proton events for a variety of the above parameters can be found in: Dierckxsens et al., 2015: **Relationship between Solar Energetic Particles and Properties of Flares and CMEs: Statistical Analysis of Solar Cycle 23 Events**  
<http://link.springer.com/content/pdf/10.1007%2Fs11207-014-0641-4.pdf>

More info on SEP events at [http://dev.sepem.oma.be/help/solpenco2\\_intro.html](http://dev.sepem.oma.be/help/solpenco2_intro.html)

:Issued: 2014 Apr 17 1325 UTC  
 :Product: documentation at http://www.sidc.be/product/s/ot  
 #-----#  
 # DAILY BULLETIN ON SOLAR AND GEOMAGNETIC ACTIVITY from the SIDC #  
 #-----#  
 SIDCURSIGRAM 40417  
 SIDCSOLAR BULLETIN 17 Apr 2014, 1304UT



SIDC FORECAST (valid from 1230UT, 17 Apr 2014 until 19 Apr 2014)  
 SOLAR FLARES : Active (M-class flares expected, probability >=50%)  
 GEOMAGNETISM : Quiet (A<20 and K<4)  
 SOLAR PROTONS : Quiet

PREDICTIONS FOR 17 Apr 2014 10CM FLUX: 180 / AP: 013  
 PREDICTIONS FOR 18 Apr 2014 10CM FLUX: 184 / AP: 007  
 PREDICTIONS FOR 19 Apr 2014 10CM FLUX: 188 / AP: 005

COMMENT: Eleven sunspot groups were reported by NOAA today. NOAA ARs 2035, 2036, and 2037 (Catania numbers 24, 25, and 26 respectively) maintain the beta-gamma configuration of the photospheric magnetic field. The strongest flare of the past 24 hours was the M1.0 flare peaking at 19:59 UT yesterday in the NOAA AR 2035 (Catania number 24). The flare was associated with an EIT wave and a weak coronal dimming, but the associated CME was narrow and is not expected to arrive at the Earth.  
 We expect further flaring activity on the C-level, especially in the NOAA ARs 2035 and 2037 (Catania numbers 24 and 26 respectively) as well as in the NOAA AR 2042 (no Catania number yet) that yesterday appeared from behind the east solar limb, with a good chance for an M-class event.

Since yesterday evening the Earth is situated inside a solar wind structure with an elevated interplanetary magnetic field magnitude (occasionally up to 10 nT). It may be a weak ICME or the compression region on the flank of an ICME that missed the Earth. The solar origin of this structure is not clear. The north-south magnetic field component Bz was not strong, so no significant geomagnetic disturbance resulted (Kindex stayed below 4). Currently the solar wind speed is around 380 km/s and the IMF magnitude is around 8 nT.

We expect quiet to unsettled (K index up to 3) geomagnetic conditions, with active geomagnetic conditions (K=4) possible, but unlikely.

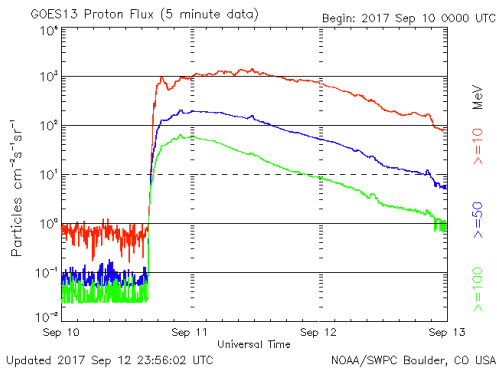
TODAY'S ESTIMATED ISN : 145, BASED ON 17 STATIONS.  
 99999

*Proton flux / events*

SOLAR INDICES FOR 16 Apr 2014  
 WOLF NUMBER CATANIA : ///  
 10CM SOLAR FLUX : 184  
 AK CHAMBON LA FORET : 012  
 AK WINGST : 004  
 ESTIMATED AP : 004  
 ESTIMATED ISN : 139, BASED ON 29 STATIONS.

NOTICEABLE EVENTS SUMMARY  
 DAY BEGIN MAX END LOC XRAY OP 10CM Catania/NOAA RADIO\_BURST\_TYPES  
 16 1954 1959 2004 S14E09 M1.0 1N 24/2035 I/2  
 END

## Exercise: proton event



- This is the GOES13 proton flux curve of a proton event associated with an X8 flare.
  - Is this a gradual or an impulsive event?
  - Is its source more likely on the eastern or the western solar hemisphere?
  - What would be its classification on the NOAA scale?

SWIC - Collaboration between STCE, Koninklijke Luchtmacht, KNMI



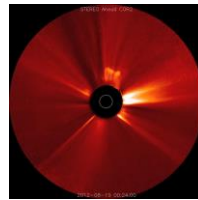
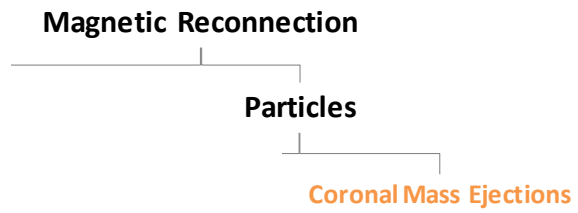
An X8 flare (R3-Strong) occurred at 10/1606 UTC with an associated 1,900 sfu Tenflare, Type II (estimated velocity 928 km/s) and Type IV radio sweeps and an asymmetric full halo CME first observed in SOHO/LASCO C2 imagery at 10/1600 UTC which had an estimated plane-of-sky speed around 2,100 km/s; however the bulk of the CME was not Earth-directed.

At 10/1645 UTC, 10 MeV protons exceeded 10 pfu (S1-Minor), reached a maximum of 1,490 pfu (S3-Strong) and decayed below the S1 level at 14/1725 UTC.

The source of the eruption, NOAA 2673, had just rotated over the west limb.

The shock of the CME arrived earlier than expected, around 20UT on 12 September.

# Solar eruptions



# Coronal Mass Ejection

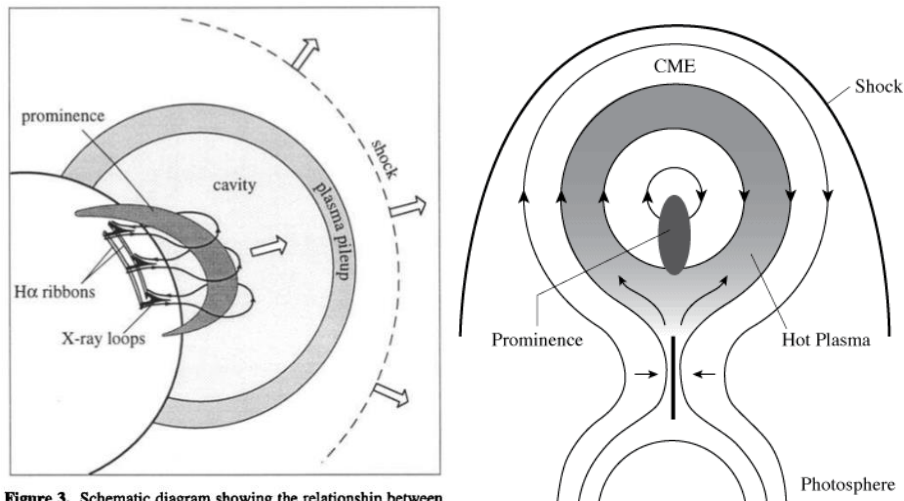


**Figure 3.** Schematic diagram showing the relationship between various features associated with a CME. The shaded region labeled “plasma pileup” refers to the outer circular arc seen in coronagraphs.

icht, KNMI

119



Figure to the right taken from [https://ase.tufts.edu/cosmos/print\\_images.asp?id=27](https://ase.tufts.edu/cosmos/print_images.asp?id=27)

A magnetic reconnection takes place at a current sheet (*dark vertical line*) beneath a prominence and above closed magnetic field lines. The coronal mass ejection, abbreviated CME, traps hot plasma below it (*hatched region*). The solid curve at the top is the bow shock driven by the CME. The closed field region above the prominence (*center*) is supposed to become a flux rope in the interplanetary medium. [Adapted from Petrus C. Martens and N. Paul Kuin (1989).]

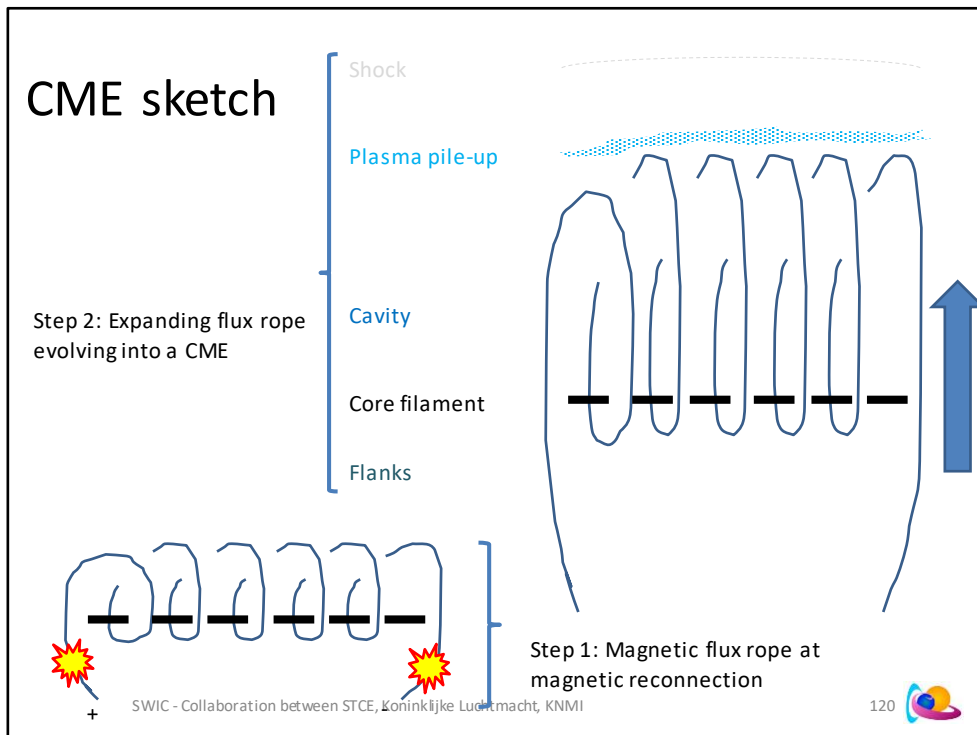
In this model of a three-part coronal mass ejection, portrayed by Terry Forbes (2000), swept-up, compressed mass and a bow shock have been added to the eruptive-flare portrayal of Tadashi Hirayama (1974). The combined representation includes compressed material at the leading edge of a low-density, magnetic bubble or cavity, and dense prominence gas. The prominence and its surrounding cavity rise through the lower corona, followed by sequential magnetic reconnection and the formation of flare ribbons at the footpoints of a loop arcade. [Adapted from Hugh S. Hudson, Jean-Louis Bougeret and Joan Burkepile (2006).]

Figure to the left taken from Forbes (2000): A review on the genesis of coronal mass ejection

<http://adsabs.harvard.edu/abs/2000JGR...10523153F>

<http://onlinelibrary.wiley.com/doi/10.1029/2000JA000005/epdf>

When CMEs were first clearly identified by Skylab in 1973, many researchers assumed that they were caused by the outward expansion of hot plasma produced by a large flare. We now know that this is not the case, for several reasons. First, less than 20% of all CMEs are associated with large flares [Gosling, 1993]. Second, CMEs that are associated with flares often appear to start before the onset of the flare [Wagner et al., 1981; Simnett and Harrison, 1985]. Finally, the thermal pressure produced by a flare is too small to blow open the strong magnetic field of the corona.



Expanding flux rope consisting of magnetic field lines and filament at bottom (left sketch) evolves into a CME with leading edge (pushed up by top of magnetic field lines from flux rope), cavity and core filament (right sketch). The shock is usually not visible, but measurable by e.g. Type II radiobursts or by observing the deflection of nearby streamers.

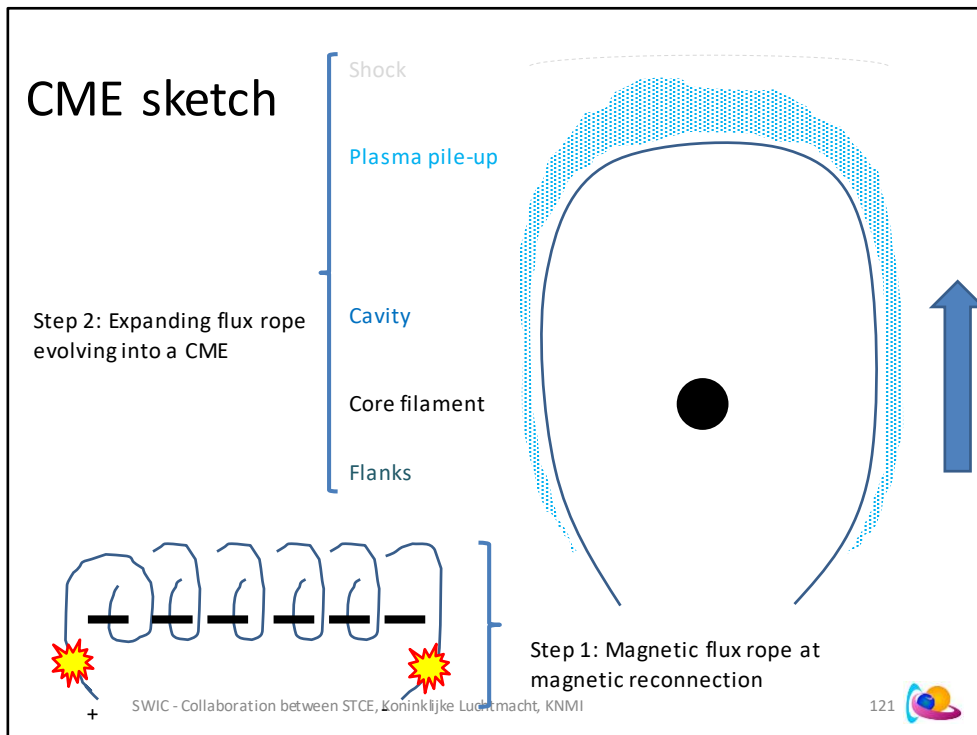
Source file: Webb et al. (2012): Coronal Mass Ejections: Observations  
<http://link.springer.com/article/10.12942/lrsp-2012-3>

However, with the larger dynamic range of LASCO rims of material detected a head of fast LASCO CMEs are now considered evidence of shock waves, and emission can be detected a head of slower speed CMEs as low-level brightness enhancements due to the expanding streamer (see Section 3.6).

The interrelationship between the various features which one can associate with CMEs is shown in Figure 3. It should be kept in mind that these features are not necessarily present in all CMEs. Not all CMEs contain a prominence, nor do all CMEs have detectable chromospheric ribbons and shock waves

\* Webb et al. (2012): Coronal Mass Ejections: Observations  
<http://link.springer.com/article/10.12942/lrsp-2012-3>

The original definition of a CME as a new, discrete brightening in the field of view over a time-scale of tens of minutes which is always observed to move outward (e.g., Webb and Hundhausen, 1987) is still generally accepted. However, some workers tend to regard any eruption from the Sun observed in the corona, no matter how faint or narrow, as a CME while others regard an eruption as a CME only if it has a certain size or structure. Although a "typical" CME is now thought to involve the eruption of a magnetic flux rope, the structure and magnitude of any CME magnetic field near the Sun can only be inferred, since we cannot directly measure coronal magnetic fields.

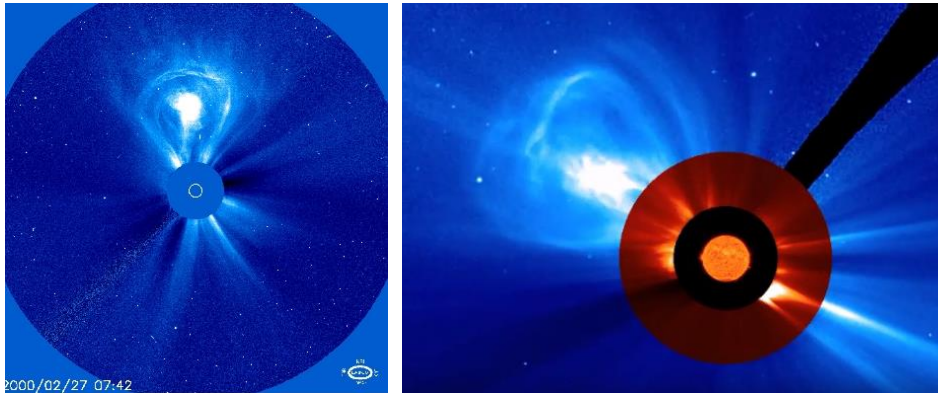


Vourlidas et al. (2013): How Many CMEs Have Flux Ropes? Deciphering the Signatures of Shocks, Flux Ropes, and Prominences in Coronagraph Observations of CMEs - <http://adsabs.harvard.edu/abs/2013SoPh..284..179V>  
 "...the 'three-part'-CME (Illing and Hundhausen, 1985) where the bright front is followed by a darker cavity, which frequently contains a bright core. It has become the archetypical morphology of a CME even though the 'three-part' morphology could be identified in only about a third of the events (Munro et al., 1979). ... "many fast ICMEs are driving a shock followed by a sheath of post-shocked plasma. The resulting five-part ICME (shock, sheath, dense front, cavity, and dense plug) does not have a coronal counterpart. ... where are the shock and sheath signatures in the coronagraph images? Shocks could deflect streamers and generally affect the ambient corona, ahead and at the flanks of a CME, thus creating complex brightness distributions in the images."

"... the brightness of the front originates from the pile-up of the overlying streamer material. ... the cavity, while not completely devoid of plasma, does contain less electrons (it is less bright) than its surroundings. ... 'three-part'-CMEs are indeed systems of ejected FRs, where the cavity is the actual FR. ..."

"... how can one be sure that the faint front is indeed related to density pile-up at a wave front and is not simply ejected material, *i.e.*, coronal loops moving ahead of the CME in direct analogy to the bright front ahead of the cavity. This can be best answered by careful inspection of excess-mass movies of these events. If the front in question is due to ejected material, then a density depletion should form behind it as it does behind the CME proper. If the front is caused by a wave, then the enhancement is due to density compression and not material transport; therefore, no density depletion should occur. ... The bright loop is the pile-up of material at the outer boundary of the erupted FR (the cavity) and hence it is bright while the outer front originates from a temporary compression of the ambient plasma as the wave (or shock) propagates through and hence is much fainter ... the large number of combined observations with LASCO (in white light) and EIT (in He I 304 Å) have shown that the cavity is not the prominence itself. They have also shown that the core does not lie in the center of the cavity as was thought in the past ... Rather the prominence lies at the bottom of the cavity, the cool plasma suspended in the dips of the FR field lines by the balance between gravity and magnetic tension forces. ... most of the cool prominence material returns to the surface and is not ejected with the rest of the CME. ... At least 41% of the CMEs exhibit clear flux rope signatures. ..."

# Coronal Mass Ejection



SWIC - Collaboration between STCE, Koninklijke Luchtmacht, KNMI

122 

Expanding flux rope consisting of magnetic field lines and filament at bottom evolves into a CME with leading edge (pushed up by top of magnetic field lines from flux rope), cavity and core filament.

Left picture: SOHO Gallery: <https://sohowww.nascom.nasa.gov/gallery/images/las02.html>

Right picture: STCE: <http://www.stce.be/news/342/welcome.html>

Coronagraph: Wiki: a telescopic attachment designed to block out the direct light from the Sun so that nearby objects – which otherwise would be hidden in the star's bright glare – can be resolved. In short: it is an instrument to create a permanent total solar eclipse.

Coronagraph Lasco: [https://lasco-www.nrl.navy.mil/index.php?p=content/handbook/hndbk\\_5](https://lasco-www.nrl.navy.mil/index.php?p=content/handbook/hndbk_5)

CMEs are mostly observed in white light by coronagraphs from space (SOHO, STEREO). In order to make the faint CMEs better visible, difference images are used (one image subtracted from the other).

Ground-based observatories can observe CMEs very close to the Sun: MLSO (K-Cor): <http://download.hao.ucar.edu/d5/www/fullres/latest/latest.kcor.gif>

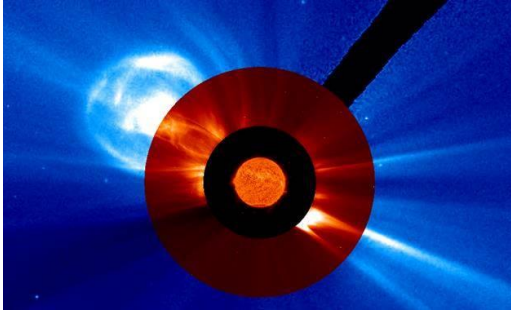
Ground-based observatories can also observe CMEs by using interplanetary scintillation (IPS).

\* Dorrian et al. (2008): Simultaneous interplanetary scintillation and Heliospheric Imager observations of a coronal mass ejection

<https://core.ac.uk/download/pdf/16283575.pdf>

Interplanetary scintillation (IPS) was first described by Hewish et al. [1964]. When the raypath from a compact radio source passes through the solar wind it encounters regions of varying plasma density, inducing phase variations. As the wave continues to the receiver these phase variations are converted into amplitude variations by interference [e.g., Coles, 1978].

## Exercise: CME feature recognition



- Which of the following CME features cannot be distinguished in this LASCO/C3 picture of the 04 Apr 2016 CME?
  - Shock
  - Plasma pile-up
  - Cavity
  - Core
  - Flanks

SWIC - Collaboration between STCE, Koninklijke Luchtmacht, KNMI

123 

See also Vourlidas et al. (2013) for more examples

<http://inspirehep.net/record/1121521/plots>

How Many CMEs Have Flux Ropes? Deciphering the Signatures of Shocks, Flux Ropes, and Prominences in Coronagraph Observations of CMEs

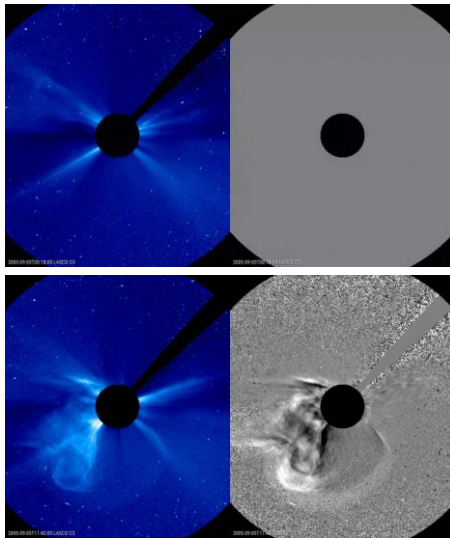
Wang et al. (2019): <https://www.frontiersin.org/articles/10.3389/fspas.2019.00018/full>

Magnetic flux ropes are generally defined as a bundle of magnetic fields that are twisted about each other and wrap around a common axis [usually the polarity inversion line].

Monga et al. (2020):

Solar filaments are high-density ... low-temperature ( $\sim 10^4$  K) structures that remain suspended by magnetic fields in the solar corona. These features when observed on-disk, are found along the polarity reversal lines between the regions of oppositely directed photospheric magnetic fields (Martin 1998). Topologically, filaments are modeled as helical magnetic flux ropes (MFRs) in which the plasma is trapped along the twisted field lines, wrapped around a guiding axis.

## Exercise: CME feature recognition



- Which of the following CME features can be distinguished in this LASCO/C3 imagery of the 05 Sep 2005 CME?

- Shock
- Plasma pile-up
- Cavity
- Core
- Flanks

SWIC - Collaboration between STCE, Koninklijke Luchtmacht, KNMI



See also Vourlidas et al. (2013) for more examples

<http://inspirehep.net/record/1121521/plots>

How Many CMEs Have Flux Ropes? Deciphering the Signatures of Shocks, Flux Ropes, and Prominences in Coronagraph Observations of CMEs

Vourlidas et al. (2003)

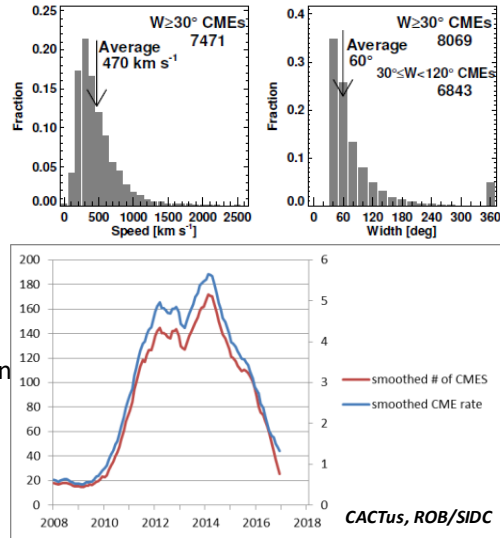
Direct Detection of a Coronal Mass Ejection-Associated Shock in Large Angle and Spectrometric Coronagraph Experiment White-Light Images

<http://adsabs.harvard.edu/abs/2003ApJ...598.1392V>

First-time observation of streamer deflection (by shock wave from CME).

# Coronal Mass Ejection

- Characteristics
  - Average speed
    - 470 km/s
  - Average width
    - 60 degrees
  - Average Mass
    - $10^{12}$  kg
    - ~ medium sized mountain
  - Number per day
    - 1-6 / day



SWIC - Collaboration between STCE, Koninklijke Luchtmacht, KNMI

Source file: Webb et al. (2012): Coronal Mass Ejections: Observations  
<http://link.springer.com/article/10.12942/lrsp-2012-3>

\* Webb et al. (2012): Coronal Mass Ejections: Observations

<http://link.springer.com/article/10.12942/lrsp-2012-3>

## 5.2 Interplanetary scintillation (IPS) observations

The IPS technique relies on measurements of the fluctuating intensity level of a large number of point-like distant meter-wavelength radio sources. They are observed with one or more ground arrays operating in the MHz–GHz range. IPS arrays detect changes to density in the (local) interplanetary medium moving across the line of sight to the source. Disturbances are detected by either an enhancement of the scintillation level and/or an increase in velocity. When built up over a large number of radio sources a map of the density enhancement across the sky can be produced. The technique suffers from relatively poor temporal (24-hour) resolution and has a spatial resolution limited to the field of view of the radio telescope. For example, high-latitude arrays such as the long-deactivated 3.5 ha array near Cambridge in the UK could not observe sources in the mid-high latitude southern hemisphere. Scattering efficiency also poses a limitation on IPS measurements as increasing the frequency at which to measure the sources allows an observer to detect disturbances closer to the Sun. Higher frequencies means fewer sources, however, so the spatial resolution is effectively decreased. Finally, ionospheric noise limits viewing near the Sun and near the horizon, and a model-dependence for interpreting the signal as density or mass. Workers have, however, been working with these difficulties for 50 years and a number of techniques have evolved to extract reliable CME measurements using IPS. Recent papers involving such measurements include Jones et al. (2007), Bisi et al. (2008), Jackson et al. (2010b), Tappin and Howard (2010), and Manoharan (2010).

# Coronal Mass Ejection

- Classification (based on speed and frequency)

EVANS ET AL.: OPINION

## Space Weather Research Center CME SCORE Scale

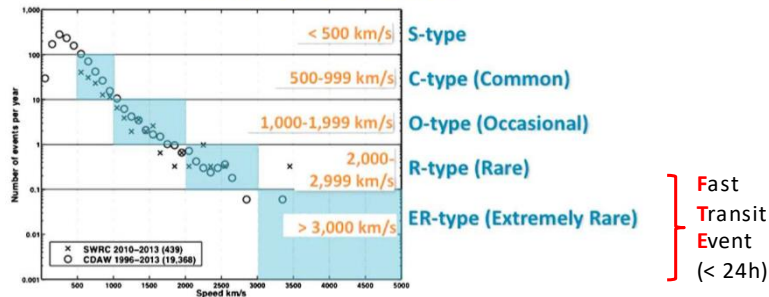


Figure 1. The frequency of CME detection, as a function of speed, from two sources: open circles represent the CDAW catalog, and the SWRC is represented by "x" marks. The numbers in parentheses in the legend indicate the total number of events in each catalog. Data are binned every 100 km/s and plotted by the bin center speed. The SWRC currently does not document all S-type CMEs, and therefore, data for this type are only shown from the CDAW catalog.

SWIC

126



Evans et al. (2013): The SCORE Scale: A Coronal Mass Ejection Typification System Based On Speed  
<http://adsabs.harvard.edu/abs/2013SpWea..11..333E>  
<http://onlinelibrary.wiley.com/doi/10.1002/swe.20058/epdf>

The relationship between the frequency of occurrence and speed of a CME in Figure 1 naturally led to the creation of five CME types, or scores (<https://swrc.gsfc.nasa.gov/main/score>). We selected the word "type" to complement, and avoid confusion with, X-ray "classes" of solar flares. In the CDAW catalog, the most numerous CMEs are those with a speed less than 500 km/s. On average, CMEs with these speeds occur more than 100 times per year. We call this group of slowest CMEs "S-type." CMEs with speeds between 500 and 999 km/s define the second type, "C-type," or a score of Common. On average, CMEs with these speeds are seen less than 100 but more than 10 times per year. CMEs with speeds between 1000 and 1999 km/s define the "O-type," with a score of Occasional. CMEs with speeds in this range take place a few times per year. CMEs with a speed between 2000 and 2999 km/s define the "R-type," with a score of Rare. On average, CMEs with these speeds occur less often than once per year. CMEs with a speed greater than 3000 km/s are scored Extremely Rare. ER-type CMEs are seen on average less than once in 10 years. In May 2012, the SCORE scale was introduced into SWRC operations in both notifications of ongoing events and Weekly Space Weather Summary Analysis provided to NASA robotic mission operators.

# Coronal Mass Ejection

- Terminology
  - Width
    - Narrow:  $<20^\circ$
    - Partial halo:  $>120^\circ$
    - (Full) halo:  $360^\circ$
  - Shape halo
    - Symmetric
    - Asymmetric
      - CMD  $>\sim 45^\circ$
  - Origin
    - Frontside/Farside
  - De- & acceleration

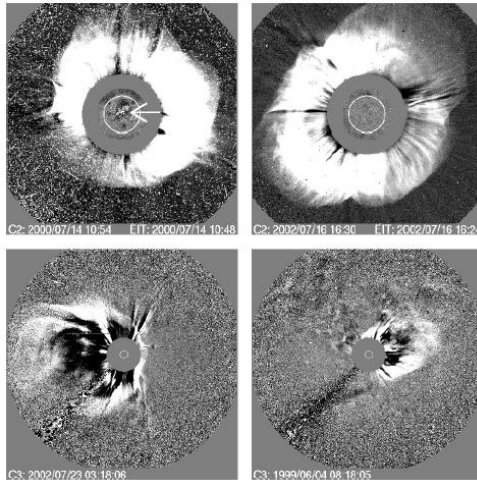


Figure 4: Examples of a variety of halo CME observations, clockwise: a frontside full halo (arrow shows likely source near Sun center); a backside full halo; a partial halo; and an asymmetric full halo. Image reproduced with permission from Gopalswamy *et al.* (2003a).

SWIC - Collaboration between STCε, Koninklijke Luchtmacht, KNMI

127

Source file: Webb *et al.* (2012): Coronal Mass Ejections: Observations  
<http://link.springer.com/article/10.12942/lrsp-2012-3>

CACTus automatically identified many more events than in the CDAW (manual) catalog but half of them were narrow ( $< 20^\circ$  of apparent angular width).

Some CMEs appear as narrow jets, some arise from pre-existing coronal streamers (the so-called streamer blowouts), while others appear as wide almost global eruptions. CMEs spanning very large angular ranges are probably not really global, but rather have a large component along the Sun-observer line and so appear large by perspective. These include the so-called halo CMEs (Howard *et al.*, 1982) – see Section 2.3. The CDAW CME catalog (Yashiro *et al.*, 2004) defines a “partial halo” as a CME with an apparent position angle range  $> 120^\circ$ . Hence, again, the definition of a CME is restricted by its viewing perspective.

Partial and full halo CMEs occur at a rate of about 10% that of all CMEs, but  $360^\circ$  halo CMEs are only detected at a rate of  $\sim 4\%$  of all CMEs.

CMEs that are aligned near the relative disk center tend to be more geoeffective while those nearer the relative solar limb are less so. The vast majority of the most intense geomagnetic storms of Cycle 23, for example, were caused by halo CMEs (Gopalswamy, 2010a).

Because of their increased sensitivity, field of view and dynamic range, the SOHO/LASCO and STEREO/COR coronagraphs now frequently observe halo CMEs, which appear as expanding, circular brightenings that completely surround the coronagraphs’ occulting disks (Figure 4). Observations of associated activity on the solar disk are necessary to help distinguish whether a halo CME was launched from the front or backside of the Sun relative to the observer. This has had limited success, as front-sided CMEs that do not have a solar surface association can be mistaken for back-sided events. In recent years several CMEs have been observed by the “three eyes” of STEREO-B, LASCO and STEREO-A by a variety of viewing points, thus reducing this latter problem.

# Coronal Mass Ejection

- Terminology
  - Width
    - Narrow:  $<20^\circ$
    - Partial halo:  $>120^\circ$
    - (Full) halo:  $360^\circ$
  - Shape halo
    - Symmetric
    - Asymmetric
      - CMD  $>\sim 45^\circ$
  - Origin
    - Frontside/Farside
  - De- & acceleration

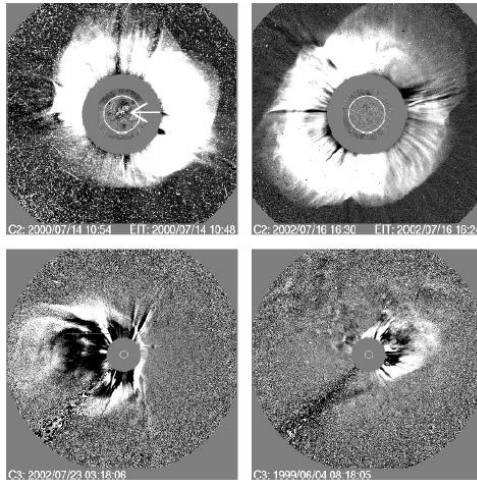


Figure 4: Examples of a variety of halo CME observations, clockwise: a frontside full halo (arrow shows likely source near Sun center); a backside full halo; a partial halo; and an asymmetric full halo. Image reproduced with permission from Gopalswamy *et al.* (2003a).

SWIC - Collaboration between STCε, Koninklijke Luchtmacht, KNMI

128

Yashiro *et al.* (2004) found that slow CMEs tend to accelerate and fast CMEs decelerated through the LASCO field of view, with those around the solar wind speed having constant speeds. Thus, CMEs attain fast acceleration low in the corona until gravity and other drag forces slow them further out. This process continues into the interplanetary medium.

She *et al.* (2014): Full Halo Coronal Mass Ejections: Arrival at the Earth

<http://adsabs.harvard.edu/abs/2014AGUFMSH43A4169S>

We found that all of the Earth-encountered CMEs satisfy a simple criterion that the angular width ( $\omega$ ) is larger than twice the deviation angle (CMD).

Gopalswamy (2009): Halo coronal mass ejections and geomagnetic storms

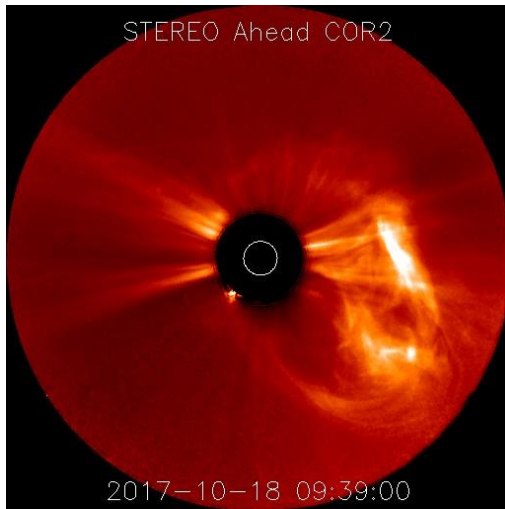
<http://adsabs.harvard.edu/abs/2009EP%26S...61..595G>

[https://cdaw.gsfc.nasa.gov/publications/gopal/gopal2009EPS61\\_1.pdf](https://cdaw.gsfc.nasa.gov/publications/gopal/gopal2009EPS61_1.pdf)

To clarify the identification of solar sources of halo CMEs, let us consider the association between CMEs and soft X-ray flares, one of the obvious indicators of disk activity. Whenever the eruption occurs on the frontside (CMD in the range  $0$  to  $90^\circ$ ), we observe a soft X-ray flare. The halo CME appears asymmetric when the solar source has a larger CMD, typically beyond  $45^\circ$ . When the eruption is behind the limb, but not too far behind, we usually observe

some EUV dimming above the concerned limb, but no soft X-ray flare is observed because the flare gets occulted by the solar limb. When a flare is partially occulted by a limb, the soft X-ray light curve tends to be very gradual and we observe the CME above the occulting limb. The extreme case is a backside CME whose associated flare is completely occulted, and we see no disk activity. In some of these cases one can see EUV dimming around most part of the solar disk, indicating a back-sided eruption. This kind of relationship between the soft X-ray flare and CMEs can be easily seen by tracking a large active region (AR) during its disk passage and eventual disappearance behind the west limb (e.g., AR 10486 reported in Gopalswamy *et al.*, 2005).

## Exercise: CME classification



- This is a STEREO-A coronagraphic image from a CME on 18 October 2017 at 09:39UT, which had a true speed of about 1080 km/s.
  - How would you label this CME?
    - Symmetric - full halo
    - Asymmetric - partial halo
  - Where would you rank this CME on the SCORE scale?
    - S-C-O-R-E
  - Would you expect this CME to be an FTE?
    - Yes / No

SWIC - Collaboration between STCE, Koninklijke Luchtmacht, KNMI



See also the STCE news item at <http://www.stce.be/news/408/welcome.html>

The CME arrived about 3 days later. See [https://stereo-ssc.nascom.nasa.gov/browse/2017/10/20/insitu\\_7day.shtml](https://stereo-ssc.nascom.nasa.gov/browse/2017/10/20/insitu_7day.shtml)

# Coronal Mass Ejection

- Typical parameters for halo CMEs

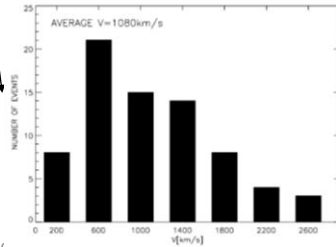
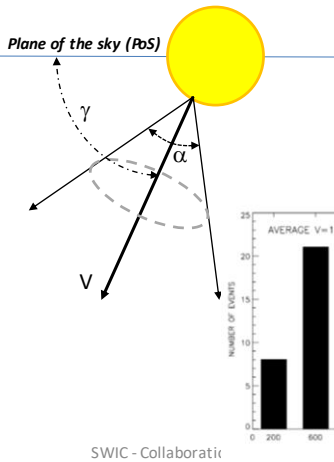


FIG. 3.—Histogram showing the distribution of  $V$  for the halo CMEs

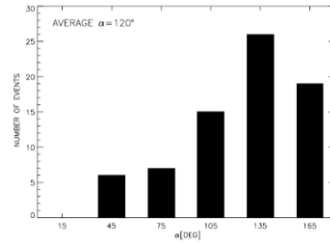


FIG. 4.—Histogram showing the distribution of  $\alpha$  for the halo CMEs

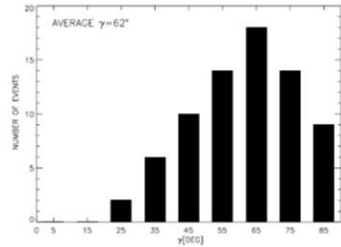


FIG. 5.—Histogram showing the distribution of  $\gamma$  for the halo CMEs

Michalek et al. (2003): A New Method for Estimating Widths, Velocities, and Source Location of Halo Coronal Mass Ejections

<http://adsabs.harvard.edu/abs/2003ApJ...584..472M>

<http://iopscience.iop.org/article/10.1086/345526/pdf>

Assuming that halo CMEs have constant velocities ( $V$ ), are symmetric, and propagate with constant angular widths.

The inclination of the symmetry axis to the sky plane is  $\gamma$ . The CME (cone) width is  $\alpha$ .

The halo CMEs date from the period 1996-2000.

Note that the width of CMEs may be solar cycle dependent:

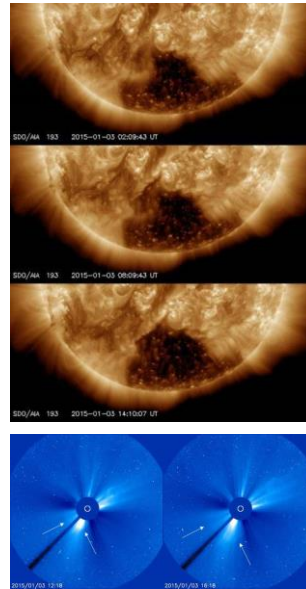
Gopalswamy et al. (2014): Anomalous expansion of coronal mass ejections during solar cycle 24 and its space weather implications

<http://adsabs.harvard.edu/abs/2014GeoRL..41.2673G>

The familiar correlation between the speed and angular width of coronal mass ejections (CMEs) is also found in solar cycle 24, but the regression line has a larger slope: for a given CME speed, cycle 24 CMEs are significantly wider than those in cycle 23. The slope change indicates a significant change in the physical state of the heliosphere, due to the weak solar activity. The total pressure in the heliosphere (magnetic + plasma) is reduced by ~40%, which leads to the anomalous expansion of CMEs explaining the increased slope. The excess CME expansion contributes to the diminished effectiveness of CMEs in producing magnetic storms during cycle 24, both because the magnetic content of the CMEs is diluted and also because of the weaker ambient fields. The reduced magnetic field in the heliosphere may contribute to the lack of solar energetic particles accelerated to very high energies during this cycle.

# Coronal Mass Ejection

- Terminology (cont'd)
  - Stealth CME
    - No obvious surface signature
    - Rather slow (<300 km/s)
    - Rather faint
  - CME cannibalism
    - 2<sup>nd</sup> CME overtakes 1<sup>st</sup>
    - Enhanced geomagn. storms
  - Fast Transit Events (FTE)
    - Sun-Earth transit < 24hrs
    - 23 July 2012!
  - Deflection



SWiC - Collaboration between STCE, Koninklijke Luchtmacht, KNMI

By CH, CME,...



## Stealth CME

Source file: Webb et al. (2012): Coronal Mass Ejections: Observations  
<http://link.springer.com/article/10.12942/lrsp-2012-3>

The absence of solar surface activity with observed CME activity is not a new observation (Howard and Harrison, 2012). The launch of STEREO in 2006, however, afforded us the opportunity to study the origins of CMEs simultaneously from multiple lines of sight. Robbrecht et al. (2009a) presented a study of a streamer blowout CME without a clear source region. The STEREO spacecraft were sufficiently widely separated (53°) that the CME and its source region could be viewed edge-on in STEREO A and face-on in STEREO B. STEREO B saw the CME as a faint halo and it was detected in-situ as a magnetic cloud 5 days later. Robbrecht et al. suggested that the CME originated high enough up in the corona such that no surface signatures were evident.

Subsequently, Ma et al. (2010) performed a statistical study of all CMEs observed during the first 8 months of 2009 when the STEREO lines of sight were nearly perpendicular to each other. They found that about a third of the CMEs were “stealth”, having no distinct surface association, and tending to be slow, i.e., < 300 km s<sup>-1</sup>. Faint coronal changes could be detected in about half of the stealth CMEs, again suggesting a higher launch site. It is noted that this period was during the recent unusual extended solar minimum, so the fraction of such CMEs may be different at other times.

A good example is in this STCE News item: The curious case of a strong storm  
<http://www.stce.be/news/290/welcome.html>

More info at Howard et al. (2012): Stealth Coronal Mass Ejections: A Perspective  
<http://adsabs.harvard.edu/abs/2013SoPh..285..269H>

# Coronal Mass Ejection

- Terminology (cont'd)

- Stealth CME

- No obvious surface signature
    - Rather slow (<300 km/s)
    - Rather faint

- CME cannibalism

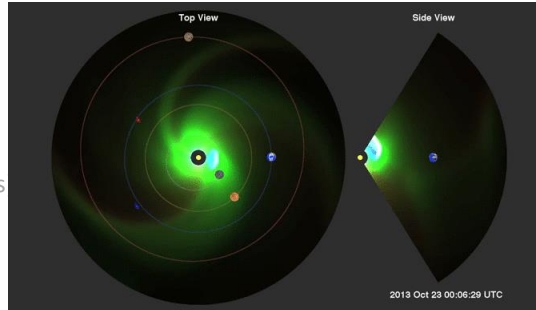
- 2<sup>nd</sup> CME overtakes 1<sup>st</sup>
    - Enhanced geomagn. storms

- Fast Transit Events (FTE)

- Sun-Earth transit < 24hrs
    - 23 July 2012!

- Deflection

SWiC - Collaboration between STCE, Koninklijke Luchtmacht, KNMI



Animation from NASA/GSFC at <https://svs.gsfc.nasa.gov/4099>

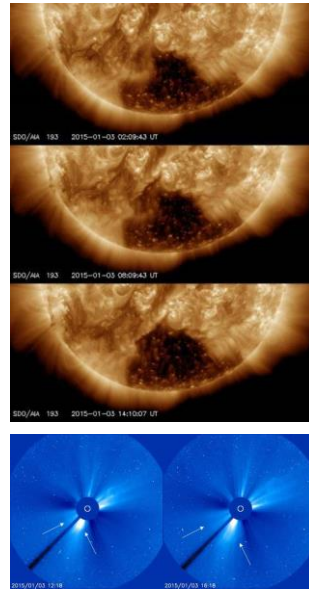
In this research model run, the Sun has launched three coronal mass ejections (CMEs) which may merge into a single front as it expands into the solar system. These events are sometimes called 'cannibal' CMEs.

This model run is based on estimated parameters from solar events of October 23-24, 2013

Also at [https://science.nasa.gov/science-news/science-at-nasa/2001/ast27mar\\_1](https://science.nasa.gov/science-news/science-at-nasa/2001/ast27mar_1)

# Coronal Mass Ejection

- Terminology (cont'd)
  - Stealth CME
    - No obvious surface signature
    - Rather slow (<300 km/s)
    - Rather faint
  - CME cannibalism
    - 2<sup>nd</sup> CME overtakes 1<sup>st</sup>
    - Enhanced geomagn. storms
  - Fast Transit Events (FTE)
    - Sun-Earth transit < 24hrs
    - 23 July 2012!
  - Deflection
    - By CH, CME,...



SWIC - Collaboration between STCE, Koninklijke Luchtmacht, KNMI

## CME cannibalism

Gopal Swamy et al. (2001): Radio Signatures of Coronal Mass Ejection Interaction: Coronal Mass Ejection Cannibalism?

<http://adsabs.harvard.edu/abs/2001ApJ...548L..91G>

<http://iopscience.iop.org/article/10.1086/318939/fulltext/>

CMEs are large-scale magnetic structures carrying ionized plasma. The physics of the interaction would therefore be very complex. One can speculate that the interaction between two CMEs may result in reconnection or simple piling up of the slower CME at the leading edge of the faster CME, resulting in a complex structure. Beyond the interaction region, one would expect a single CME consisting of magnetic field lines and plasma from both CMEs. We can describe this process as "CME cannibalism." The final structure and composition of the resulting CME would depend upon the nature of the interaction between the two CMEs. An analogous situation exists in the high-latitude solar wind: it is well known that high-latitude CMEs and the fast solar wind from coronal holes have similar composition (Galvin 1997). Even though the high-latitude CME originates from closed field lines and the fast solar wind originates from open field lines, they end up having similar composition, suggesting a possible interaction between the two magnetized plasma systems.

A nice example can be found in the STCE News item: The Sun in August 2011

<http://www.stce.be/news/x139x/welcome.html>

Cannibal CMEs can lead to enhanced geomagnetic storms.

# Coronal Mass Ejection

- Terminology (cont'd)

- Stealth CME
  - No obvious surface signature
  - Rather slow (<300 km/s)
  - Rather faint
- CME cannibalism
  - 2<sup>nd</sup> CME overtakes 1<sup>st</sup>
  - Enhanced geomagn. storms
- Fast Transit Events (FTE)
  - Sun-Earth transit < 24 hrs
  - 23 July 2012!
- Deflection

TABLE III  
"Fast-transit" events, 1859–2003.

| Flare date   | Transit time (h)  | References    |
|--------------|-------------------|---------------|
| 04 Aug. 1972 | 14.6              | 1, 2, 3       |
| 01 Sep. 1859 | 17.6              | 4, 5, 6, 7, 8 |
| 06 Feb. 1946 | 17.8              | 3, 9          |
| 28 Feb. 1941 | 18.4              | 10            |
| 16 Jul. 1959 | 19.4              | 11            |
| 28 Feb. 1942 | 19.5              | 8, 12         |
| 17 Sep. 1941 | 19.8              | 8, 13         |
| 29 Oct. 2003 | ~20 <sup>a</sup>  | 14            |
| 28 Oct. 2003 | 20.3 <sup>a</sup> | 14            |
| 15 Apr. 1938 | 21.2              | 8, 15         |
| 12 Nov. 1960 | 21.2              | 11            |
| 16 Jan. 1938 | 21.8              | 15, 16        |

References: (1) Dryer *et al.*, 1975; (2) Vaisberg and Zastenker, 1976; (3) Cliver *et al.*, 1990b; (4) Carrington, 1860; (5) Hodgson, 1860; (6) Hale, 1931; (7) Bartels, 1937; (8) Newton, 1943; (9) Nicholson and Hickox, 1946; (10) Newton, 1941a; (11) Ellison, McKenna, and Reid, 1961; (12) Newton, 1942; (13) Newton, 1941b; (14) Skoug *et al.*, 2004; (15) Bartels, 1940; (16) Bartels, Heck, and Johnston, 1939.  
<sup>a</sup>Preliminary.

SWIC - Collaboration between STCE, Koninklijke Luchtmacht, KNMI



## Fast transit event

Cliver *et al.* (2004): The 1859 Solar-Terrestrial Disturbance And the Current Limits of Extreme Space Weather Activity

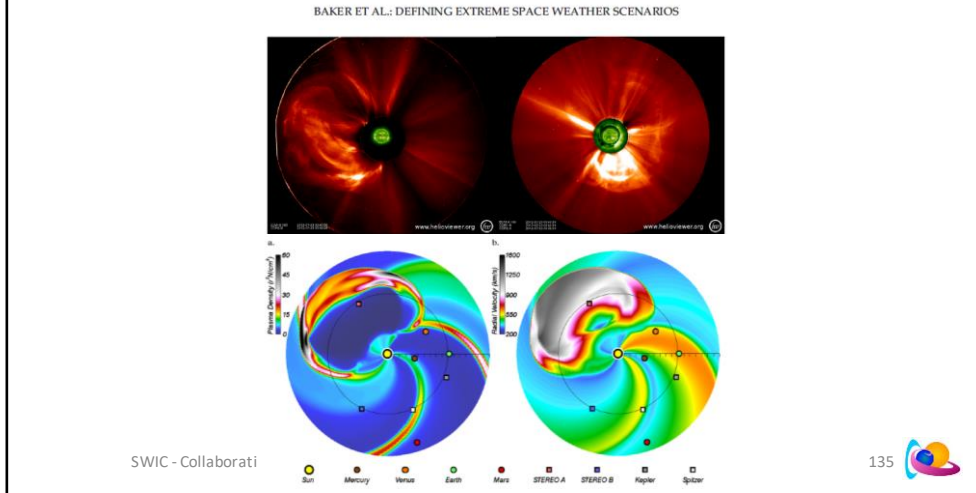
[adsabs.harvard.edu/abs/2004SoPh..224..407C](https://adsabs.harvard.edu/abs/2004SoPh..224..407C)

### 2.3. SUN-EARTH TRANSIT TIME

Cliver, Feynman, and Garrett (1990a,b) compiled a list of 10 "fast transit" events occurring from 1859–1989 in which a solar flare was followed within ~20 h by the sudden commencement of a geomagnetic storm. Table III is an update of their list through 2003. The shortest transit time (measured from inferred/observed flare onset to geomagnetic storm sudden commencement) for the listed events is 14.6 h for the 4 August 1972 flare-storm pair. The 1859 event had the second shortest delay, 17.6 h. On average, fast transit events appear to occur 1–2 times per solar cycle, but the temporal distribution is very uneven, with 6 such events occurring from 1938–1946 and a 31-year gap between the 4 August 1972 and 28 October 2003 events followed by a one day gap between the two October 2003 events. Solar wind measurements for the three modern events on the list (4 August 1972 (Vaisberg and Zastenker, 1976; d'Uston *et al.*, 1977) and 28 and 29 October 2003 (Skoug *et al.*, 2004)) indicate peak speeds ~ 2000 km/s.

# Coronal Mass Ejection

- Example of FTE during SC24



A nice example of the most recent FTE can be found in the STCE News item: A CME with an Olympic Speed

<http://www.stce.be/news/152/welcome.html>

This CME had a transit time of about 19 hours, but was directed towards ST-A, not Earth.

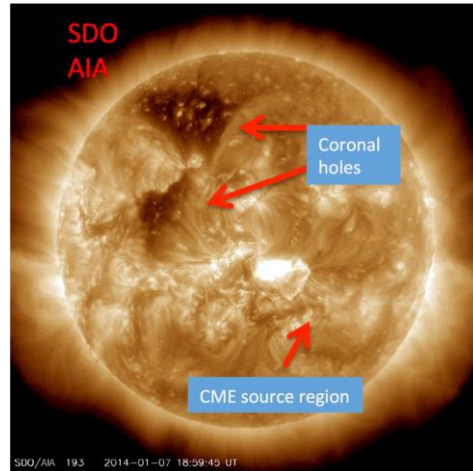
It is believed that, if the CME had been earth-directed, the space weather consequences would have been similar to the Carrington event.

Baker et al. (2013): A major solar eruptive event in July 2012: Defining extreme space weather scenarios

<http://adsabs.harvard.edu/abs/2013SpWea..11..585B>

# Coronal Mass Ejection

- Terminology (cont'd)
  - Stealth CME
    - No obvious surface signature
    - Rather slow (<300 km/s)
    - Rather faint
  - CME cannibalism
    - 2<sup>nd</sup> CME overtakes 1<sup>st</sup>
    - Enhanced geomagn. storms
  - Fast Transit Events (FTE)
    - Sun-Earth transit < 22hrs
    - 23 July 2012!
  - Deflection
    - By CH, CME,...



[https://science.gsfc.nasa.gov/674/swl\\_research.html](https://science.gsfc.nasa.gov/674/swl_research.html)

SWIC - Collaboration between STCE, Koninklijke Luchtmacht, KNMI

136 

## Deflections

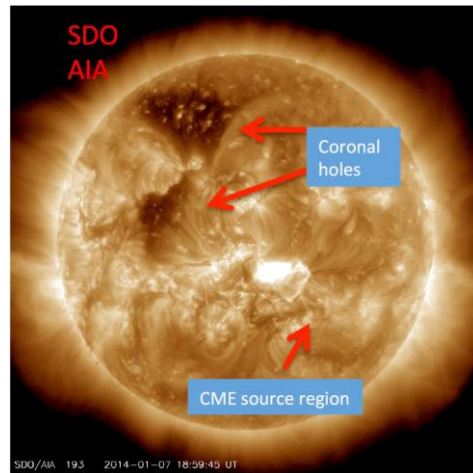
Kay et al. (2015): Global Trends of CME Deflections Based on CME and Solar Parameters

<http://adsabs.harvard.edu/abs/2015ApJ...805..168K>

Forecasting space weather effects relies on knowledge of the path of a CME. Observations commonly show significant non-radial deviations in the CME trajectories. Understanding these deflections will allow for more accurate space weather predictions. Coronal observations show that CMEs can undergo significant deflection close to the Sun, but it is often hard to disentangle the effects of deflection, rotation, and non-uniform expansion in the lower corona (Nieves-Chinchilla et al. 2012). Byrne et al. (2010) measure a latitudinal deflection of  $30^\circ$  below  $7 \odot R$  for the 2008 December 12 CME. Kilpua et al. (2009) suggest that CMEs may not be able to penetrate the open magnetic field emanating from coronal holes (CHs). The CH magnetic field then guides CMEs toward the Heliospheric Current Sheet (HCS). Shen et al. (2011) and Gui et al. (2011) attribute the deflection to gradients in the background magnetic energy density, which would also cause CMEs to tend to deflect toward the HCS. As with the observed CMEs, the MHD CMEs tend toward regions of lower magnetic energy. In some cases, magnetic reconnection creates an imbalance in the magnetic energy, which causes a CME to deflect early in the eruption (Zuccarello et al. 2012; Lynch & Edmondson 2013). MHD simulations also show that CMEs can deflect due to interactions with other CMEs (Lugaz et al. 2012). Finally, there are also effects of CME rotation due to a torque created by differential forces along the CME's toroidal axis.

# Coronal Mass Ejection

- Terminology (cont'd)
  - Stealth CME
    - No obvious surface signature
    - Rather slow (<300 km/s)
    - Rather faint
  - CME cannibalism
    - 2<sup>nd</sup> CME overtakes 1<sup>st</sup>
    - Enhanced geomagn. storms
  - Fast Transit Events (FTE)
    - Sun-Earth transit < 22hrs
    - 23 July 2012!
  - Deflection
    - By CH, CME,...



[https://science.gsfc.nasa.gov/674/swl\\_research.html](https://science.gsfc.nasa.gov/674/swl_research.html)

SWIC - Collaboration between STCE, Koninklijke Luchtmacht, KNMI

137



A good example of deflections is at [https://science.gsfc.nasa.gov/674/swl\\_research.html](https://science.gsfc.nasa.gov/674/swl_research.html)

## Extreme Solar Wind Deflects CMEs

A very fast CME was observed on January 7, 2014. Preliminary data analysis and all 8 community forecasts reported in GSFC's Space Weather Scoreboard indicated rapid arrival at Earth and a major geo-magnetic storm. However, the CME arrived at Earth ~19 hr **after the predicted time**, and the geomagnetic storm was weak ( $K_p < 3$ ). What happened?

Detailed analysis by the CCMC/SWRC team identified possible causes for the gap between predicted vs. actual outcome.

The solar wind coming from the nearby coronal holes was extremely fast – 950 km/s at Earth (very rare!) and deflected the CME away from the Earth. However, the solar wind speed assumed at the lower boundary of the CME transport model (WSA-ENLIL) was too low – 750 km/s (maximum allowed value). Therefore the model CME propagated to Earth much too slowly. Previously the same coronal hole did not produce such high speed wind, so the strong deflection was a surprise. We know that CMEs can be deflected by a coronal hole, so a CME that seems to be Earth-directed can be deflected from the Earth-Sun line. The simulations did not predict that the deflection would be so large that the CME only hit a glancing blow to the Earth.

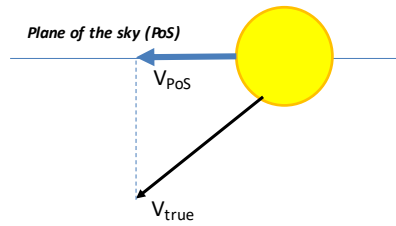
Wang et al. (2004) - Deflection of coronal mass ejection in the interplanetary medium

<http://adsabs.harvard.edu/abs/2004SoPh..222..329W>

Under the effect of the Parker spiral magnetic field, a fast CME will be blocked by the background solar wind ahead and deflected to the east, whereas a slow CME will be pushed by the following background solar wind and deflected to the west. ... slow CMEs can be deflected more easily than fast ones. ...

# Coronal Mass Ejection

- Speed
  - We see the projected speed
    - Plane of the sky (PoS)
  - We use the true speed
    - = Corrected PoS speed
      - $V_{true} \geq V_{PoS}$
    - From Type II radio bursts
      - = shock speed
      - NOAA event listing
      - SWS
        - » Learmonth
        - » Culgoora



```

:Created: 2012 Jul 15 0332 UT
:Date: 2012 07 12
# Prepared by the U.S. Dept. of Commerce, NOAA, Space Weather Prediction Center
# Please send comments and suggestions to SWPC.Website@noaa.gov
#
# Missing data: ////
# Updated every 30 minutes.
#
# Edited Events for 2012 Jul 12
#-----
#Event  Begin  Max  End  Obs  Q  Type  Loc/Frq  Particulars  Reg#
#-----
9900 + 1537 1649 1730 G15 5 XRA 1-8A X1.4 4.6E-01 1520
9900 1610 //// 1638 PAL C RSP 108-180 1520
9900 + 1614 1649 1732 SAG G RBR 410 6600 1520
9900 + 1614 1652 1706 SAG G RBR 1415 1100 1520
9900 + 1614 1653 1705 SAG G RBR 2695 800 1520
9900 + 1614 1653 1714 SAG G RBR 4995 480 1520
9900 + 1615 1653 1824 SAG G RBR 9800 430 1520
9900 1615 1652 2010 SAG G RBR 245 3900 1520
9900 1620 1655 1814 SAG G RBR 610 2400 1520
9900 + 1621 1654 1815 SAG G RBR 15400 230 1520
9900 + 1625 //// 1653 SAG C RSP 025-082 T3/2 1260 1520
9900 + 1638 //// 2359 PAL C RSP 025-180 1772 1520
  
```

SWIC - Collaboration between STCE, Koninklijke Lu

Source file: Webb et al. (2012): Coronal Mass Ejections: Observations  
<http://link.springer.com/article/10.12942/lrsp-2012-3>

Studies performed using SOHO data seem to confirm that metric type II bursts arise from shock waves driven by CMEs (Cliver et al., 1999) although the association between metric type II bursts and solar activity has been established since their discovery in the 1950s. Type II bursts in various wavelength domains appear to be organized by the kinetic energy of the CMEs: metric type II bursts ( $< 2 R_{\odot}$ ) are associated with CMEs with above-average kinetic energy; those extending into decameter-hectometric (DH) wavelengths ( $> 2 R_{\odot}$ ) have moderate CME kinetic energy; and type II bursts seen in both the metric and DH domains and extending to kilometric (km) wavelengths (covering the entire Sun-Earth distance) are associated with CMEs of the largest energy. This hierarchical relationship implies that all type II bursts are associated with CMEs, i.e., mass ejecta (e.g., Gopalswamy et al., 2005).

Some additional information on the relation between CMEs, CME shocks and Type II radio bursts can be found at [http://www.ovsa.njit.edu/fasr/Chapter\\_15.pdf](http://www.ovsa.njit.edu/fasr/Chapter_15.pdf) (Gopalswamy: Interplanetary Radio bursts, in Solar and Space Weather Radiophysics – Chapter 15).

As well as in Gopalswamy et al. (2008): Coronal mass ejections, type II radio bursts, and solar energetic particle events in the SOHO era  
<http://adsabs.harvard.edu/abs/2008AnGeo..26.3033G>  
<http://www.ann-geophys.net/26/3033/2008/angeo-26-3033-2008.pdf>

Some good examples on how to calculate/deduce the CME speed:  
 - NASA: <http://rodshome.com/TLA/sunspots/CMEveloctiry%20calc.pdf>  
 - Pohjolainen et al. (2007): CME Propagation Characteristics from Radio Observations  
<http://adsabs.harvard.edu/abs/2007SoPh..244..167P>

Data of Type II bursts with derived shock speeds:  
 NOAA: <https://www.swpc.noaa.gov/products/solar-and-geophysical-event-reports>  
 SWS: <http://www.sws.bom.gov.au/Solar/2/3>  
 Attention: The shock speed is usually (a bit / a lot) higher than the (corrected) CME speed.

# Coronal Mass Ejection

- Speed calculation

## Forecasting the Arrival of ICMEs: The Drag-Based Model

Basic DBM | **Advanced DBM** | Documentation

CME take-off date: Feb 3 2017

CME take-off time (UTC): 16 h 37 min

$R_0$  - starting radial distance of CME ( $R_A$ ): 20

$V_0$  - speed of CME at  $R_0$  (km/s): 1000

$\Gamma$  - drag parameter ( $10^{-7} \text{ km}^{-1}$ ): 0.2

$w$  - asymptotic solar wind speed (km/s): 450

$R_{\text{target}}$  - target heliocentric distance (AU): 1

Calculate | Reset

Drag-Based Model has performed 1799 successful calculations (since 26.12.2012).

Results | v-R-t plots | Documentation

**Output:**

CME arrival at target (date & time): 05.02.2017 at 18h:36min  
 Transit time: 45.99 h  
 Impact speed at target (at 1 AU): 636 km/s

**Input parameters:**

CME take-off date & time: 03.02.2017 at 16h:37min  
 $R_0=20$   $R_A=1000$  km/s,  $\Gamma=0.2 \times 10^{-7} \text{ km}^{-1}$ ,  $w=450$  km/s,  $R_{\text{target}}=1$  AU

Calculated in 0.26 seconds.

The true speed of a CME can be quite accurately determined by triangulation of images from 2 spacecraft, e.g. SOHO/LASCO C3 and STEREO-A/COR2.

For this purpose, the tool STEREOCAT developed by NASA's GSFC/CCMC can be used. The tool is online publicly available at <https://ccmc.gsfc.nasa.gov/analysis/stereo/>

It provides the true speed of the CME which can then be used as an input for the drag based model, which then calculates the arrival time at Earth.

The true speed of a CME is usually a bit less than the shock speed derived from Type II radio burst data.

# Coronal Mass Ejection

- Bz
  - North-South component of magnetic field (nT) perpendicular to the ecliptic
  - Intensity varies much more than speed
  - *Negative (« south »), strong and long-lasting Bz is necessary to get a strong geomagnetic storm*
  - Need to predict both orientation and intensity
    - Not easy + potentially changing during Sun-Earth transit!

SWIC - Collaboration between STCE, Koninklijke Luchtmacht, KNMI



Ecliptic: The ecliptic is the apparent path of the Sun on the celestial sphere, and is the basis for the ecliptic coordinate system. It also refers to the plane of this path, which is coplanar with the orbit of Earth around the Sun (and hence the apparent orbit of the Sun around Earth).

From Wikipedia: <https://en.wikipedia.org/wiki/Ecliptic>

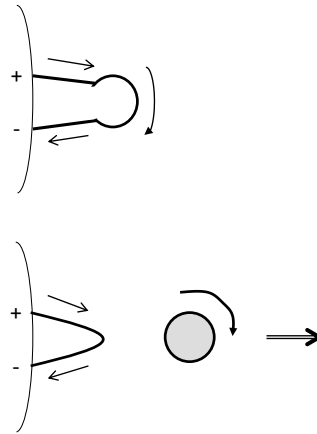
Zhukov (2017): Predicting Geomagnetic Storms on the Base of Solar Observations

<https://events.oma.be/indico/event/21/>

The solar wind-magnetosphere coupling is governed by the duskward electric field  $E_y \sim vB_z$ . However,  $v$  varies only by a factor of 2 (maybe 5 in extreme events).  $B_z$  varies by a factor of 10 and is thus a parameter more important for predictions. To be geoeffective, the CME-associated disturbance should have a suitable magnetic field configuration: the interplanetary magnetic field (IMF)  $B_z$  component should be negative (southward), strong enough and long-lasting.

# Coronal Mass Ejection

- Bz: Orientation
  - Proxies of erupting flux ropes:
    - Post-eruption arcades
    - Magnetograms
    - CME shape from coronagraphic imagery
  - May change during Sun-Earth transit!
    - See « Deflections »!



SWIC - Collaboration between STCE, Koninklijke Luchtmacht, KNMI



Bothmer et al. (1998): The structure and origin of magnetic clouds in the solar wind  
<http://adsabs.harvard.edu/abs/1998AnGeo..16....1B>  
<http://www.ann-geophys.net/16/1/1998/angeo-16-1-1998.pdf>

The term magnetic cloud (MC) was introduced by Burlaga et al. (1981) to characterize the magnetic field and plasma signatures of an interplanetary post-shock flow observed by five spacecraft separated over more than 30 in solar longitude between 0.9 and 2 AU. The outstanding feature of this solar wind transient was the smooth rotation of the magnetic field vector nearly parallel to a plane over a time interval of the order of one day at 1 AU. MCs are often, but not always associated with interplanetary shocks (Klein and Burlaga, 1982; Zhang and Burlaga, 1988).

## Configurations and orientations of MCs in interplanetary space

The concept of cylindrical flux tubes allows different magnetic configurations. In the context of the investigation of the orientations of MCs in interplanetary space, it will be shown that all the predicted types of flux-tubes actually occur in the solar wind. Assume as in Fig. 3 that the axis of a MC lies in the ecliptic plane, normal to the sun-spacecraft line. A flux tube (MC) cloud possess one of the four different magnetic configurations presented in Table 2, which differ in the orientation of the magnetic field lines at the cloud's outer boundaries and on its axes. These MCs would produce different characteristic magnetic signatures when passing over a spacecraft. According to Table 2, MCs can be classified into SEN (SWN) clouds where the magnetic field vector turns from south (S) to east (E) (west, W) on the cloud's axis and finally to the north (N) at its rear boundary, and vice versa into NES (NWS) clouds. More generally we can define  $\Delta\theta > 0$  for SN- clouds ( $\Delta\theta < 0$  for NS clouds) with  $180 < \theta < 360$  for SEN, NES (SWN, NWS) clouds. The classification introduced here involves the property of magnetic helicity (see Burlaga, 1988; Lepping et al., 1990). SEN and NWS clouds possess left-handed (LH), SWN and NES clouds, right-handed (RH) helicity as viewed by an observer looking towards the Sun.

# Coronal Mass Ejection

- **Bz: Orientation**
  - Proxies of erupting flux ropes:
    - Post-eruption arcades
    - Magnetograms
    - CME shape from coronagraphic imagery
  - May change during Sun-Earth transit!!
    - See « Deflections »!
- **Bz: intensity**
  - CME solidness
  - CME Speed
  - ...

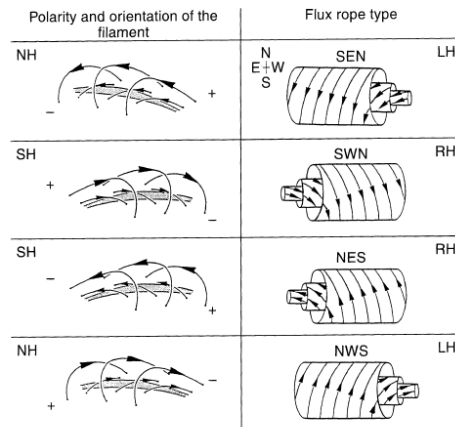


Fig. 17. Inferred magnetic structure of filaments in the Sun's northern and southern hemispheres (NH, SH) and that of associated MCs in interplanetary space (adapted from Bothmer and Schwenn, 1994). The abbreviations for the magnetic field structures have been chosen in analogy to the different flux tube types of MCs presented in Table 2. LH (left-handed) and RH (right-handed) denote the corresponding magnetic helicity

SWIC - Collaboration between STCE, Koninklijke Lu

Bothmer et al. (1998): The structure and origin of magnetic clouds in the solar wind  
<http://adsabs.harvard.edu/abs/1998AnGeo..16....1B>  
<http://www.ann-geophys.net/16/1/1998/angeo-16-1-1998.pdf>

The term magnetic cloud (MC) was introduced by Burlaga et al. (1981) to characterize the magnetic field and plasma signatures of an interplanetary post-shock flow observed by five spacecraft separated over more than 30 in solar longitude between 0.9 and 2 AU. The outstanding feature of this solar wind transient was the smooth rotation of the magnetic field vector nearly parallel to a plane over a time interval of the order of one day at 1 AU. MCs are often, but not always associated with interplanetary shocks (Klein and Burlaga, 1982; Zhang and Burlaga, 1988).

## Configurations and orientations of MCs in interplanetary space

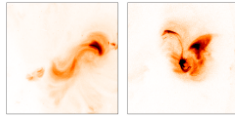
The concept of cylindrical flux tubes allows different magnetic configurations. In the context of the investigation of the orientations of MCs in interplanetary space, it will be shown that all the predicted types of flux-tubes actually occur in the solar wind. Assume as in Fig. 3 that the axis of a MC lies in the ecliptic plane, normal to the sun-spacecraft line. A flux tube (MC) cloud possess one of the four different magnetic configurations presented in Table 2, which differ in the orientation of the magnetic field lines at the cloud's outer boundaries and on its axes. These MCs would produce different characteristic magnetic signatures when passing over a spacecraft. According to Table 2, MCs can be classified into SEN (SWN) clouds where the magnetic field vector turns from south (S) to east (E) (west, W) on the cloud's axis and finally to the north (N) at its rear boundary, and vice versa into NES (NWS) clouds. More generally we can define  $\Delta\theta > 0$  for SN- clouds ( $\Delta\theta < 0$  for NS clouds) with  $180 < \theta < 360$  for SEN, NES (SWN, NWS) clouds. The classification introduced here involves the property of magnetic helicity (see Burlaga, 1988; Lepping et al., 1990). SEN and NWS clouds possess left-handed (LH), SWN and NES clouds, right-handed (RH) helicity as viewed by an observer looking towards the Sun.

# Coronal Mass Ejection

## Sigmoids:

- forward-S → RH
- reverse-S → LH

(Pevtsov et al., 1997)

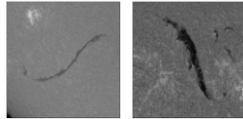


Hinode/XRT Soft X-ray

## Filament H $\alpha$ details:

filament barbs (right bearing = LH), threads, and spine shape

(Martin et al., 1994)

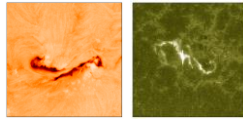


BBSO 6563 Å

## Flare ribbons:

- forward-J → RH
- reverse-J → LH

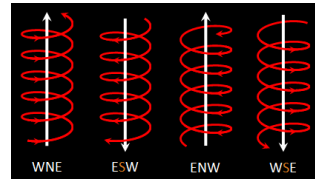
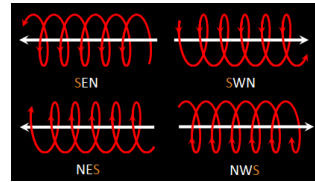
(Démoulin et al., 1996)



Hinode/SOT 6563 Å

SDO/AIA 1600 Å

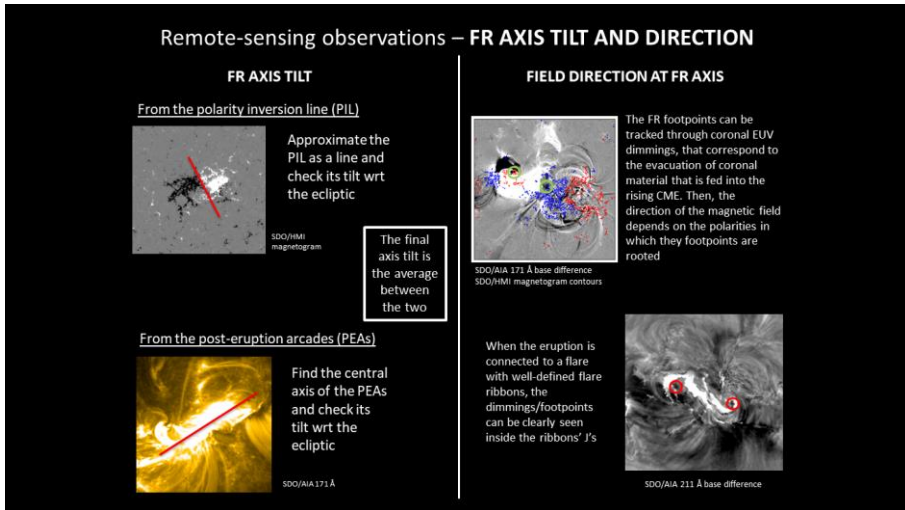
- SEN and NWS clouds possess LH (left-hand) chirality
- SWN and NES clouds possess RH (right-hand) chirality
- ESW and WSE flux ropes produce strongest geo. effects; WNE and ENW are weakest



Figures from Seminar by Erika Palmerio (19 April 2017)



# Coronal Mass Ejection



Figures from Seminar by Erika Palmerio (19 April 2017)

SWIC - Collaboration between STCE, Koninklijke Luchtmacht, KNMI

FR: Flux rope

# Interplanetary CME

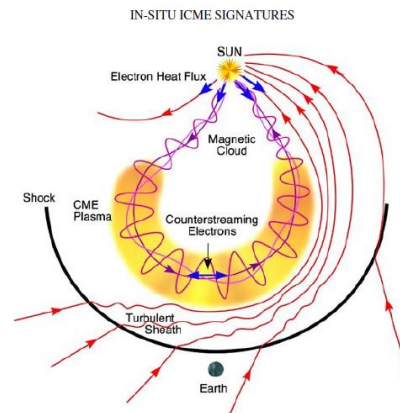
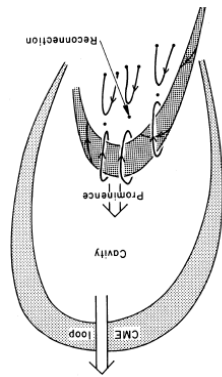


Figure 2. Schematic of the three-dimensional structure of an ICME and upstream shock, relating magnetic field, plasma, and BDE signatures.

SWIC - Collaboration between STCE, Koninklijke Luchtmacht, KNMI

145 

Figure right:

Zurbuchen et al. (2006): In-Situ Solar Wind and Magnetic Field Signatures of Interplanetary Coronal Mass Ejections

<http://adsabs.harvard.edu/abs/2006SSRv..123...31Z>

An interplanetary CME (ICME) is a CME of which the solar wind features are measured in situ by spacecraft at Earth or in the solar system.

Pending the mutual positions of the Earth and the CME, Earth may experience the following impacts from this (I)CMEs:

1. Nothing
2. Shock + Sheath
3. Shock + Sheath + Magnetic Cloud leg (long)
4. Shock + Sheath + Magnetic Cloud (head-on) + rarefied region
5. No shock, still magnetic cloud

These all give different signatures in the various solar wind parameters.

The figure on the left was taken from:

Priest (1988): The initiation of solar coronal mass ejections by magnetic nonequilibrium

<http://adsabs.harvard.edu/abs/1988ApJ...328..848P> (Fig. 1c, upside down)

Rodriguez et al. (2016): Typical Profiles and Distributions of Plasma and Magnetic Field Parameters in Magnetic Clouds at 1 AU

<http://adsabs.harvard.edu/abs/2016SoPh..291.2145R>

# Interplanetary CME

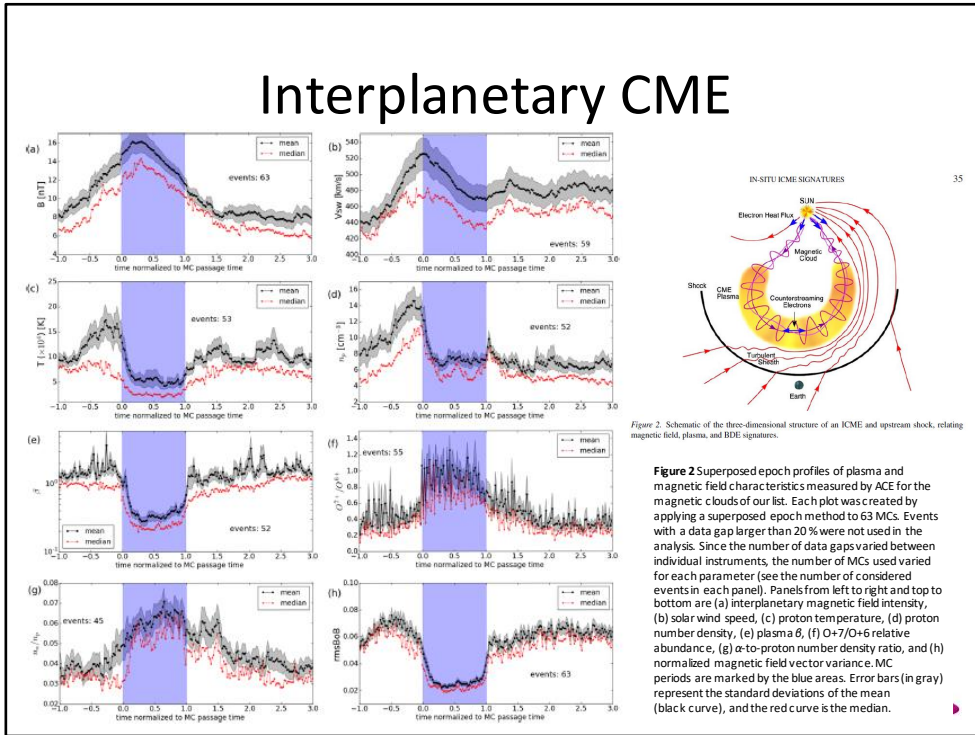


**Figure 2** Superposed epoch profiles of plasma and magnetic field characteristics measured by ACE for the magnetic clouds of our list. Each plot was created by applying a superposed epoch method to 63 MCs. Events with a data gap larger than 20% were not used in the analysis. Since the number of data gaps varied between individual instruments, the number of MCs used varied for each parameter (see the number of considered events in each panel). Panels from left to right and top to bottom are (a) interplanetary magnetic field intensity, (b) solar wind speed, (c) proton temperature, (d) proton number density, (e) plasma  $\beta$ , (f) O+7/O+6 relative abundance, (g)  $\alpha$ -to-proton number density ratio, and (h) normalized magnetic field vector variance. MC periods are marked by the blue areas. Error bars (in gray) represent the standard deviations of the mean (black curve), and the red curve is the median.

Small figure to the right: Zurbuchen et al. (2006): In-Situ Solar Wind and Magnetic Field Signatures of Interplanetary Coronal Mass Ejections  
<http://adsabs.harvard.edu/abs/2006SSRv..123...31Z>

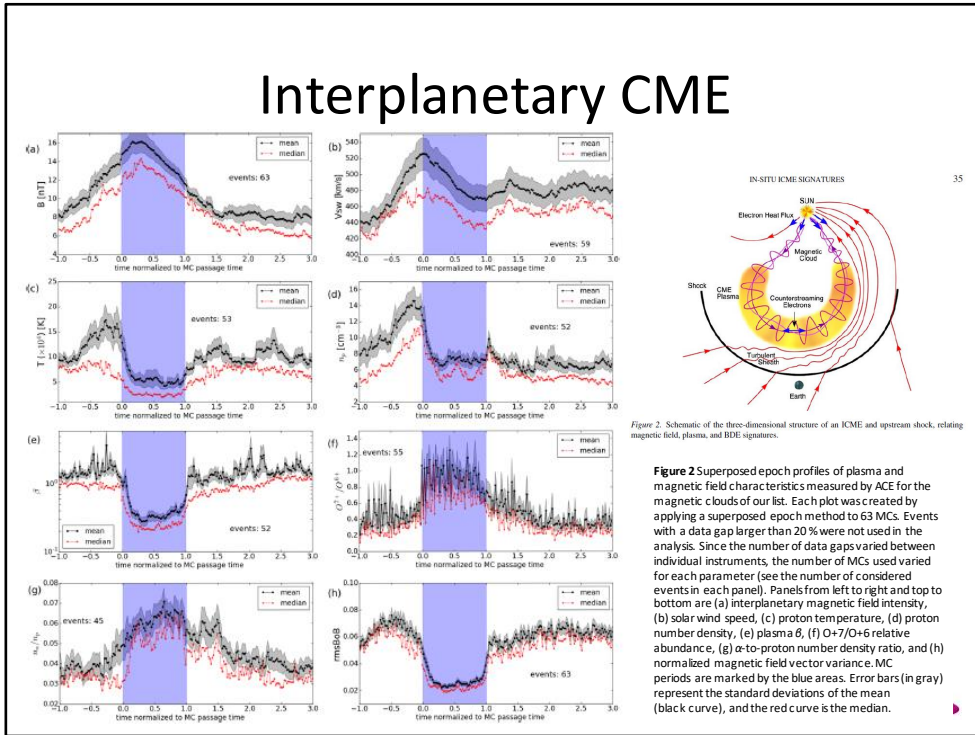
Figure to the left: Rodriguez et al. (2016): Typical Profiles and Distributions of Plasma and Magnetic Field Parameters in Magnetic Clouds at 1 AU  
<http://adsabs.harvard.edu/abs/2016SoPh..291.2145R>

Coronal mass ejections (CMEs) are large-scale solar eruptive events in which large amounts of plasma carrying magnetic flux and helicity (see e.g. Démoulin, Janvier, and Dasso, 2016, and references therein) are expelled into the interplanetary space. When sampled *in situ* by a spacecraft in the interplanetary medium, they are called interplanetary CMEs (ICMEs). Magnetic clouds (MCs) are an important subset of ICMEs that exhibit a particular internal magnetic field configuration resembling that of a flux rope. This is characterized by an enhanced magnetic field intensity, smooth rotation of its magnetic field vector, and low temperature (e.g. Burlaga, 1991).

The classical three-part structure of a CME (bright front, dark cavity, and dense core) is commonly also interpreted in terms of a magnetic flux rope propagating in the corona (see e.g. Illing and Hundhausen, 1986; Vourlidas et al., 2013). The bright front corresponds to the plasma pile-up in front of the flux rope, the cavity represents the bulk of the flux rope, and the dense core is the erupting prominence that is located in the bottom (concave-out) parts of the flux rope field lines. However, it is very difficult to identify the corresponding three-part morphology in ICMEs detected *in situ* (e.g. Kilpua et al., 2013a).

The plasma  $\beta$  and the level of fluctuations in the magnetic field vector are the best parameters to define the boundaries of MCs. We find that one third of the events shows a peak in plasma density close to the trailing edge of the flux ropes.

# Interplanetary CME



Firstly, the magnetic field magnitude is found to peak inside the cloud, reaching values twice as high as those found in the ambient solar wind (as can be seen from panel a of Figure 2). In addition, the peak is asymmetric toward the leading edge. Next, the proton density (panel d) and temperature (panel c) peak before the arrival of the flux rope and represent a clear signature of the compressed pile-up plasma region in front of the flux rope. The proton temperature then decreases and reaches a minimum in the MC region, which is also a consequence of the internal expansion (Gosling, Pizzo, and Bame, 1973; Richardson and Cane, 1995). As mentioned in Section 1, the proton density peak observed close to the flux rope leading edge probably corresponds to the bright front of the associated CME observed by coronagraphs. The negative slope of the speed profile (panel b) marks the typical expansion of magnetic clouds (e.g. Klein and Burlaga, 1982; Gulisano *et al.*, 2010). The plasma  $\beta$  (panel e) is low within the clouds, meaning that these are magnetically dominated structures. The magnetic field within the MC is found to vary very smoothly, and its normalized variation [ $rmsBoB$ ] is a factor of three smaller than in the ambient solar wind.

The magnetic field variation can be considered as a very reliable parameter for MC identification. Furthermore, together with the plasma  $\beta$ , the variation of the magnetic field unit vector clearly marks the boundaries of the clouds. The O+7/O+6 shown in Figure 2 (panel f) is clearly increased within the MC, indicating high temperatures in the source region of the CME (Henke *et al.*, 1998; Rodriguez *et al.*, 2004; Song *et al.*, 2015). This parameter provides a very good signature for identifying magnetic cloud material (see also Figure 8 of Richardson and Cane, 2004). The magnetic field intensity and the temperature (panels a and c) have the most progressive transition from the MC to typical solar wind conditions, followed by the composition ratios (panels f and g). All these features could be a consequence of the formation of a back region in magnetic clouds that is due to reconnection of the flux rope with the surrounding solar wind (see Dasso *et al.*, 2006, 2007; Ruffenach *et al.*, 2015). Still, the rear boundary of this extended flux rope is not well defined (no sharp transition).

In summary, compression by trailing HSSs seems to be the most promising explanation for the creation of the trailing density peaks in MCs. This mechanism, together with intrinsic processes corresponding to flux tubes with different plasma and magnetic field properties, could explain the majority of the observed peaks.

:Issued: 2014 Apr 17 1325 UTC  
 :Product: documentation at http://www.sidc.be/product/s/ot  
 #-----#  
 # DAILY BULLETIN ON SOLAR AND GEOMAGNETIC ACTIVITY from the SIDC #  
 #-----#  
 SIDCURSIGRAM 40417  
 SIDCSOLAR BULLETIN 17 Apr 2014, 1304UT



SIDC FORECAST (valid from 1230UT, 17 Apr 2014 until 19 Apr 2014)  
 SOLAR FLARES : Active (M-class flares expected, probability >=50%)  
 GEOMAGNETISM : Quiet (A<20 and K<4)  
 SOLAR PROTONS : Quiet

PREDICTIONS FOR 17 Apr 2014 10CM FLUX: 180 / AP: 013  
 PREDICTIONS FOR 18 Apr 2014 10CM FLUX: 184 / AP: 007  
 PREDICTIONS FOR 19 Apr 2014 10CM FLUX: 188 / AP: 005

COMMENT: Eleven sunspot groups were reported by NOAA today. NOAA ARs 2035, 2036, and 2037 (Catania numbers 24, 25, and 26 respectively) maintain the beta-gamma configuration of the photospheric magnetic field. The strongest flare of the past 24 hours was the M1.0 flare peaking at 19:59 UT yesterday in the NOAA AR 2035 (Catania number 24). The flare was associated with an EIT wave and a weak coronal dimming, but the associated CME was narrow and is not expected to arrive at the Earth.

We expect further flaring activity on the C-level, especially in the NOAA ARs 2035 and 2037 (Catania numbers 24 and 26 respectively) as well as in the NOAA AR 2042 (no Catania number yet) that yesterday appeared from behind the east solar limb, with a good chance for an M-class event.

Since yesterday evening the Earth is situated inside a solar wind structure with an elevated interplanetary magnetic field magnitude (occasionally up to 10 nT). It may be a weak ICME or the compression region on the flank of an ICME that missed the Earth. The solar origin of this structure is not clear. The north-south magnetic field component Bz was not strong, so no significant geomagnetic disturbance resulted (Kindex stayed below 4). Currently the solar wind speed is around 380 km/s and the IMF magnitude is around 8 nT.

~~We expect quiet to unsettled (K-index up to 2) geomagnetic conditions, with active geomagnetic conditions (K=4) possible, but unlikely.~~

TODAY'S ESTIMATED ISN : 145, BASED ON 17 STATIONS.  
 99999

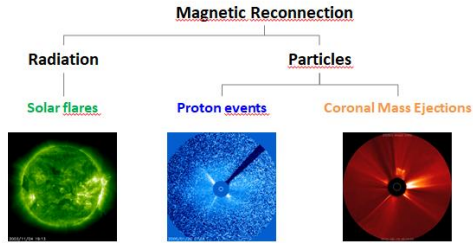
SOLAR INDICES FOR 16 Apr 2014  
 WOLF NUMBER CATANIA : ///  
 10CM SOLAR FLUX : 184  
 AK CHAMBON LA FORET : 012  
 AK WINGST : 004  
 ESTIMATED AP : 004  
 ESTIMATED ISN : 139, BASED ON 29 STATIONS.



NOTICEABLE EVENTS SUMMARY  
 DAY BEGIN MAX END LOC XRAY OP 10CM Catania/NOAA RADIO\_BURST\_TYPES  
 16 1954 1959 2004 S14E09 M1.0 1N 24/2035 I/2  
 END

# Summary 1/2

- Solar Eruptions



- **Solar flares**

- Standard model
  - Outlook & Features
- Classification
  - H $\alpha$ , x-ray, NOAA scale (R)
- Different types
  - Spotless flares, WLF,...
- Radio bursts
- Flare predictions
  - McIntosh, Hale, filaments

# Summary 2/2

- **Proton events**

- $\geq 10$  MeV proton flux  $\geq 10$  pfu
- Classification
  - Impulsive vs. Gradual
  - SEP vs. ESP
  - NOAA Scale (S)
- Forecasting
  - Strong flare
  - Wide and fast CME
  - Western solar hemisphere

- **Coronal Mass Ejection**

- Morphology
- Classification & Terminology
  - SCORE (speed), width/shape,...
  - Stealth, Cannibalism, FTE, Deflection
- True vs. Plane-of-the-Sky speed
- Bz
- ICME